Investigating the effects of environmental stress on coastal zooplankton populations: from mechanistic drivers to trophic impacts

Amy C. Wyeth

A dissertation

submitted in partial fulfillment of the

requirements for the degree of

Doctor of Philosophy

University of Washington

2024

Reading Committee:

Daniel Grünbaum, Co-chair

Julie E. Keister, Co-chair

Parker MacCready

Program Authorized to Offer Degree:

Oceanography

University of Washington

Abstract

Investigating the effects of environmental stress on coastal zooplankton populations: from mechanistic drivers to trophic impacts

Amy C. Wyeth

Chairs of the Supervisory Committee:

Daniel Grünbaum

Julie E. Keister

Oceanography

Environmental stressors, such as hypoxia and acidification, are increasing in intensity, duration, and extent in coastal waters and estuaries. Environmental stressors are known to affect a wide range of marine species, including zooplankton. Zooplankton are a critical link in marine food webs, connecting phytoplankton to higher trophic levels such as economically important fish, and are thought to be informative indicators of ecosystem change. For this reason, increased attention has been paid to understanding the mechanisms shaping zooplankton populations. Previous studies have shown that zooplankton exhibit both lethal and sublethal responses to changes in dissolved oxygen and pH. However, there is a range of species-specific responses to

stressors. Different responses across species alter zooplankton community composition and spatial distributions, directly impacting predator-prey interactions and the trophic dynamics in coastal environments. This dissertation integrates laboratory experiments, in situ observations, and field work to understand how environmental stressors affect coastal zooplankton populations and nearshore food webs. In Chapter 1, I conducted laboratory experiments to investigate whether the copepod, *Calanus pacificus*, showed behavioral responses to stressors, and whether these responses lead to changes in vertical population distributions. Our laboratory experiments demonstrated significant effects of bottom water hypoxia and acidification on behavioral avoidance, swimming statistics, and apparent mortality rates in *C. pacificus*. In Chapter 2, I used a remote camera system to quantify in situ behavioral responses of zooplankton to stressors, using results from Chapter 1 to generate hypotheses about observations in the field. Our in situ videos revealed that copepods in stressful conditions exhibited significantly slower swimming speeds than copepods in non-stressful conditions, while amphipods showed significantly decreased abundances within stressful conditions. Finally, in Chapter 3, I collected zooplankton net tows in an intertidal estuary to investigate the transport of pelagic species into eelgrass beds and the role of eelgrass beds as potential sinks of pelagic zooplankton over the tidal cycle, potentially due to predation by juvenile fish. We found evidence of transport of pelagic species into intertidal habitats and measured large spatial and temporal variability, highlighting the need for sampling programs that can capture small-scale variability. This dissertation provides insight into the mechanisms that link the effects of environmental stressors across individual responses to population, community, and ecosystem level scales and suggests novel methodologies to help advance our understanding of changing zooplankton dynamics.

Table of Contents

List of Figures

List of Tables

Acknowledgements

Thank you to my advisors, Julie Keister and Danny Grünbaum, for their encouragement and support over the last 6 years. I came into graduate school knowing very little about zooplankton and even less about coding. Thank you for taking me under your wings and providing me with a range of different field, lab, and critical thinking tools. You gave me the freedom to learn, make mistakes, and come out of graduate school feeling like, with the right google search, I can do anything. I will carry so many aspects of your scientific approach and mentorship style into the next steps of my career. Truely, thank you.

Thank you to my committee members (past and current), Alex Gagnon for all things carbonate chemistry, Parker MacCready for all things estuarine circulation, and Jennifer Ruesink for all things nearshore ecology.

Thank you to my mentors at the Padilla Bay National Estuary Research, Sylvia Yang, Nicole Burnett, and Heath Bolhmann. Chapter 3 would not have been possible without the deep knowledge of Padilla Bay that you shared with me. Thank you for all the hours you spent with me in the field figuring out how to sample pelagic species in such a shallow system. My experience working with you in the federal sector has helped shape my career ambitions.

A massive thank you to Captain Brian Bare and all the amazing crew I have sailed with on the R/V Rachel Carson. Every single person on the Carson cares deeply about the research they facilitate. Thank you for some of the most creative and fun problem-solving sessions. Brian, you have been an unwavering source of support for me over the last six years and have helped me navigate around more obstacles that I can count. I could not have finished Chapter 1 if you hadn't collected samples for me from your personal boat during the COVID lockdown. Being in the field fills my cup and it has been a pleasure sailing with people who feel the same.

Thank you to Jan Newton for being the busiest person I know and still always finding the time to offer me guidance when I was feeling a little lost. I was given advice early on in graduate school to find mentors that aren't your official mentor. You filled that role for me, and I wouldn't have gotten here without your support.

Thank you to all the other faculty and staff I have worked with who truly keep the School of Oceanography running and who have made coming to work more fun. From the Keister lab, Amanda, BethElLee, and Olga, I have learning everything I know about zooplankton taxonomy from you. Thank you for all the hours you've spent helping me. For making my life easier

whenever you could, Loren, Kathy, Tor, Dave, Michelle, Taylor, Shannon, and Mikelle, you are the real MVPs in my book.

To all my fellow graduate students!! We are trauma bonded forever and there aren't words to describe how essential you have been in my graduate experience. Thank you to my amazing lab mates Anna, Sasha, Robert, and Haila for always popping in to talk about life or research and showing up to my 3-hour long practice talks. Thank you to my friends and cohort members Rita, Natalie, Evan, Zinka, Laura C., Laura M., Erin, Jade, and Susan. Second Thursdays are some of my fondest graduate school memories. I have pulled so much inspiration and motivation from all of you and I am so proud of what we have and will accomplish.

I have loved mentoring several undergraduate students who have worked alongside me and helped advance our research over the years. Thank you to Ricky, Dina, and Benny for bringing joy and energy into the lab and helping me figure out how to be a good mentor. Thank you to the UW CICOES program for funding their summer internships.

Thank you to my funders over the years: NSF, NOAA's Margaret A. Davidson Graduate Fellowship, Washington Ocean Acidification Center, and the Beatrice Crosby Booth Endowed Fellowship.

Thank you to my family, Mom, Dad, and Kate. I was raised in a household that valued education and curiosity above all else. Every morning as he left for work my dad would shout "Ask good questions!!" Safe to say I took that a little too far. You have supported me through every twist and turn of my life and I would never have made it to this point without you.

And last, but certainly not least, I would not have wanted to do any of this without the love and constant support of my fiancé and partner in all things Robby. I'm thrilled that on our first date, learning I was zero years into a six-year program didn't scare you away. Thank you for helping me code, run lab experiments, shuttle equipment around, and remember to do the one thing I hate most in life, drink water. You have been my ultimate hype man these last six years, and I will spend the rest of my life trying to repay the favor.

Dedication

To Robby.

Sorry I never listed you as a co-author on anything, but hopefully this makes up for it. I couldn't have done any of this without you. Thank you.

Introduction

Fossil fuel combustion, deforestation, and changes in agricultural practices are altering the chemistry of the oceans on a global scale (Doney 2010, IPCC 2021). Increases in atmospheric carbon dioxide drive the acidification, warming, and deoxygenation of the oceans. The oceans have absorbed approximately one third of anthropogenic carbon dioxide emissions, altering the carbonate chemistry and increasing the acidity of seawater. Additionally, increases in water temperature decrease the carrying capacity of dissolved oxygen while stratifying the water column, inhibiting the ventilation of oxygen-depleted waters (Isensee et al. 2016). Coastal systems are especially subject to chemical stresses, such as hypoxia (oxygen concentration less than 2 mg L^{-1}) and acidification (Breitburg et al. 2018). Coastal environments also increasingly experience severe pulse events such as heat shock, desiccation, and increased turbidity (Orth et al. 2006).

Environmental stressors are known to affect a wide range of marine species, including fish and zooplankton. An important group of organisms impacted by environmental stressors is copepods—crustaceous zooplankton that are ubiquitous in the world's oceans and play major roles in marine food webs and biogeochemical cycling (Verity & Smetacek 1996). Hypoxia results in increased mortality rates for many species of copepods. While there is variation in mortality among species, many copepods have a steep mortality threshold around 1 mg O2 L^{-1} (Auel & Verheye 2007, Grodzins et al. 2016). Adult copepods are thought to be robust to moderate decreases in pH (Mayor et al. 2012, Weydmann et al. 2012). However, there is increasing evidence that mortality rates vary across life stages, with nauplii showing the strongest lethal responses to decreased pH (Cripps et al. 2014).

In addition to lethal responses, sub-lethal responses to hypoxia and acidification, such as behavioral avoidance and changes in swimming speed, are also known to affect zooplankton populations. Zooplankton exhibit a range of swimming behaviors to reposition themselves in the water column, feed, find mates, and avoid predation (Van Duren & Videler 1996). An important behavior for many species is diel vertical migration (DVM), in which animals most commonly swim downwards during the day into darker water to avoid visual predation, and upwards at night to feed on phytoplankton near the surface (Frost 1988). The ability of copepods to perform DVM determines vertical population distributions and plays an important role in predator-prey interactions. Changes in swimming speed also affect trophic interactions because predator-prey encounter rates typically increase with speed (Frost 1972; Visser 2007). Because sub-lethal stress responses have individual, population, and community level implications, changes in swimming behavior are informative metrics for understanding ecosystem impacts of environmental change.

Species-specific responses to environmental stressors often alter zooplankton community composition and spatial distributions. In general, decreased DO results in lower copepod abundances and shifts the community composition toward smaller species (Roman et al. 1993, Uye 1994, Elliot et al. 2012, Roman et al. 2019, Keister et al. 2020). Hypoxia also affects species composition by altering mortality, growth, and reproduction differently between species. It is thought that smaller species of copepods fare better in hypoxic environments because they have a larger surface area to volume ratio, and therefore have more efficient gas exchange (Stalder & Marcus 1997, Pörtner 2010, Roman et al. 2019). In situ measurements of copepod distributions have shown that when stressful bottom waters are present, the distribution of copepod populations shifts upwards. In Chesapeake Bay, the Gulf of Mexico, and the intermediate oxygen minimum layer in the northern Benguela Current upwelling region, copepod abundances were

lower within hypoxic water, with distributions shifting upwards in the water column (Keister et al. 2000, Auel & Verheye 2007, Roman et al. 2012).

Due to their trophic linkages, changes in the distribution and abundance of deep-water, pelagic zooplankton communities likely affect nearshore systems. Throughout my dissertation, I will refer to deeper stations within the Salish Sea but away from its coastline as "deep-water" and the zooplankton associated with these waters as pelagic species. Additionally, I will refer to the shallow subtidal and intertidal waters as "nearshore" and the organisms typically associated with these waters as epibenthic or benthic. Nearshore environments, such as eelgrass beds, are known to be important habitats, providing food and protection for juvenile fish and many other marine species (Thayer et al. 1975, Adams 1976). Nearshore eelgrasses are connected to neighboring deep-water environments through tides. Daily tides, which transport pelagic zooplankton over the eelgrasses, may offer a significant feeding opportunity for small fish within the beds.

Puget Sound, a deep, glacially carved fjord connected to the Pacific Ocean by the Strait of Juan de Fuca, provides a useful study site to measure the effects of environmental stress on zooplankton. Puget Sound is home to many ecologically important species of mammals, fish, birds, and invertebrates which are vital in supporting local fisheries and coastal economies. The four basins of Puget Sound (Whidbey Basin, Main Basin, South Sound, and Hood Canal) vary in circulation patterns, deep water residence times, and flushing, resulting in a range of environmental conditions experienced between the basins (Babson et al. 2006). Whidbey Basin, Main Basin, and South Sound typically do not experience episodes of hypoxia and acidification, whereas Hood Canal regularly experiences both. The duration and extent of hypoxia varies annually, but parts of southern Hood Canal can be hypoxic for 2-6 months of the year (Newton et

al. 2007). In the summertime, the deep waters of Hood Canal are also highly acidic with pH values ranging from 7.3 to 7.8, and pH less than 7.4 reaching as shallow as 50 m (Feely et al. 2010). Puget Sound is a variable and important ecosystem and understanding the impacts of environmental stress on the system is a priority for both the scientific community and coastal managers.

The overarching question of this dissertation work is: How do environmental changes affect coastal zooplankton populations and the higher trophic levels that rely on them? I will approach this question using a tiered framework, with chapters of my dissertation moving through levels of ecological organization from individual to population, community, and ecosystem level responses. In Chapter 1, I conducted laboratory experiments to investigate whether zooplankton show behavioral responses to chemical stressors, and whether these responses lead to changes in vertical population distributions. In Chapter 2, I used a remote camera system to quantify *in situ* behavioral responses of zooplankton to stressors, using results from Chapter 1 to generate hypotheses about observations in the field. Finally, in Chapter 3, I investigated the transport of pelagic species into eelgrass beds and the role of eelgrass beds as potential sinks of pelagic zooplankton over the tidal cycle, potentially due to predation by juvenile fish.

In each chapter of my dissertation, I attempt to identify the mechanistic drivers behind observed responses to environment change, whether that be individual behavioral responses, changes in regional community compositions, or tidally influenced interactions between neighboring environments. To better understand and characterize these mechanisms, new approaches to monitoring coastal ecosystems are required. An additional outcome of my dissertation work includes the development of tools and methodologies that facilitate an

improved understanding of the critical role zooplankton play in supporting coastal ecosystems and the resources they provide.

Literature Cited

Adams, S. M. (1976). The ecology of eelgrass, Zostera marina (L.), fish communities. II. Functional analysis. Journal of Experimental Marine Biology and Ecology, 22(3), 293–311. https://doi.org/10.1016/0022-0981(76)90008-3

Auel, H., & Verheye, H. M. (2007). Hypoxia tolerance in the copepod *Calanoides carinatus* and the effect of an intermediate oxygen minimum layer on copepod vertical distribution in the northern Benguela Current upwelling system and the Angola-Benguela Front. Journal of Experimental Marine Biology and Ecology, 352(1), 234–243. https://doi.org/10.1016/j.jembe.2007.07.020

Babson, A. L., Kawase, M., & MacCready, P. (2006). Seasonal and interannual variability in the circulation of Puget Sound, Washington: A box model study. Atmosphere - Ocean, 44(1), 29–45. https://doi.org/10.3137/ao.440103

Breitburg, D., Levin, L. A., Oschlies, A., Grégoire, M., Chavez, F. P., Conley, D. J., Garçon, V., Gilbert, D., Gutiérrez, D., Isensee, K., Jacinto, G. S., Limburg, K. E., Montes, I., Naqvi, S. W. A., Pitcher, G. C., Rabalais, N. N., Roman, M. R., Rose, K. A., Seibel, B. A., Zhang, J. (2018). Declining oxygen in the global ocean and coastal waters. Science, 359(6371). https://doi.org/10.1126/science.aam7240

Cripps, G., Lindeque, P., & Flynn, K. J. (2014). Have we been underestimating the effects of ocean acidification in zooplankton? Global Change Biology, 20(11), 3377–3385. https://doi.org/10.1111/gcb.12582

Doney, S. C. (2010). The growing human footprint on the planet. Science, 328(10058), 1512–1516. https://doi.org/10.1126/science.1185198

Elliott, D. T., Pierson, J. J., & Roman, M. R. (2012). Relationship between environmental conditions and zooplankton community structure during summer hypoxia in the northern Gulf of Mexico. Journal of Plankton Research, 34(7), 602–613. https://doi.org/10.1093/plankt/fbs029

Feely, R. A., Alin, S. R., Newton, J., Sabine, C. L., Warner, M., Devol, A., Krembs, C., & Maloy, C. (2010). The combined effects of ocean acidification, mixing, and respiration on pH and carbonate saturation in an urbanized estuary. Estuarine, Coastal and Shelf Science, 88(4), 442–449. https://doi.org/10.1016/j.ecss.2010.05.004

Frost, B. W. (1972). Effects of size and concentration of food particles on the feeding behavior of the marine planktonic copepod Calanus pacificus. Limnology and Oceanography, 17(6), 805–815.

Frost, B. W. (1988). Variability and possible adaptive significance of diel vertical migration in Calanus pacificus, a planktonic marine copepod. Bulletin of Marine Science, 43(3), 675–694.

Grodzins, M. A., Ruz, P. M., & Keister, J. E. (2016). Effects of oxygen depletion on field distributions and laboratory survival of the marine copepod Calanus pacificus. Journal of Plankton Research, 38, 1412–1419. https://doi.org/10.1093/plankt/fbw063

Isensee, K., Levin, L. A., Breitburg, D., Gregoire, M., Veronique, Garcon., & Valdes, L. (2016). The Ocean is Losing its Breath. Ocean and Climate Scientific Notes, ed 2, 20–31. www.ocean-climate.org

Keister, J. E., Houde, E. D., & Breitburg, D. L. (2000). Effects of bottom-layer hypoxia on abundances and depth distributions of organisms in Patuxent River, Chesapeake Bay. Marine Ecology Progress Series, 205, 43–59.

Keister, J. E., Winans, A. K., & Herrmann, B. E. L. (2020). Zooplankton community response to seasonal hypoxia: A test of three hypotheses. Diversity, 12(1). https://doi.org/10.3390/d12010021

Mayor, D. J., Everett, N. R., & Cook, K. B. (2012). End of century ocean warming and acidification effects on reproductive success in a temperate marine copepod. Journal of Plankton Research, 34(3), 258–262. https://doi.org/10.1093/plankt/fbr107

Newton J, Bassin C, Devol A, Kawase M, Ruef W, Warner M, Hannafious D, Rose R (2007) Hypoxia in Hood Canal: An overview of status and contributing factors.

Orth, R. J., Carruthers, T. J. B., Dennison, W. C., Duarte, C. M., Fourqurean, J. W., Heck, K. L., Hughes, A. R., Kendrick, G. A., Kenworthy, W. J., Olyarnik, S., Short, F. T., Waycott, M., & Williams, S. L. (2006). A global crisis for seagrass ecosystems. BioScience, 56(12), 987–996. https://doi.org/10.1641/0006-3568(2006)56[987:AGCFSE]2.0.CO;2

Pörtner H (2010) Oxygen- and capacity-limitation of thermal tolerance: a matrix for integrating climate-related stressor effects in marine ecosystems. J Exp Biol 213:881–893.

Roman, M. R., Brandt, S. B., Houde, E. D., & Pierson, J. J. (2019). Interactive effects of Hypoxia and temperature on coastal pelagic zooplankton and fish. Frontiers in Marine Science, 6(MAR), 1–18. https://doi.org/10.3389/fmars.2019.00139

Roman, M. R., Gauzens, A. L., Rhinehart, W. K., & White, J. R. (1993). Effects of low oxygen waters on Chesapeake Bay zooplankton. Limnology and Oceanography, 38(8), 1603–1614. https://doi.org/10.4319/lo.1993.38.8.1603

Roman, M. R., Pierson, J. J., Kimmel, D., & Boicourt, W. C. (2012). Impacts of Hypoxia on Zooplankton Spatial Distributions in the Northern Gulf of Mexico. Estuaries and Coasts, 35, 1261–1269. https://doi.org/10.1007/s12237-012-9531-x

Stalder, L. C., & Marcus, N. H. (1997). Zooplankton responses to hypoxia: behavioral patterns and survival of three species of calanoid copepods. Marine Biology, 127, 599–607.

Thayer, G. W., Wolfe, D. A., & Williams, R. B. (1975). The impact of man of seagrass systems. American Scientist, 63(3), 288–296. https://doi.org/10.1007/BF01060519

Uye, S. (1994). Replacement of large copepods by small ones with eutrophication of embayments: cause and consequence. Hydrobiologia, 292–293(1), 513–519. https://doi.org/10.1007/BF00229979

Van Duren, L. A., & Videler, J. J. (1996). The trade-off between feeding, mate seeking and predator avoidance in copepods: Behavioural responses to chemical cues. Journal of Plankton Research, 18(5), 805–818. https://doi.org/10.1093/plankt/18.5.805

Verity, P. G., & Smetacek, V. (1996). Organism life cycles, predation, and the structure of marine pelagic ecosystems. Marine Ecology Progress Series, 130(1–3), 277–293. https://doi.org/10.3354/meps130277

Visser, A. W. (2007). Motility of zooplankton: Fitness, foraging and predation. Journal of Plankton Research, 29(5), 447–461. https://doi.org/10.1093/plankt/fbm029

Weydmann, A., Søreide, J. E., Kwasniewski, S., & Widdicombe, S. (2012). Influence of CO 2-induced acidification on the reproduction of a key Arctic copepod Calanus glacialis. Journal of Experimental Marine Biology and Ecology, 428, 39–42. https://doi.org/10.1016/j.jembe.2012.06.002

Chapter 1: Effects of hypoxia and acidification on *Calanus pacificus*: behavioral changes in response to stressful environments

This manuscript was previously published as: Wyeth, A.C., Grünbaum D., Keister J.E. (2022). Effects of hypoxia and acidification on *Calanus pacificus*: behavioral changes in response to stressful environments. Marine Ecology Progress Series, 697: 15-29. https://doi.org/10.3354/meps14142.

Abstract

Copepods, which play major roles in marine food webs and biogeochemical cycling, frequently undergo diel vertical migration (DVM) swimming downwards during the day to avoid visual predation and upwards at night to feed. Natural water columns that are stratified with chemical stressors, such as hypoxia and acidification, at depth are increasing with climate change. Understanding behavioral responses of copepods to these stresses—in particular, whether copepods alter their natural migration—is important to anticipating impacts of climate change on marine ecosystems. We conducted laboratory experiments using stratified water columns to measure the effects of bottom water hypoxia and pH on mortality, distribution, and swimming behaviors of the calanoid copepod, *Calanus pacificus*. When exposed to hypoxic (0.65 mg O_2 L^{-1}) bottom waters, the height of *C. pacificus* from the bottom increased 20% within hypoxic columns, swimming speed decreased 46% at the bottom of hypoxic columns and increased 12% above hypoxic waters. When exposed to low pH (7.48) bottom waters, swimming speeds decreased by 8 and 9% at the base of the tanks and above acidic waters, respectively. Additionally, we found a 118% increase in "moribund" (immobile on the bottom) copepods when exposed to hypoxic, but not to acidic, bottom waters. Some swimming statistics differed

between copepods collected from sites with versus without historical hypoxia and acidity. Observed responses suggest potential mechanisms underlying *in situ* changes in copepod population distributions when exposed to chemical stressors at depth.

1. Introduction

Hypoxia (oxygen concentration less than 2 mg L^{-1}) and acidification are two chemical stressors that are increasing in duration and extent in many coastal waters. Hypoxia and acidification can occur in productive coastal systems when excess organic matter sinks from the surface and is respired at depth, drawing down O_2 and releasing CO_2 (Melzner et al. 2013, Isensee et al. 2016, Breitburg et al. 2018, Doney 2019). Stratification of the water column due to differences in temperature and salinity limits mixing of oxygen-poor, more acidic bottom waters with surface waters, leading to stressful conditions that commonly occur at depth (Breitburg et al. 2018). Hypoxia and acidification within deep coastal waters can also be caused by seasonal upwelling of cold, dense, O_2-poor, and CO_2-rich waters (Feely et al. 2010). Hypoxia and acidification have historically occurred in areas with high productivity and poor flushing, but can be exacerbated by anthropogenic-influenced processes such as development of coastal areas and increased nutrient runoff, as well as by increased atmospheric CO_2 and warmer surface waters (Doney 2010).

Changes in bottom water chemistry are known to impact a range of marine species, including fish and zooplankton (Wu 2002). An important group of organisms impacted by changing bottom waters are copepods—crustaceous zooplankton that are ubiquitous in the world's oceans and play major roles in marine food webs and biogeochemical cycling (Verity & Smetacek 1996). Hypoxia results in increased mortality rates for many species of copepods.

Previous experiments have tested the mortality thresholds across a range of species and, while there is variation among species, many copepods have a steep mortality threshold around 1 mg O_2 L^{-1} (Auel & Verheye 2007, Grodzins et al. 2016). Adult copepods are thought to be fairly robust to moderate decreases in pH (Mayor et al. 2012, Weydmann et al. 2012). However, there is increasing evidence that mortality rates vary across life stages, with nauplii showing the largest lethal responses to decreased pH (Cripps et al. 2014). Adult copepods may exhibit sublethal responses to low pH, such as adverse effects on reproduction (Fitzer et al. 2012, Cripps et al. 2014).

Copepods exhibit a range of swimming behaviors to reposition themselves in the water column, feed, find mates, and avoid predation (Van Duren & Videler 1996). An important behavior for many species is diel vertical migration (DVM), in which animals most commonly swim downwards during the day into darker water to avoid visual predation, and upwards at night to feed on phytoplankton near the surface (Frost 1988). The ability of copepods to perform DVM determines vertical population distributions and plays an important role in predator-prey interactions. However, in areas with stressful bottom waters, DVM can increase exposure to stressful conditions, imposing a tradeoff between predation risk at the surface and adverse effects of chemical stress at depth.

In situ measurements of copepod distributions have shown that when bottom waters are stressful, the distributions of copepod populations often shift upwards. In Chesapeake Bay, the Gulf of Mexico, and the intermediate oxygen minimum layer in the northern Benguela Current upwelling region, copepod abundances are lower within hypoxic water, with distributions shifting upwards (Keister et al. 2000, Auel & Verheye 2007, Roman et al. 2012). Two potential mechanisms that could cause an upward shift in population distributions are increased mortality

within stressful bottom waters, leading to an apparent upward shift, and behavioral avoidance of stressful layers, leading to upward movement of individual animals. The extent to which copepods modify their swimming behaviors to avoid stressful bottom waters is largely unknown.

Sub-lethal responses to chemical stress, such as behavioral avoidance, vary among stressors, species, and populations. In one of the few laboratory studies quantifying behavior, the copepod, *Calanus euxinus*, spent more time swimming as oxygen concentrations declined from 10 to 0.5 mg L^{-1}, potentially to avoid sinking into anoxic bottom waters. (Svetlichny et al. 2000). In pH-stratified experimental water columns, larval sand dollars reversed the direction and shape of their swimming trajectory upon encountering the boundary between ambient and acidic water (Maboloc et al. 2020). Historical exposure to chemical stressors can also result in different behavioral responses between populations of the same species, through local adaptation or behavioral plasticity. Individuals from the copepod species *Acartia tonsa* avoided artificial hypoxic bottom waters when they were collected from an area that experiences hypoxia, but did not when they were collected from a non-hypoxic area (Decker et al. 2003). Behavioral avoidance has the potential to shift copepod distributions, but more work is needed to quantify its importance under changing chemical conditions.

The goals of this study were to assess the relative impacts of mortality versus behavioral avoidance in shaping vertical distributions of copepods when exposed to laboratory analogs of habitats with chemically stressful bottom waters. Puget Sound, a deep, glacially carved fjord connected to the Pacific Ocean by the Strait of Juan de Fuca, provides a useful region in which to measure effects of chemical stressors on copepods. The four basins of Puget Sound (Whidbey Basin, Main Basin, South Sound, and Hood Canal) vary in circulation patterns, deep water residence times, and flushing, resulting in different chemical conditions across the basins.

Whidbey Basin, Main Basin, and South Sound typically do not experience episodes of hypoxia and acidification, whereas Hood Canal regularly experiences both. The duration and extent of hypoxia varies annually, but parts of southern Hood Canal can be hypoxic for 2-6 months of the year (Newton et al. 2014). In the summertime, the deep waters of Hood Canal are also highly acidic, with pH values ranging from 7.3 to 7.8, and pH less than 7.4 reaching as shallow as 50 m (Feely et al. 2010).

We hypothesized that, when exposed to stressful bottom waters, copepods would change their behavior in one or both of two ways: 1) avoid the stressful bottom waters; or 2) descend into the stressful waters, and over time show increased mortality or increasing signs of sub-lethal stress such as changes in swimming speed. We hypothesized that copepods collected from areas that regularly experience hypoxia and acidification (such as Hood Canal) would experience lower rates of mortality and larger sub-lethal stress responses. Without a practical means of observing copepod behaviors in the field, we tested these hypotheses using a laboratory study that aimed to replicate some aspects of naturally occurring behaviors. We chose the calanoid copepod *C. pacificus* as our study organism because the species is ubiquitous in the Northeast Pacific and is an important food source for higher trophic levels due to their size and large lipid reserves. We designed laboratory experiments to quantify behavioral responses of *C. pacificus* collected from different basins of Puget Sound to bottom water hypoxia and acidification levels relevant to many coastal estuaries.

2. Methods

2.1 Organism Collection and Handling

Calanus pacificus were collected from within Puget Sound, Washington, USA between June and October of 2019 and 2020 (Table S.1). Collection sites (Figure 1) were chosen for their differences in chemical histories.

Samples were collected using either a 60-cm diameter, 200-μm mesh ring net with a non-filtering codend or a 60-cm diameter, 335-μm mesh bongo net with non-filtering codends, lifted vertically from 10 m off the seafloor. Samples were stored in a cooler and air-bubbled for <24 hours until actively–swimming adult female *C. pacificus* were manually sorted under a microscope into 1-L jars filled with 200-μm filtered seawater. 20 females were sorted into each jar. A single sex was used to exclude mate-seeking behaviors (Van Duren & Videler 1996). Copepods were kept at 14°C and fed a premade mixture of five marine microalgae (*Isochrysis, Pavlova, Tetraselmis, Thalassiosira weissflogii and Thalassiosira pseudonana*) daily, for no more than two weeks until they were used in a single laboratory experiment. *C. pacificus* continued to produce fecal pellets and had visibly full guts throughout the culture period, indicating they were feeding.

2.2 Laboratory Experiments/Experimental Design

C. pacificus behaviors and vertical distributions in response to either hypoxic or acidic bottom waters were observed in an array of four replicate 0.1 x 0.1 x 1-m acrylic tanks, installed in an environmental chamber set to 14°C (Figure 2). Stressful water layers (or non-stressful controls) were placed at the bottoms of salinity-stratified tanks, modeled after conditions experienced in the field. In preliminary daytime trial runs, we observed that *C. pacificus* consistently swam downwards when introduced to the top of experimental tanks, confirming that they continue behaviors consistent with natural DVM under these laboratory conditions. After

being added to the top of the tanks, the first copepods reached the bottom in 2-5 minutes. Because we manipulated only one chemical characteristic at a time, acidification experiments were conducted after hypoxia experiments, and therefore used *C. pacificus* collected later in the season.

Water treatments of two different salinities (29 and 31) were made using Instant Ocean (~36 g L^{-1} and ~39 g L^{-1}) and verified with a YSI Pro 2030 salinity probe. Replicate two-layer water columns with stable haloclines were created by pumping light (low salinity) water into the bottom of the tanks using a peristaltic pump until the water level was 500 mm from the bottom. Then, heavy (high salinity) water was pumped slowly to avoid mixing into the bottom, displacing the light water upwards until the water columns were 780 mm deep with the haloclines located 280 mm above the bottom.

In each set of experiments, two tanks were randomly selected to be treatment tanks and the other two were control tanks. In the two treatment tanks, the "treatment bottom water" was heavy artificial seawater (ASW) bubbled either with N_2 (hypoxia experiments) or CO_2 (acidification experiments) (see water chemistry section below). In the two control tanks, the "control bottom water" was heavy, non-bubbled ASW to control for potential behavioral responses to the change in salinity across the halocline. The "surface water" in all four tanks was light, non-bubbled ASW.

Before being added to the experimental array, 80 adult female *C. pacificus* were acclimated overnight in light ASW, identical to the surface water in the experimental tanks. To start each experiment, 20 animals were gently introduced to the top of each of the four tanks. Swimming behavior was then observed for 90 minutes using 5-megapixel IR USB cameras. Experiments were run during the day in the dark with the tanks backlit with IR LED strips

behind and around the base of each tank. Two front-facing cameras (the "Bottom Camera" and "Surface Camera") recorded swimming in the X (left, right) and Z (up, down) directions, observing true vertical motion and projected horizontal motion (see Section 2.4). An upwards-facing "Base Camera" was added to each tank in 2020 to improve tracking and behavioral analysis of copepods near the bottom. Base cameras recorded the bottom 2 cm of each tank in the X (left, right) and Y (front, back) directions, and therefore observed true horizontal motion but not vertical motion (Figure 2).

2.3 Water Chemistry

2.3.1 Hypoxia Experiments

To create the different oxygen conditions, bottom water was split into two buckets of equal volume to use in treatment and control tanks. Treatment bottom water was then bubbled with pure N_2 gas until dissolved oxygen was <0.2 mg L^{-1}, as measured by a PreSens oxygen dipping probe. Surface water and control bottom water were not bubbled, and were left at ambient oxygen concentrations (~10 mg L^{-1}). At the end of each experiment, oxygen was measured at the surface, upper halocline, lower halocline, and bottom of each tank by lowering the oxygen probe slowly through the water column so as not to disrupt the halocline.

2.3.2 Acidification Experiments

To manipulate pH conditions, bottom water was split into two buckets of equal volume to use in treatment and control tanks. Treatment bottom water was bubbled with CO_2 until it reached the desired pH. In the first 5 pH experiments, treatment bottom water was bubbled with 2000 ppm CO_2-air mixture for approximately 40 minutes. The final pH in this treatment was

approximately 7.6, as measured by a Star A221 pH meter with a Ross ultra gel pH/ATC electrode that was calibrated daily prior. In the last 5 experiments, treatment bottom water was made using a feedback-control system that supplied mixed lab air and pure CO_2 gas at 3000 ppm at 4.1 liters per minute through an airstone. pH was measured with a Sunburst AFT (assumed constant salinity of 31) during bubbling, to ensure a pH of 7.4 was maintained. The acidification method was altered halfway through experiments because 2000 ppm CO_2-air mixture refills became unavailable in 2020 due to supply chain shortages. At that time, the CO_2 concentration was also altered to more closely match conditions experienced in conjunction with hypoxia *in situ*. Control bottom water and surface water were not bubbled and were left at ambient CO_2 concentrations.

At the end of each experiment, pH was measured above the halocline by dipping the pH probe into the top of each tank to measure the pH of the light ASW. The pH of the bottom water was measured by filling scintillation vials from ports at the bottom of each tank, and measuring the pH of the water sample with the pH probe. Additionally, bottle samples were collected for laboratory analysis, first from the top port of one randomly selected control tank and one randomly selected treatment tank, then from the bottom port of all four tanks. Bottle samples were poisoned with mercuric chloride and stored for less than 6 months before analysis. Dissolved inorganic carbon (DIC) and alkalinity were measured from the bottle samples using a DIC VINDTA system with an electrochemical cell UIC Coulometer for DIC as well as a Dickson Total Alkalinity Titrator for alkalinity. Samples from all the experimental trials were run in random order over the course of 5 days. An internal standard was run at the beginning and end of each day to check for accuracy and drift throughout the day. A replicate DIC measurement was taken for every other sample. Only one alkalinity measurement was taken for

each sample. Three samples of laboratory seawater were analyzed each day to check instrument precision.

2.4 Video Processing and Movement Analysis

Videos were processed with the software Fosica (Wallingford Imaging, WA, USA) to distinguish moving copepods from stationary background and noise, and to extract copepod pixel coordinates. Pixel coordinates were converted into physical space units, and then assembled into individual swimming paths using the Matlab software package Tracker3D (Chan & Grünbaum 2010), neglecting parallax in the camera field of view (an example output is provided in Figure S.1). A smoothing spline was applied to remove features changing faster than 6 Hz, which were dominated by frame rate noise. X and Z (or, for the Base Cameras, X and Y) pixel coordinates for each object and the total projected speed and velocities were calculated at every frame for each swimming path. Swimming paths included only animals actively moving in the tank, excluding motionless (moribund) animals at the bottom of the tank.

Copepod swimming paths were used to calculate the mean height from the bottom of the tank, mean number of copepod localizations per frame, and mean swimming speeds. The Surface Camera and Bottom Camera recorded velocity in the X and Z directions, and therefore observed true vertical movement components (VS_{tr}) but only projected horizontal movement components (HS_{proj}), i.e., horizontal movement in the X-Z plane but not in the X-Y plane. We assumed anisotropic swimming (no preferred direction) in the horizontal direction, implying true horizontal speeds (HS_{tr}) were on average proportional to projected horizontal speeds (HS_{proj}). We calculated the constant of proportionality using Equation 1, where HS_{proj} is measured and HS_{tr} is inferred from the equation.

(1) $$HSproj = HStr \times (1/2\pi) \times \int_0^{2\pi} |cos(x)|dx = HStr \times (2/\pi)$$

Using the mean HS_{tr} and the measured mean VS_{tr}, we estimated the mean total speed (*TS*) using Equation 2.

(2) $$TS = \sqrt{(HStr)^2 + (VStr)^2}$$

Raw vertical and projected horizontal speeds are provided in Figures S.2 and S.3.

Base Cameras recorded speed in the X and Y directions, observing true horizontal speed (HS_{tr}), near the bottom of the tank. To ensure that copepod pixel coordinates were not double counted in both the Bottom Camera and the Base Cameras, we determined the height above the bottom in the Bottom Camera (Z direction) at which copepods came into view in the Base Cameras, which was 26 mm. Any copepod coordinates in the Bottom Camera below 26 mm were dropped from the analysis, so that those points were only stitched into swimming paths in the Base Camera analysis. The total copepod counts from the Surface, Bottom, and Base Cameras were calculated for a subset of frames and experiments to ensure that we were able to continually track individuals in each tank throughout the duration of the experiment.

Our video system could not distinguish between individuals that were dead and those that were lying immobilized on the bottom for extended periods (a behavior leading, at least in hypoxia, to a high likelihood of eventual mortality). Therefore, for 2020 experiments, we developed a video-based metric using the Base Cameras to classify copepods at the bottom of tanks that were "moribund." Remaining motionless on the bottom of the tank is an uncommon behavior for *C. pacificus*, and we conservatively estimated that copepods motionless for a two-minute threshold were in a "moribund" or stressed state. To quantify moribundity, we calculated the mean brightness values for each pixel from frames in each of the last 1-min sections (89th and 90th minutes). Because the videos were recorded in dark field with IR back-lighting, copepods

appeared as bright spots in the videos. The brightness of pixels representing a copepod in these 1-min means was a direct function of the number of frames in which it remained stationary. We then used a brightness threshold to classify copepods as moribund if pixel brightness indicated they had not moved during the last two minutes of video observations.

In both 2019 and 2020 hypoxia experiments, the positions of living copepods were visually counted above the halocline, below the halocline but above the base, and at the base of each tank at the end of the 90-minute runs. A visual count of the number of moribund animals on the bottom of each tank was made. No visual counts were done for the acidification experiments because we assessed the video metric to be as good as or better than visual counts during the hypoxia experiments.

2.5 Statistics

Metrics from the processed videos were analyzed to test hypotheses about distribution changes and behavioral responses of *C. pacificus* when exposed to stressful bottom waters. From preliminarily analysis, it was determined that copepod vertical position and behaviors approached a steady state within 30 minutes of being added to the experimental tanks. Therefore, to optimize processing time, only the first 30-minutes of video were analyzed. In 10 of the 23 experiments conducted in 2020, one of the four Base Cameras malfunctioned (for an equal number of experimental and control tanks across the 10 runs). In statistical analyses that required Base Camera video, those individual tanks were dropped. A single batch of zooplankton collected from South Sound in 2020, used in 3 hypoxia experiments, behaved differently from all other experimental replicates: this one batch of copepods did not swim downwards when added to the top of the experimental tanks, did not interact with the sub-halocline hypoxic water, and

therefore did not test our set of hypotheses. Those three experiments were dropped from all further analysis. The two bubbling methods used for making acidified water (premixed CO2/air and a feedback control system) differed in their final pH value. However, results from the two sets of experiments were not significantly different from each other, so they were pooled for all analyses. There was only one pH experiment using copepods collected from South Sound, so for pH experiments only, South Sound was dropped as a collection site in post-hoc statistical analysis due to the insufficient replication for that site. All statistics were generated using the software *R* (version 4.2.0).

2.5.1 Moribund Counts

To test for treatment effects on the video-based moribund counts from 2020, a 2-way ANOVA was performed to compare the effect of treatment, collection site, and a treatment*collection site interaction. Visual inspection of residual plots, Shapiro-Wilk, and Levene's test did not reveal any deviations from normality or homoscedasticity. Visual counts of moribund copepods from 2019 and 2020 were pooled. Visual counts did not meet the assumptions of normality or homoscedasticity, so a negative binomial regression was used to test for treatment and collection site effects using the *MASS* package (version 7.3-57) (Venables & Ripley 2002).

2.5.2 Mean Height

The mean height above the bottom of copepod swimming tracks was calculated over 5-minute intervals for the first 30 minutes of each experiment. Copepods observed by the Base Camera during this time interval were included in the mean height metric by assigning counts

from the Base Camera a height of 0 mm. To test for treatment effects on the mean height, mixed-effects models were generated using the *lme4* package (version 1.1-29) (Bates et al. 2015). Nested models were generated using different combinations of treatment, experimental time (linear and quadratic term) and copepod collection site as main effects. Experiment was included as a random effect to account for differences between copepod collections and batches. The best model was identified using AIC values (see Tables S.2 and S.3). A visual inspection of the Q-Q plots of model residuals and model residuals against the fitted values plots did not reveal any deviations from normality or homoscedasticity.

2.5.3 Swimming Speeds

Calculated mean total swimming speeds (*TS*) observed by the Surface Camera and Bottom Camera in 2019 and 2020 were pooled for analysis. True horizontal speed (HS_{tr}) at the bottom of the tanks was observed by the Base Cameras only in 2020. Mixed-effects models were generated using the *lme4* package in *R*. Nested models were generated using different combinations of treatment, experimental time (linear and quadratic term) and copepod collection site as main effects and experiment as a random effect. The best models were identified using AIC values (see tables S.4 - S.9). A visual inspection of residual plots did not reveal any deviations from normality or homoscedasticity.

2.5.4 Differences Among Collection Sites

Additional post-hoc analyses were used to evaluate the effect of collection site on total swimming speed (*TS*). A Tukey pairwise comparison of treatment and collection site was generated using the *emmeans* package in *R* (version 1.7.3) (Lenth 2021). To visualize the effect

of treatment among different collection sites, the mean *TS* from control tanks was subtracted from the mean *TS* from the treatment tanks, and a pooled standard error was calculated, for each collection site, time interval, and camera view combination.

3. Results

3.1 Water Chemistry

In the twenty hypoxia experiments conducted, mean dissolved oxygen (DO) concentration and standard error (SE) was 0.65 ± 0.03 mg L^{-1} in the treatment bottom water compared to 10.2 ± 0.04 mg L^{-1} in control bottom water (Table 1).

In the ten acidification experiments conducted, treatment bottom water made using premixed CO_2/air had a mean pH and SE of 7.58 ± 0.01 and treatment bottom water made using a feedback control system had a mean pH and SE of 7.39 ± 0.01. Control bottom water had a mean pH and SE of 8.06 ± 0.02 and 8.03 ± 0.03 during experiments using the premixed CO_2/air and feedback control system methods, respectively (Table 2).

3.2 Moribundity

The number of moribund animals was significantly higher in hypoxic tanks than in control tanks after 90 minutes, using both visual (NB reg; $p = 0.001$) (Figure 3a) and video (ANOVA; $F = 10.4$, $p = 0.003$) (Figure 3b) metrics. A 118% increase in moribund individuals was observed using the video-based metric.

The number of moribund animals was not significantly different between acidic tanks versus controls using the video-based metric (ANOVA; Treatment: $F = 0.088$, $p = 0.77$; Site: F =

0.703, p = 0.5). At the end of each experiment, a mean and SE of 3.4 ± 0.56 and 3.2 ± 0.39 moribund animals were counted in acidic and control tanks, respectively (Figure 3c).

3.3 Mean Height

Swimming animals were significantly higher in the water column in hypoxic tanks compared to control tanks (Figure 4a). Mixed effects model results indicated that treatment and time had significant effects on mean height (treatment: $p < 0.0001$, time: $p < 0.0001$, time^2: $p < 0.0001$). Over the full 30 minutes, the mean height and SE of animals in hypoxic tanks was 36 ± 8.7 mm higher in the water column than animals in control tanks, a 20% increase. In the last 5 minutes only (25-30 minutes), animals in hypoxic tanks were 59 ± 39.9 mm higher in the water column than animals in control tanks, a 25% increase. The mean position of copepods in hypoxic tanks during the last 5 minutes was only 10 mm below the estimated halocline (280 mm), whereas copepods in control tanks were 70 mm below. Including experiment as a random effect explained significant variability in the model.

There was no difference between the mean height of copepods in acidic versus control tanks. The mean height of copepods in each tank decreased with time (time: $p < 0.0001$, time^2: $p < 0.0001$). During the last 5 minutes (25-30 minutes), the mean height and SE of copepods was 84.6 ± 11.1 mm in control tanks and 93.0 ± 14.7 mm in acidic tanks, both well below the halocline height (Figure 4b).

3.4 Swimming Speed

Across all hypoxia experiments in 2019 and 2020, there was a general trend that animals exposed to hypoxic bottom waters swam slower in bottom and base waters but faster in surface

waters than animals in control tanks (Figure 5). Over the first 30 minutes of video, the mean horizontal speed (HS_{tr}) from copepod swimming paths at the base of the tanks (observed by Base Cameras during the 2020 experiments) varied with time and treatment (time: $p < 0.0001$, treatment: $p < 0.0001$, time^2: $p = 0.0004$). At the final time point the mean and SE true horizontal speed (HS_{tr}) was 0.04 ± 0.007 mm s^{-1} slower at the base of hypoxic tanks, a 58% decrease relative to copepods at the base of control tanks (Figure 5a). Within the bottom waters (observed by the Bottom Camera and not including the base of the tanks) in 2019 and 2020, there was an 8% decrease in the mean total swimming speeds (*TS*) from the first 30 minutes of video recorded in hypoxic tanks relative to controls, with a significant collection site effect (Figure 5b). Within the surface waters (observed by the Surface Camera), mean total swimming speed (*TS*) increased gradually with time ($p = 0.002$) and there was a significant interaction between treatment and collection site ($p = 0.0002$) (Figure 5c). Copepods in the surface water of hypoxic tanks showed a 12% increase in swimming speed, moving 0.60 ± 0.10 mm s^{-1} faster than copepods in control tanks ($p < 0.0001$). The copepod counts per frame for each camera view can be found in Figure S.4, which approximates the number of swimming paths included in the above speed statistics.

Overall, copepods exposed to acidic bottom waters swam slower in surface waters and at the base of tanks compared to copepods in control tanks, with some significant differences in the swimming speeds of copepods from different collection sites (Figure 6). At the base of the tanks, the mean horizontal speed (HS_{tr}) and SE was 0.006 ± 0.002 mm s^{-1} slower in acidic tanks than in control tanks, an 8% decrease, with speeds decreasing over time (time: $p < 0.0001$, treatment: $p = 0.007$) (Figure 6a). A majority of the total copepod counts were observed by the Base Cameras (see Figure S.5). Within the bottom water (but above the base), total swimming speed (*TS*) varied with time, with no significant difference between treatments (time: $p = 0.003$, time^2: $p = 0.002$)

(Figure 6b). Within surface waters, total swimming speed (*TS*) significantly varied with treatment (but not time) with a significant treatment by collection site interaction (treatment: $p = 0.0003$, treatment*site: $p = 0.02$) (Figure 6c).

3.5 Differences Among Collection Sites

Changes in swimming speed in both bottom and surface waters in response to hypoxia, and in surface waters in response to acidification, varied depending on collection site (Figure 7). In hypoxia experiments, mean total swimming speed (*TS*) within the bottom water was significantly slower in hypoxic tanks relative to controls for copepods collected from the Main Basin ($p = 0.008$) and South Sound ($p = 0.004$), but not from Hood Canal (Figure 7a). Mean total swimming speed (*TS*) within surface waters was significantly faster in hypoxic tanks relative to controls for copepods from Hood Canal ($p < 0.0001$) and to a lesser extent South Sound ($p = 0.054$) but not Main Basin (Figure 7b).

In acidification experiments, there were no differences in swimming speeds among copepods from different collection sites within the bottom waters (Figure 7c). However, in surface waters, the mean speed and SE of copepods from Hood Canal was 0.51 ± 0.14 mm s^{-1} slower in acidic tanks than in control tanks ($p = 0.002$), but copepods collected from Main Basin did not exhibit differences (Figure 7d).

Changes in moribundity, mean height, and swimming speed at the base of the tanks (observed by the Base Cameras) did not vary among collection sites in response to either hypoxia or acidification.

4. Discussion

Due to a combination of natural conditions, climate change, and increased development in coastal areas, the oceans are predicted to experience widespread oxygen deficiency and acidification by the end of the century (Doney 2010, Melzner et al. 2013, Breitburg et al. 2018). Our laboratory experiments demonstrated significant effects of bottom water hypoxia and acidification on behavioral avoidance, swimming statistics, and apparent mortality rates in the copepod, *Calanus pacificus* (summarized in Table 3). Copepods showed strong responses to hypoxia, and weaker but significant responses to acidification. When exposed to hypoxic (0.65 mg O_2 L^{-1}) bottom waters, *C. pacificus* were higher in the water column, exhibited slower swimming speeds within bottom waters, faster swimming speeds within non-stressful surface waters, and had higher apparent mortality rates relative to controls. When exposed to acidic (7.48 pH) bottom waters, *C. pacificus* swam slower but did not show changes in apparent mortality or vertical position. Interestingly, for a subset of our swimming speed measurements, we observed a significant effect of collection site on the magnitude of differences between treatment and control tanks. These may suggest an evolved or learned difference in response to historical presence or absence of chemical stressors between animals from different locations.

4.1 Changes in Moribundity

We interpret the moribundity metric to imply a high likelihood of impairment or impending mortality, because lying immobilized on the bottom of the tank is not a normal behavior for *C. pacificus*, and because oxygen levels of 0.65 mg L^{-1} have been shown to cause 100% mortality in *C. pacificus* within 60 minutes (Grodzins et al. 2016). Increased moribundity in our experiments suggests potential increases in mortality under analogous natural conditions,

which are increasingly encountered by copepods in eastern Pacific habitats. Oxygen conditions in our experiments resulted in 25% mortality after 90 minutes—a 118% increase relative to controls, but still low compared to Grodzins et al. (2016). A possible interpretation for the difference is that, in our experiments, a subset of *C. pacificus* periodically sought refuge in normoxic waters above the halocline. In the absence of avoidance, hypoxia experienced *in situ* in present-day Hood Canal and other coastal areas, is likely to result in even higher mortality than observed in our 90-minute experiments.

Consistent with previous findings that copepods are generally robust to the low pH conditions they encounter *in situ* (Mayor et al. 2012, Weydmann et al. 2012), we found no significant difference in moribundity between control and treatment tanks during acidification experiments. In many coastal and upwelling systems, where hypoxia and acidification occur in conjunction, our results imply that oxygen stress will have a larger impact on copepod mortality *in situ* relative to acidification. Overall moribundity was higher in acidification experiments, with an average of 1.2 more moribund copepods in the control tanks during acidification experiments than in control tanks during hypoxia experiments. However, we hypothesize that copepods collected later in the season for acidification experiments than for hypoxia experiments were in a different physiological state, possibly due to seasonal changes in food availability. We speculate that the later collection date may have resulted in marginally increased moribundity rates in both treatment and control tanks.

4.2 Changes in Depth Distributions

Our laboratory observations suggest that avoidance may be an important mechanism contributing to observed *in situ* shifts in copepod vertical distributions when stressful bottom

waters are present. A majority of copepods, whose normal downward swimming behavior would have kept them within quickly lethal concentrations of dissolved oxygen, survived the duration of the 90-minute experiment. Our interpretation is that individual copepods periodically sought refuge in normoxic surface waters. The upwards shift in vertical position in hypoxic tanks, the ongoing presence of swimming paths within lethally stressful bottom waters, and low moribundity together suggest that copepods attempted to continue their normal downward swimming, but when hypoxic bottom waters were present, periodically reversed that behavior to move above the hypoxic layer.

There are important differences between laboratory and field conditions to consider when translating results to the field. Notably for our experiments, downward migrations in the field occur over much larger water columns across broader chemical gradients (typically on the order of meters versus millimeters). As a result, copepods in the laboratory may be more likely to sense changes in water chemistry as they experience steeper gradients and more rapid changes with depth. This difference suggests tank experiments might overestimate some behavioral responses relative to *in situ* water columns. Conversely, swimming across broader natural gradients would provide more time for physiological effects to induce behavioral responses, such as up-swimming to escape stressful bottom layers, before full impacts of stressors become incapacitating. In that case, tank experiments might overestimate *in situ* behavioral responses. Despite the unclear implications of these limitations, recording copepod swimming paths in the laboratory yielded new insights into specific mechanisms leading to the apparent upwards shift in population distributions above stressful waters observed in many natural systems.

Interference with DVM into deep waters and a resultant congregation of copepods near the oxycline could have profound influences on predator-prey interactions. Hypoxic bottom

waters can compress available habitat and shift copepod distributions upwards (Pierson et al. 2009, Keister et al. 2000, Roman et at. 2012, Elliot et al. 2013, Keister & Tuttle, 2013). In Hood Canal, the oxycline separating oxygen-rich surface waters and hypoxic bottom waters can be as shallow as 15 m in a 120 m water column (ORCA 2022), apparently compressing available habitat by as much as 88%. Our laboratory results suggest that *in situ* congregations of copepods observed near the halocline could be due to copepods attempting their normal downward migration but periodically ascending to recover from exposure to hypoxic conditions (Ludsin et al. 2009, Zhang et al. 2009). Encounter rates and foraging efficiency of both visual and non-visual predators are likely to increase if copepods aggregate near the oxycline during the day (Craig, 2012), with commensurate increases in copepod mortality.

Suppression of downward migration may also impact carbon transport to depth. In shallower systems, such as hypoxic estuaries, a large percentage of the carbon flux to depth is the direct sinking of organic matter from the surface, which in summer, is primarily composed of fixed carbon associated with phytoplankton blooms (Baker et al. 1985, Turner 2002, Svensen et al. 2006). Zooplankton mediate the flux of fixed carbon through grazing on phytoplankton (Lorenzen et al. 1981). When bottom waters are not stressful, zooplankton may transport carbon into deeper waters during DVM. However, when downward migration is suppressed, fecal pellets produced in surface waters will likely be recycled through consumption and bacterial decomposition before sinking to the seafloor (Kiørboe 1997, Turner 2002). This shallow remineralization may act to retain nutrients in the surface waters, reducing the carbon flux to depth, acting as a negative feedback on hypoxia.

Finally, shallower migrations could increase population losses from estuaries and upwelling regions, where net transport of surface water is typically oceanward (Peterson et al.

1979, Falkenhaug et al. 1997, Giddings & MacCready 2017). In the absence of hypoxic bottom waters, migrating copepods spend part of the day in deeper waters where net flow is landward, acting to retain them in coastal environments (Hill 1991, Falkenhaug et al. 1997, Batchelder et al. 2002, Tommasi et al. 2013). The extent to which shallower copepods are advected offshore is location- and time-specific, mediated by bathymetry and local climatic and oceanographic conditions such as freshwater runoff, tidal currents, and wind patterns (Falkenhaug et al. 1997).

4.3 Changes in Swimming Speed

We observed significant changes in swimming speeds when *C. pacificus* were exposed to either hypoxic or acidic bottom waters. Copepods in hypoxic tanks swam slower below the halocline and faster above the halocline relative to controls. We hypothesize that this observed change in swimming speed indicates a behavioral avoidance mechanism used to regulate and ultimately survive exposure to hypoxic bottom waters. A reduction in swimming speed within the hypoxic bottom layer could prolong the time copepods can tolerate metabolic stress. Conversely, an increase in swimming speed may reflect behavior used to swim out of the stressful layer. In acidification experiments, copepods in tanks with acidic bottom waters swam significantly slower than those in control tanks both at the base of the tanks (observed by the Base Cameras) and above the halocline (observed by the Surface Camera). To our knowledge this laboratory study is the first to report a significant behavioral response of a calanoid copepod to changes in pH, potentially indicating a sub-lethal stress response to acidic waters that may be observable in the field.

While potentially important in avoiding chemical stress, significant increases in swimming speed increase copepods' metabolic demands. The total metabolism of *C. euxinus* is

2-4 times higher at maximal locomotion compared to basal metabolism (Svetlichny et al. 2000). An organism's metabolism is also influenced by environmental variables such as temperature and dissolved oxygen. While temperature was constant in our experimental tanks, temperatures *in situ* are typically warmer in surface waters, exacerbating the metabolic costs of increased swimming above the halocline (Roman et al. 2019, Svetlichny et al. 2000). However, the potential for increased feeding on phytoplankton near the surface may be able to offset some of the increased metabolic costs associated with exposure to chemical stress.

Changes in swimming speed also affect trophic interactions by directly influencing encounter rates between predators and prey (Visser 2007). Many calanoid copepods are cruise feeders, using their mouth appendages to propel them through the water while also bringing food particles towards them (Van Duen & Videler 1996). The encounter rate of cruise feeders is determined by prey density and swimming speed, with encounter rates increasing with speed (Frost 1972). Additionally, rheotactic predators that consume copepods detect their prey through fluid signals, making faster swimming prey easier to detect (Kiørboe et al. 2014). We hypothesize that stress-induced increases in swimming speed will increase predation on copepods, because of increased encounters and increased detection by rheotactic predators (Lima & Dill 1990, Visser 2007).

With hypoxia and acidification typically occurring in conjunction in natural systems, it will be important to understand how encountering the two stressors simultaneously may affect swimming speed. Tomasetti et al. (2018) observed additive negative effects of low pH combined with moderately low DO on larval crustacean survival. In both our hypoxia and acidification experiments, *C. pacificus* showed significant changes in swimming speed above the halocline, but the direction and magnitude of change differed. In addition, *in situ* surface waters are

typically warmer than deep waters, which may further impact copepod responses to stressful bottom waters. Although constraints on our experimental design prevented us from assessing interactions, understanding co-occurring stressor effects on swimming speed is a priority for future research.

4.4 Differences among Collection Sites – Evidence for Local Adaptation?

In our experiments, copepods from Hood Canal (which regularly experiences both hypoxia and acidification) showed significantly different responses in swimming speed to both hypoxia and pH compared to copepods from Main Basin (and South Sound, during hypoxia experiments). Copepods from the different sub-basins of Puget Sound are genetically distinct and differ in population structuring across basin-wide spatial scales (Nuwer 2008). We hypothesize that these behavioral differences reflect local adaptation of a subpopulation of *C. pacificus* from Hood Canal, driven by the site's historical chemical conditions.

Localized, potentially adaptive behavioral variations have been previously observed in copepods. *Acartia tonsa* from areas historically exposed to low oxygen move vertically to avoid hypoxic bottom waters, while *A. tonsa* from high oxygen areas do not (Decker et al. 2003). Similarly, respiration rates after exposure to elevated pCO_2 differ between populations of *Pseudocalanus acuspes* from areas differing in natural fluctuations of pCO_2 (Thor & Oliva 2015).

The specific mechanisms enabling local adaptation could include physiological adaptations such as enhanced ventilatory capability, large surfaces, short diffusion distances, and respiratory proteins with high oxygen affinity (Childress & Seibel 1998)–or behavioral adaptations in responses to a sensory input (Dam 2013). In our experiments, increased swimming

speeds above hypoxic waters, paired with maintained swimming speeds within hypoxic waters may reflect adaptive behavior in a subpopulation of copepods to escape lethal bottom waters common in Hood Canal. If so, local adaptation merits further study as a potential indicator of long-term resilience of copepods to increasing chemical stress.

4.5 Conclusions

With coastal systems continuing to change, our observations in stratified laboratory water columns are important for understanding ecosystems currently stressed by hypoxia and acidification, and for predicting future ecosystem responses. Our experimental results indicated changes in depth and swimming speed when exposed to hypoxic bottom waters, and in swimming speed when exposed to acidic bottom waters. These sublethal effects have implications for the distribution and abundance of copepods, predator-prey interactions, and biogeochemical cycling. These behavioral changes may have contributed to observed mortality estimates, which were much lower than expected under prolonged exposure to hypoxia. Sub-lethal effects of hypoxic and especially acidic conditions on copepods are only just starting to be explored in the literature. With advances in ocean technology and the improving ability to observe individual organisms in the field, our results suggest metrics for *in situ* swimming characteristics, such as changes in swimming speed, that could prove a useful tool for monitoring ecosystems impacted by climate and anthropogenic changes.

Acknowledgements

The authors gratefully acknowledge Alex Gagnon, Dan Anderson, and Amy Larson for assistance with experimental design and lab techniques regarding carbonate chemistry protocols,

Dan Anderson for processing DIC and alkalinity samples, Rick Wright for assistance constructing the experimental array, Anna McLaskey and Sasha Seroy for statistical advice, Brian Bare for organism collection, Kathy Newell for assistance with experimental set-up, Robert Levine for programming guidance, and three anonymous reviewers for providing helpful feedback. This work was funded by NSF Grant OCE-1657992 to J. Keister and the Beatrice Crosby Booth Endowed Scholarship.

Literature Cited

Auel H, Verheye HM (2007) Hypoxia tolerance in the copepod *Calanoides carinatus* and the effect of an intermediate oxygen minimum layer on copepod vertical distribution in the northern Benguela Current upwelling system and the Angola-Benguela Front. J Exp Mar Bio Ecol 352:234–243.

Baker ET, Feely RA, Landry MR, Lamb M (1985) Temporal variations in the concentration and settling flux of carbon and phytoplankton pigments in a deep fjordlike estuary. Estuar Coast Shelf Sci 21:859–877.

Batchelder HP, Edwards CA, Powell TM (2002) Individual-based models of copepod populations in coastal upwelling regions: Implications of physiologically and environmentally influenced diel vertical migration on demographic success and nearshore retention. Prog Oceanogr 53:307–333.

Bates D, Mächler M, Bolker B, Walker S (2015) Fitting Linear Mixed-Effects Models Using lem4. J Stat Softw 67:1–48.

Breitburg D, Levin LA, Oschlies A, Grégoire M, Chavez FP, Conley DJ, Garçon V, Gilbert D, Gutiérrez D, Isensee K, Jacinto GS, Limburg KE, Montes I, Naqvi SWA, Pitcher GC,

Rabalais NN, Roman MR, Rose KA, Seibel BA, Telszewski M, Yasuhara M, Zhang J (2018) Declining oxygen in the global ocean and coastal waters. Science 359:1-11.

Chan KYK, Grunbaum D (2010) Temperature and diet modified swimming behaviors of larval sand dollars. Mar Ecol Prog Ser 415:49–59.

Childress JJ, Seibel BA (1998) Life at stable low oxygen levels: Adaptation of animals to oceanic oxygen minimum layers. J Exp Biol 201:1223–1232.

Craig JK (2012) Aggregation on the edge: Effects of hypoxia avoidance on the spatial distribution of brown shrimp and demersal fishes in the Northern Gulf of Mexico. Mar Ecol Prog Ser 445:75–95.

Cripps G, Lindeque P, Flynn KJ (2014) Have we been underestimating the effects of ocean acidification in zooplankton? Glob Chang Biol 20:3377–3385.

Dam HG (2013) Evolutionary adaptation of marine zooplankton to global change. Ann Rev Mar Sci 5:349–370.

Decker MB, Breitburg DL, Marcus NH (2003) Geographical differences in behavioral responses to hypoxia: Local adaptation to an anthropogenic stressor? Ecol Appl 13:1104–1109.

Doney SC (2010) The growing human footprint on the planet. Science 328:1512–1516.

Falkenhaug T, Tande K, Timonin A (1997) Spatio-temporal patterns in the copepod community in Malangen, Northern Norway. J Plankton Res 19:449–468.

Feely RA, Alin SR, Newton J, Sabine CL, Warner M, Devol A, Krembs C, Maloy C (2010) The combined effects of ocean acidification, mixing, and respiration on pH and carbonate saturation in an urbanized estuary. Estuar Coast Shelf Sci 88:442–449.

Fitzer SC, Caldwell GS, Close AJ, Clare AS, Upstill-Goddard RC, Bentley MG (2012) Ocean acidification induces multi-generational decline in copepod naupliar production with

possible conflict for reproductive resource allocation. J Exp Mar Bio Ecol 418–419:30–36.

Frost BW (1972) Effects of size and concentration of food particles on the feeding behavior of the marine planktonic copepod *Calanus pacificus*. Limnol Oceanogr 17:805–815.

Frost BW (1988) Variability and possible adaptive significance of diel vertical migration in *Calanus pacificus*, a plankton marine copepod. Bulletin Mar Sci 43:675–694.

Giddings SN, MacCready P (2017) Reverse estuarine circulation due to local and remote wind forcing, enhanced by the presence of along-coast estuaries. J Geophys Res Ocean 122:10184–10205.

Grodzins MA, Ruz PM, Keister JE (2016) Effects of oxygen depletion on field distributions and laboratory survival of the marine copepod *Calanus pacificus*. J Plankton Res 00:1–8.

Hill AE (1991) A mechanism for horizontal zooplankton transport by vertical migration in tidal currents. Mar Biol 111:485–492.

Isensee K, Levin LA, Breitburg D, Gregoire M, Veronique G, Valdes L (2016) The Ocean is Losing its Breath. Ocean Clim Sci Notes ed 2:20–31.

Keister JE, Houde ED, Breitburg DL (2000) Effects of bottom-layer hypoxia on abundances and depth distributions of organisms in Patuxent River, Chesapeake Bay. Mar Ecol Prog Ser 205:43–59.

Keister JE, Tuttle LB (2013) Effects of bottom-layer hypoxia on spatial distributions and community structure of mesozooplankton in a sub-estuary of Puget sound, Washington, U.S.A. Limnol Oceanogr 58:667–680.

Keister JE, Winans AK, Herrmann BEL (2020) Zooplankton community response to seasonal hypoxia: A test of three hypotheses. Diversity 12.

Kiørboe T (1997) Population regulation and role of mesozooplankton in shaping marine pelagic food webs. Hydrobiologia 363:13–27.

Kiørboe T, Jiang H, Gonçalves RJ, Nielsen LT, Wadhwa N (2014) Flow disturbances generated by feeding and swimming zooplankton. Proc Natl Acad Sci USA 111:11738–11743.

Lenth RV (2021) Emmeans: estimated marginal means, aka least-squares means. R package version 1.7.2. https:// CRAN.R-project.org/package=emmeans

Lima SL, Dill LM (1990) Behavioral decisions made under the risk of predation: a review and prospectus. Can J Zool 68:619–640.

Lorenzen CJ, Shuman FR, Bennett JT (1981) In situ calibration of a sediment trap. Limnol Oceanogr 26:580–585.

Ludsin SA, Zhang X, Brandt SB, Roman MR, Boicourt WC, Mason DM, Costantini M (2009) Hypoxia-avoidance by planktivorous fish in Chesapeake Bay: Implications for food web interactions and fish recruitment. J Exp Mar Bio Ecol 381:121–131.

Maboloc EA, Batzel G, Grünbaum D, Chan KYK (2020) Vertical distribution of echinoid larvae in pH stratified water columns. Mar Biol 167:1–9.

Mayor DJ, Everett NR, Cook KB (2012) End of century ocean warming and acidification effects on reproductive success in a temperate marine copepod. J Plankton Res 34:258–262.

Melzner F, Thomsen J, Koeve W, Oschlies A, Gutowska MA, Bange HW, Hansen HP, Körtzinger A (2013) Future ocean acidification will be amplified by hypoxia in coastal habitats. Mar Biol 160:1875–1888.

Newton J, Bassin C, Devol A, Kawase M, Ruef W, Warner M, Hannafious D, Rose R (2007) Hypoxia in Hood Canal: An overview of status and contributing factors.

Nuwer ML (2008) Genetic Structure and Speciation in Planktonic Copepods: Global Phylogeography of the *Calanus helgolandicus* clad. PhD dissertation, University of Washington, Seattle, WA.

ORCA Mooring Data, Applied Physics Lab, University of Washington (2022) NW Environmental Moorings. https://nwem.apl.washington.edu/prod_PS_Hoodsport.shtml (accessed 14 Dec 2021).

Peterson WT, Miller CB, Hutchinson A (1979) Zonation and maintenance of copepod populations in the Oregon upwelling zone. Deep Sea Res Part A, Oceanogr Res Pap 26:467–494.

Pierson JJ, Roman MR, Kimmel DG, Boicourt WC, Zhang X (2009) Quantifying changes in the vertical distribution of mesozooplankton in response to hypoxic bottom waters. J Exp Mar Bio Ecol 381:S74–S79.

Roman MR, Brandt SB, Houde ED, Pierson JJ (2019) Interactive effects of Hypoxia and temperature on coastal pelagic zooplankton and fish. Front Mar Sci 6:1–18.

Roman MR, Pierson JJ, Kimmel D, Boicourt WC (2012) Impacts of Hypoxia on Zooplankton Spatial Distributions in the Northern Gulf of Mexico. Estuaries and Coasts 35:1261–1269.

Svensen C, Viličić D, Wassmann P, Arashkevich E, Ratkova T (2007) Plankton distribution and vertical flux of biogenic matter during high summer stratification in the Krka estuary (Eastern Adriatic). Estuar Coast Shelf Sci 71:381–390.

Svetlichny LS, Hubareva ES, Erkan F, Gucu AC (2000) Physiological and behavioral aspects of *Calanus euxinus* females (Copepoda: Calanoida) during vertical migration across temperature and oxygen gradients. Mar Biol 137:963–971.

Thor P, Oliva EO (2015) Ocean acidification elicits different energetic responses in an Arctic and a boreal population of the copepod *Pseudocalanus acuspes*. Mar Biol 162:799–807.

Tomasetti SJ, Morrell BK, Merlo LR, Gobler CJ (2018) Individual and combined effects of low dissolved oxygen and low pH on survival of early stage larval blue crabs, *Callinectes sapidus*. PLoS One 13.

Tommasi D, Hunt BPV, Pakhomov EA, Mackas DL (2013) Mesozooplankton community seasonal succession and its drivers: Insights from a British Columbia, Canada, fjord. J Mar Syst 115–116:10–32.

Turner JT (2002) Zooplankton fecal pellets, marine snow and sinking phytoplankton blooms. Aquat Microb Ecol 27:57–102.

Venables WN, Ripley B. (2002) Modern Applied Statistics with S, 4th ed. Springer, New York.

Van Duren LA, Videler JJ (1996) The trade-off between feeding, mate seeking and predator avoidance in copepods: Behavioural responses to chemical cues. J Plankton Res 18:805–818.

Verity PG, Smetacek V (1996) Organism life cycles, predation, and the structure of marine pelagic ecosystems. Mar Ecol Prog Ser 130:277–293.

Visser AW (2007) Motility of zooplankton: Fitness, foraging and predation. J Plankton Res 29:447–461.

Weydmann A, Søreide JE, Kwasniewski S, Widdicombe S (2012) Influence of CO 2-induced acidification on the reproduction of a key Arctic copepod *Calanus glacialis*. J Exp Mar Bio Ecol 428:39–42.

Wu RSS (2002) Hypoxia: From molecular responses to ecosystem responses. Mar Pollut Bull 45:35–45.

Zhang H, Ludsin SA, Mason DM, Adamack AT, Brandt SB, Zhang X, Kimmel DG, Roman MR, Boicourt WC (2009) Hypoxia-driven changes in the behavior and spatial distribution of pelagic fish and mesozooplankton in the northern Gulf of Mexico. J Exp Mar Bio Ecol 381:S80–S91.

Tables

Table 1. Mean (+/- SE) realized conditions during 2019 and 2020 hypoxia experiments.

Treatment	n	Temp (°C)	Salinity (ppt)	Density (σ_t)	DO (mg L^{-1})	Percent Saturation
Surface - control	40	14	29.0	21.6	10.1 ± 0.05	117 ± 0.6
Surface - treatment	40	14	29.0	21.6	10.0 ± 0.05	116 ± 0.6
Bottom - control	40	14	31.0	23.1	10.2 ± 0.04	119 ± 0.5
Bottom - treatment	40	14	31.0	23.1	0.65 ± 0.03	7.7 ± 0.9

Table 2. Mean (+/- SE) realized conditions during pH experiments for the two different bubbling methods (Pre-mix= premixed CO2/air, Feedback=feedback control system).

Bubbling Method	Treatment	n	Temp (°C)	Salinity (ppt)	Alkalinity (μmol kg^{-1})	DIC (μmol kg^{-1})	pCO_2 (μatm)	pH (total scale)
Pre-mix	Surface - control	5	14	29.0	3081 ± 24.7	2777 ± 33.0	386 ± 24.5	8.18 ± 0.02
	Surface - treatment	5	14	29.0	3008 ± 29.9	2703 ± 34.1	367 ± 22.2	8.19 ± 0.02
	Bottom - control	10	14	31.0	3085 ± 40.1	2840 ± 26.5	537 ± 29.7	8.06 ± 0.02
	Bottom - treatment	10	14	31.0	3266 ± 20.7	3239 ± 19.8	1889 ± 38.4	7.58 ± 0.01
Feedback	Surface - control	5	14	29.0	3035 ± 40.0	2735 ± 42.1	378 ± 15.9	8.18 ± 0.01
	Surface - treatment	5	14	29.0	2985 ± 36.4	2684 ± 37.8	365 ± 14.8	8.19 ± 0.01
	Bottom - control	10	14	31.0	3035 ± 53.7	2735 ± 36.6	559 ± 40.2	8.03 ± 0.03
	Bottom - treatment	10	14	31.0	3236 ± 28.6	3284 ± 27.8	2936 ± 42.9	7.39 ± 0.01

Table 3. Summary of responses to hypoxic or acidic bottom waters. An asterisk (*) designates a significant treatment effect and a dagger (†) designates a significant treatment*collection site interaction.

Stressor	**Metric**	**Camera View**	**Change relative to control**
Hypoxia	Moribundity	Base Camera	Increase *
	Mean Height	All cameras	Increase *
	Calculated Total Speed (*TS*)	Surface Camera	Increase *,†
	Calculated Total Speed (*TS*)	Bottom Camera	Decrease †
	True horizontal speed (HS_{tr})	Base Camera	Decrease *
Acidification	Moribundity	Base Camera	No change
	Mean Height	All cameras	No change
	Calculated Total Speed (*TS*)	Surface Camera	Decrease *,†
	Calculated Total Speed (*TS*)	Bottom Camera	No change
	True horizontal speed (HS_{tr})	Base Camera	Decrease *

Figures

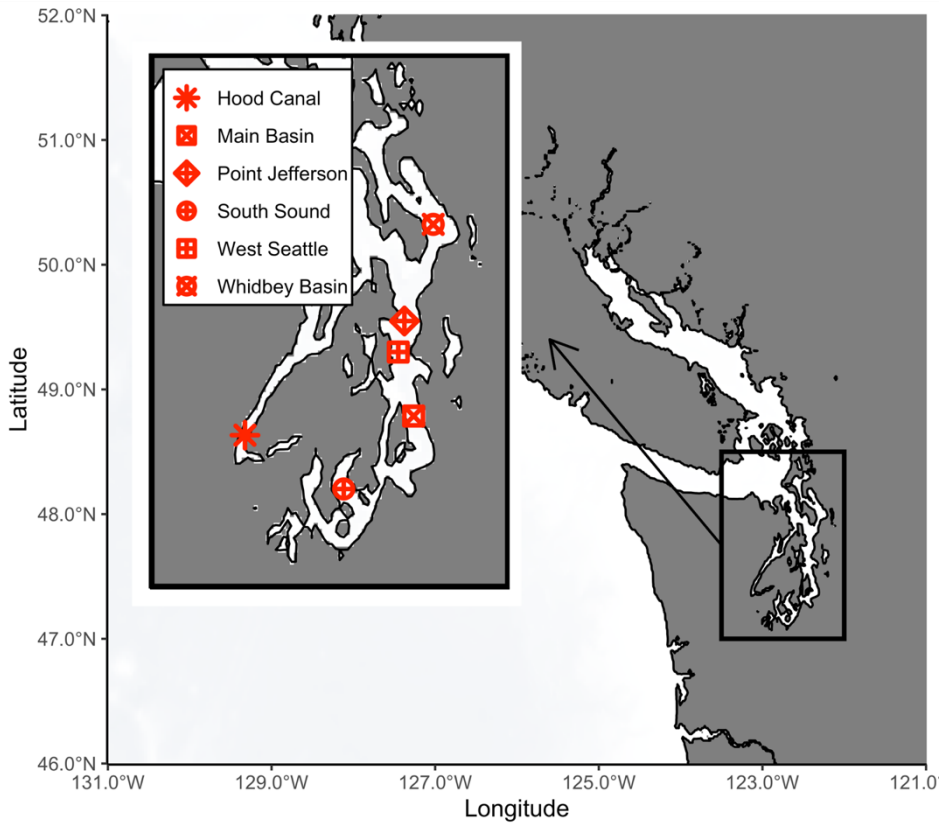

Figure 1. Map of Puget Sound, WA and stations where Calanus pacificus were collected over the summers of 2019 and 2020.

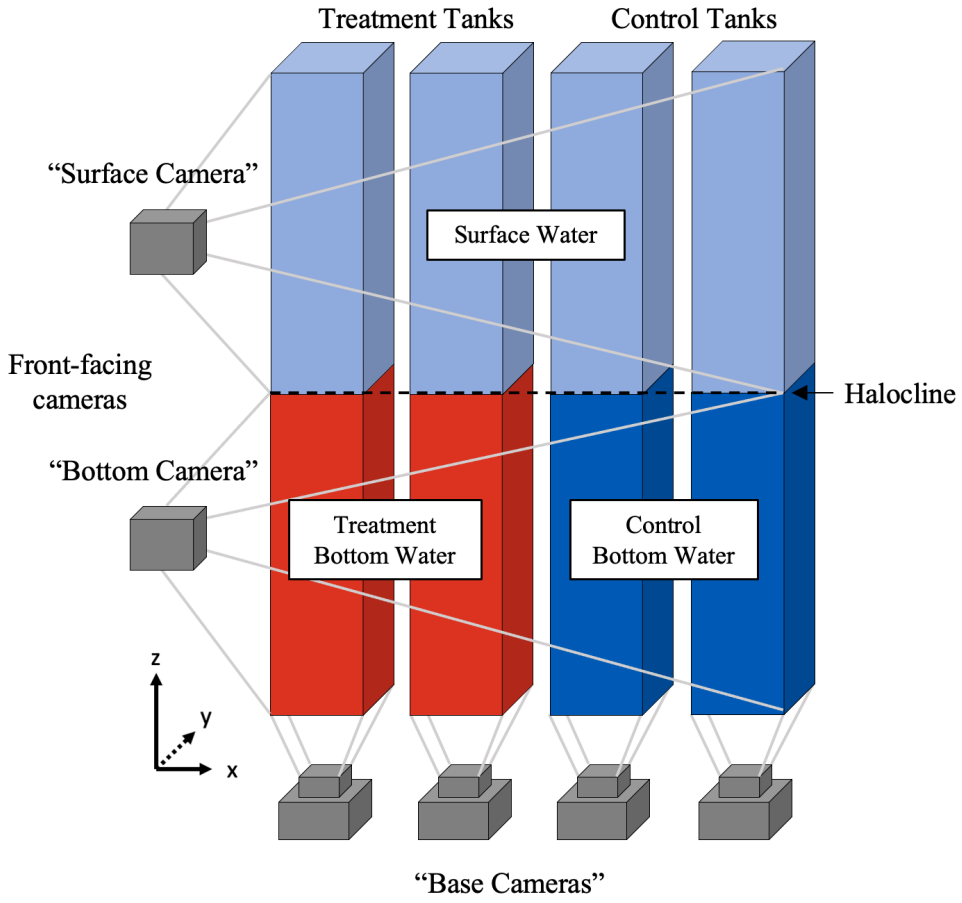

Figure 2. Experimental schematic highlighting the 0.1 x 0.1 x 1 m two-layer water columns, front-facing cameras (observing motion X and Z directions), and Base Cameras (observing motion in the X and Y directions). Allocation of treatment and control tanks was randomized in every experiment. The same colors will be used in later figures for continuity.

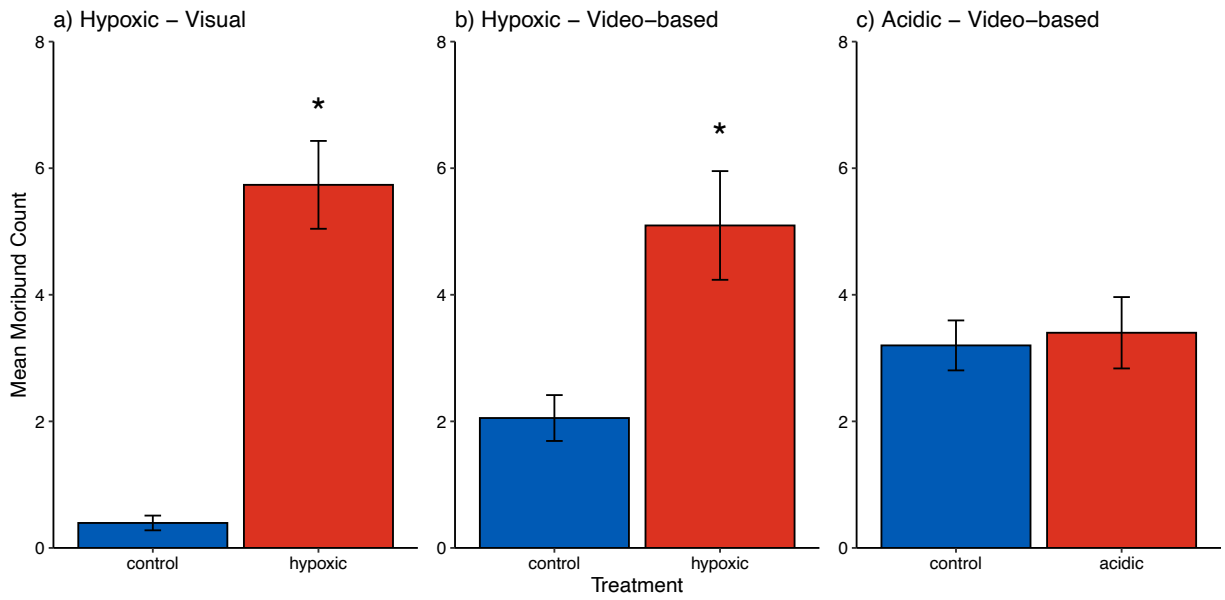

Figure 3. Number of "moribund" (immobilized or dead) (+/- SE) copepods in control (blue) and treatment (red) tanks after 90 minutes (out of 20 copepods). **(a)** Visual "moribundity" metric at the end of all 2019 and 2020 hypoxia experiments. Asterisks indicate significant differences between treatments ($p<0.0001$). **(b)** Video-based "moribundity" metric from 2020 hypoxia experiments. Asterisk indicates a significant difference between treatments ($p=0.003$). **(c)** Video-based "moribundity" metric from 2020 acidification experiments. There was no significant difference between treatments.

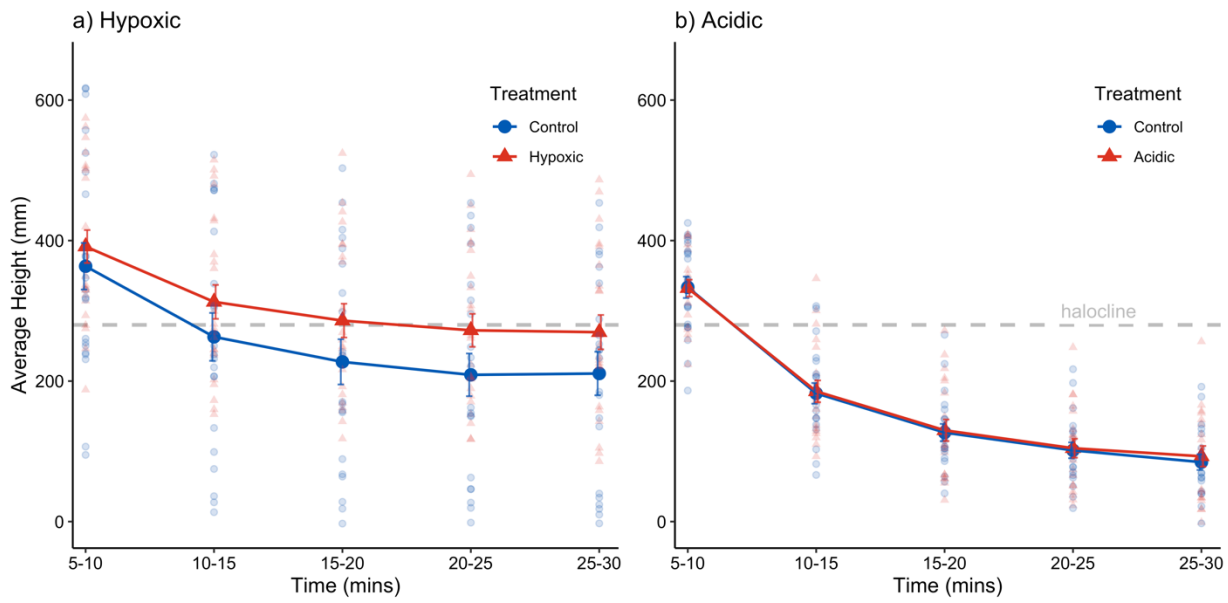

Figure 4. Mean height above bottom (+/- SE) of copepods over 5-minute intervals from 2020 **(a)** hypoxia and **(b)** acidification experiments. The blue line shows the mean height for control tanks and the red line shows treatment tanks. Grey dashed line shows the location of the halocline. The hypoxic treatment and control were significantly different from each other ($p<0.0001$). The acidic treatment and control were not significantly different.

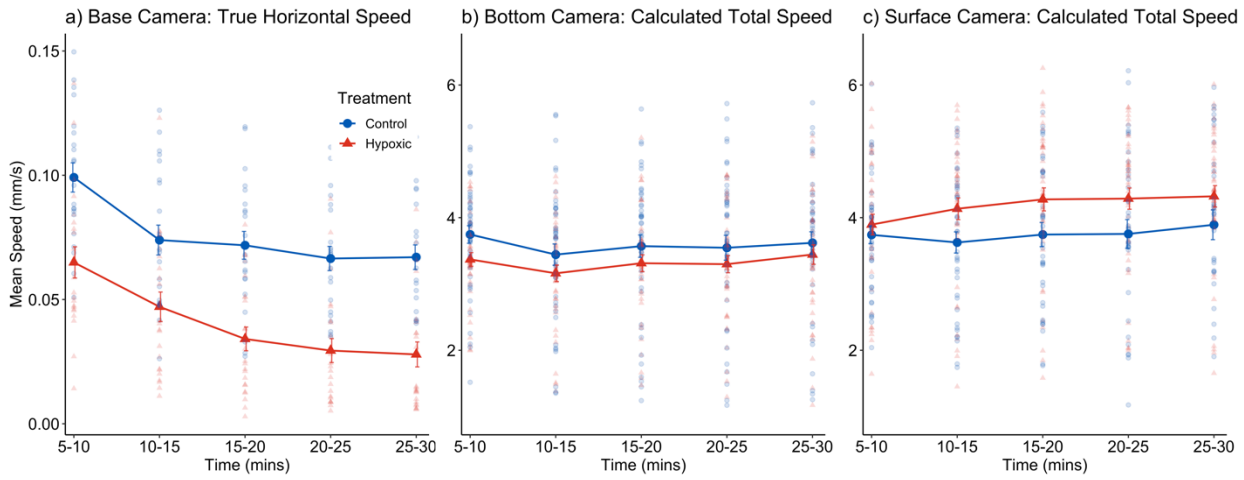

Figure 5. Calculated swimming speeds from different camera views during the hypoxia experiments. **(a)** Mean true horizontal speed (HS_{tr}) (mm/s) (+/- SE) observed by the Base Camera during the 2020 hypoxia experiments. Treatment and control tanks were significantly different from each other ($p<0.0001$). **(b)** Mean calculated total speed (TS) (mm/s) (+/-SE) observed by the front-facing Bottom Camera (below the halocline and above the base) and **(c)** Surface Camera (above the halocline) during 2019 and 2020 hypoxia experiments. Swimming speeds significantly differed in the Surface Camera and there was a significant treatment*collection site interaction in both the Bottom and Surface Cameras. In all plots the blue line shows mean speed in control tanks and the red line shows mean speed in treatment tanks. Note the difference of scale in plot (a).

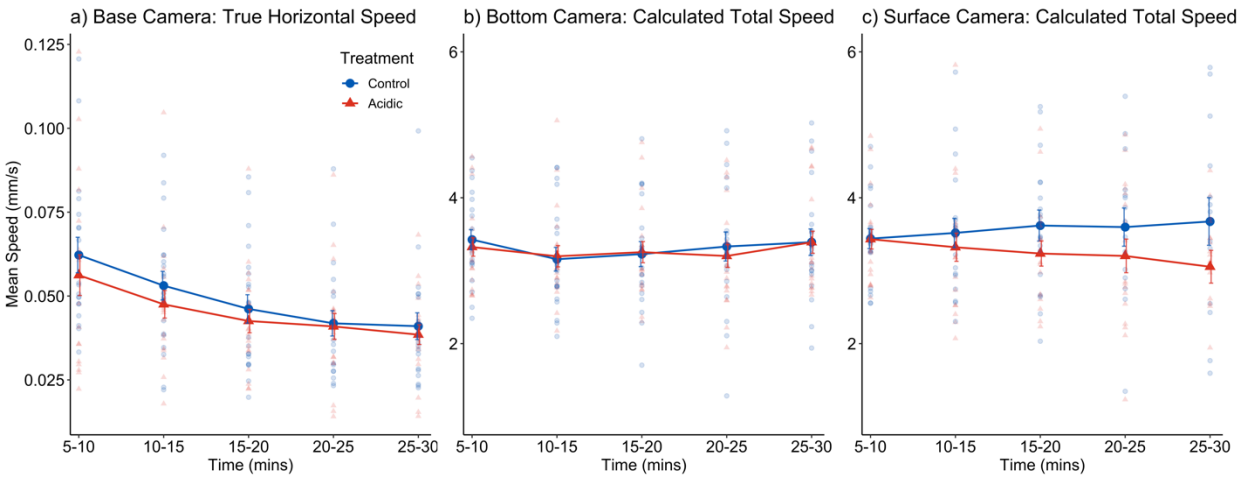

Figure 6. Calculated swimming speeds from different camera views during the acidification experiments. **(a)** Mean true horizontal speed (HS_{tr}) (mm/s) (+/- SE) observed by the Base Cameras. Treatment and control tanks were significantly different from each other (p=0.007). **(b)** Mean calculated total speed (TS) (mm/s) (+/-SE) from front-facing Bottom Camera (below the halocline and above the base) and **(c)** Surface Camera (above the halocline) during pH experiments. There was a significant treatment*collection site interaction for the Surface Camera. In all plots the blue line shows mean speed in control tanks and the red line shows mean speed in treatment tanks. Note the difference of scale in plot (a).

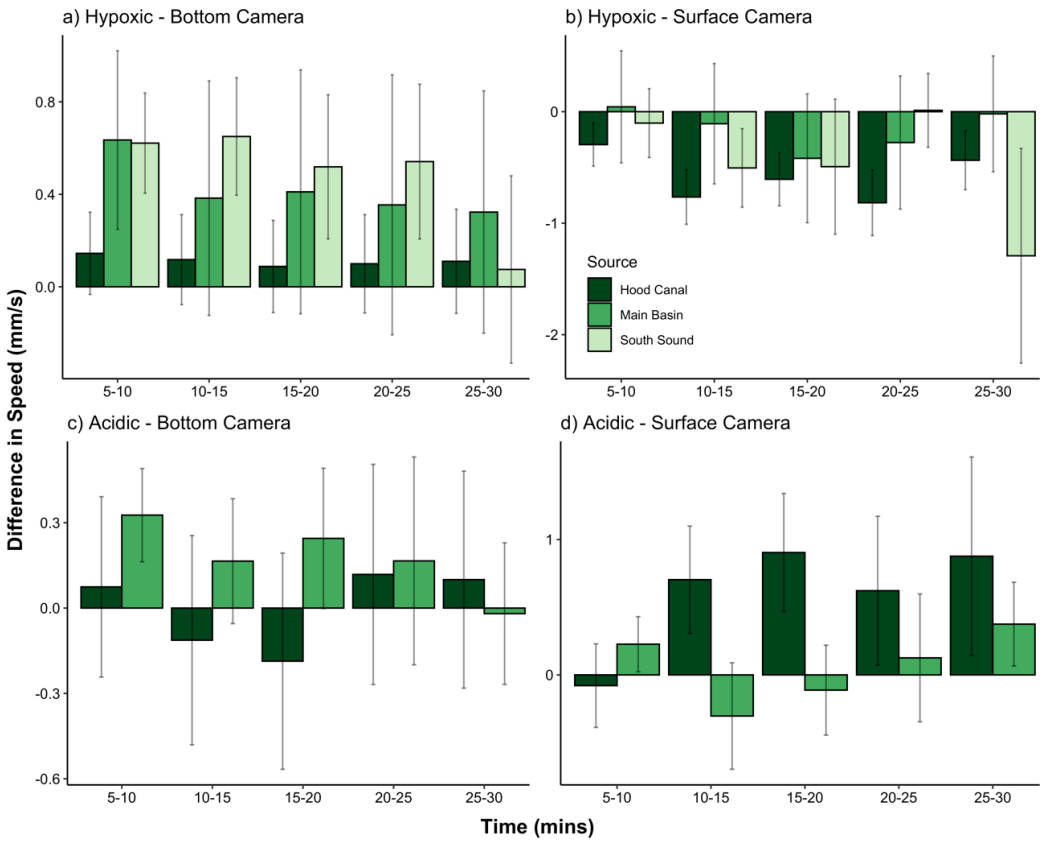

Figure 7. The difference (control – treatment) in the mean swimming speed (mm/s) (+/- pooled SE) between control and treatment tanks among copepods collected from Hood Canal (dark), Main Basin (medium), and South Sound (light). In hypoxia experiments, **(a)** changes in mean total swimming speeds (TS) observed by the Bottom Camera (but not including the base) was significantly slower in hypoxic tanks relative to control among copepods collected from the Main Basin ($p = 0.008$) or South Sound ($p = 0.004$), but not Hood Canal. **(b)** In surface waters, the largest swimming speed differences were observed among copepods from Hood Canal ($p < 0.0001$). In acidification experiments, **(c)** there was no significant difference in swimming speed responses among copepods from different collection sites in bottom waters. **(d)** In surface waters, only copepods from Hood Canal swam significantly slower in acidic tanks relative to control tanks ($p = 0.002$).

Chapter 2: In situ observations of zooplankton show changes in abundance and swimming speed in response to hypoxia and acidification

This manuscript was previously published as: Wyeth, A.C., Grünbaum D., Keister J.E., Crouser, D., Roberts, P. (2024). In situ observations of zooplankton show changes in abundance and swimming speed in response to hypoxia and acidification. Limnology and Oceanography, 9999: 1-11. https://doi.org/10.1002/lno.12668

Abstract

Zooplankton exhibit diverse swimming behaviors to reposition themselves in the water column, feed, find mates, and avoid predation. Environmental stressors that modify behavior can have cascading effects on population distributions and predator-prey interactions. Understanding zooplankton population dynamics is challenging, largely because traditional methods for quantifying zooplankton distributions are costly, limited in scope, and require extended analysis by trained analysts. We developed a novel methodology that combined remotely deployed camera systems, machine learning-based identification of zooplankton, and video-based tracking technology to quantify copepod and amphipod in situ swimming behavior in Hood Canal, WA, USA, a seasonally hypoxic and acidified fjord. Behavioral analysis showed copepods of all sizes swam on average 24% slower in stressful (hypoxic and acidified) waters relative to non-stressful waters. Copepods exhibited less frequent escape responses in stressful waters, with a 68% decrease in the amount of time spent “jumping” for copepods 1-2 mm in length. Interestingly, abundances of small copepods increased in stressful waters, with 56% more 1-2 mm long copepods in stressful versus non-stressful conditions. In contrast, amphipods' average “darting”

speeds did not differ between environmental conditions, but the abundance of amphipods significantly decreased in stressful waters relative to non-stressful waters, suggesting avoidance of stressful conditions. Changes in swimming behavior are informative metrics in understanding ecosystem impacts of environmental stress because swimming speed has individual, population, and community level implications. Our results suggest that, among copepods, in situ behaviors may be useful proxies in monitoring impacts of climate change on coastal ecosystems.

1. Introduction

Coastal systems are increasingly subject to chemical stresses such as hypoxia (oxygen concentration less than 2 mg/L) and acidification (Breitburg et al. 2018). Increases in atmospheric carbon dioxide, changes in agriculture, and climate change drive the acidification and deoxygenation of the oceans (Doney 2010; IPCC 2023). In addition to changes driven by increases in anthropogenic CO_2, coastal hypoxia and acidification are also the result of bacterial respiration of organic matter at depth which draws down O_2 and releases CO_2, leading to stressful conditions that commonly occur at depth (Doney 2010; Melzner et al. 2013; Breitburg et al. 2018). Because of the overlap in processes that drive them, coastal hypoxia and acidification, frequently occur in conjunction.

Sub-lethal responses to hypoxia and acidification, such as behavioral avoidance and changes in swimming speed, are known to affect zooplankton under laboratory conditions. In one study, the fraction of time that the copepod *Calanus euxinus* spent swimming increased as the oxygen concentration declined from 10 to 0.5 mg/L, potentially as a behavioral response to avoid sinking into anoxic bottom waters (Svetlichny et al. 2000). In pH-stratified experimental water columns, larval sand dollars *Dendraster excentricus* reversed the direction and shape of their swimming trajectories upon encountering the boundary between ambient and acidified

water (Maboloc et al. 2020). In the laboratory, copepods of the species *Calanus pacificus* partially avoided hypoxic bottom waters, but not acidified waters (Wyeth et al. 2022). Individuals that entered hypoxic (dissolved O_2 0.65 mg/L) or acidified (pH 7.48) water showed significant decreases in swimming speed. Low pH waters also altered the proportion of some swimming behaviors, such as shelter use, in a laboratory experiment using the gammarid amphipod *Gondogeneia antarctica* (Park et al. 2020). However, these studies, and laboratory experiments in general, do not resolve how zooplankton behaviors change in response to environmental stressors in situ, or the consequences of behavioral changes for population distributions.

In situ observations are essential to understanding the effects of co-occurring stressors, and new technologies provide new methods for conducting these observations. Traditional methods for sampling in situ zooplankton populations include ship-board net tows, combined with taxonomic analysis of samples by trained analysts in the laboratory. These methods are typically costly, limited in duration and scope, and biased against certain groups of zooplankton, such as strong swimmers that can avoid the nets and gelatinous species that are damaged by nets (Ohman et al. 2019). Additionally, net tows typically integrate plankton data over space and do not permit the fine-scale study of individuals or their behaviors. A combination of three rapidly-developing technologies offer solutions to the limitations of traditional net tows: remotely deployed camera systems (Cowen and Guigand 2008; Ohman et al. 2019; Campbell et al. 2020; Orenstein et al. 2020), machine learning-based identification of individual zooplankton from in situ imaging (Ellen et al. 2019; Li et al. 2021), and video-based tracking technologies (Chan and Grünbaum 2010; Lard et al. 2010; Wyeth et al. 2022). To our knowledge, our study is the first to

combine these three technologies to observe in situ zooplankton behavioral responses to environmental stress.

Because swimming speed has individual, population, and community level implications, changes in swimming behavior are informative metrics for understanding ecosystem impacts of environmental change. On the individual level, decreased oxygen concentrations or increased temperatures can cause respiratory stress, which can be further exacerbated by increased metabolic demands due to increased swimming (Svetlichny et al. 2000). Changes in swimming speed also affect trophic interactions because predator-prey encounter rates typically increase with speed (Frost 1972; Visser 2007). Additionally, rheotactic predators detect their prey through fluid signals, making faster-swimming prey easier to detect (Kiørboe et al. 2014). Increases in swimming speed also increase hydrochemical signals, and therefore encounter distances, of individuals seeking mates (Van Duren and Videler 1996).

The goals of this study were to develop and implement a novel methodology to observe in situ zooplankton behavioral responses to environmental conditions, and to assess whether in situ behavioral responses to hypoxia and acidification are likely to exacerbate physiological stresses, mitigate them, or have no effect. We collected in situ videos under a range of oceanographic conditions, by deploying a remote camera system in Hood Canal, a seasonally hypoxic and acidified fjord located in Puget Sound. The duration and extent of hypoxia in Hood Canal varies annually, but parts of southern Hood Canal can be hypoxic for 2-6 months of the year (Newton et al. 2007). In Summer, the deep parts of Hood Canal are also highly acidified, with pH values ranging from 7.3 to 7.8. Levels of pH less than 7.4 reaches depths as shallow as 50 m (Feely et al. 2010), well within the range of typical zooplankton diel vertical migrations. We hypothesized that zooplankton adjust their swimming, either to avoid stressful water or to

mitigate the physiological impacts of hypoxia and acidification by reducing their swimming speed. To test our hypotheses, we combined in situ videos, particle tracking technology, and machine learning-based classification of zooplankton to extract swimming statistics of individual copepods and amphipods under a range of environmental conditions.

2. Methods

2.1 Field site and video collection

A high-resolution camera, constructed by the Jaffe Laboratory for Underwater Imaging (Scripps Institute of Oceanography) (Campbell et al. 2020) (Fig. S1), was modified for IR-illuminated video capture and mounted on the profiling package of an Oceanic Remote Chemical Analyzer mooring over the summer of 2018. Oceanic Remote Chemical Analyzer moorings are profiling systems that collect real-time oceanographic and atmospheric data. The mooring was located near Hoodsport, Washington, in southern Hood Canal with a station depth of 120 m (Fig. S2).

The camera moved with the profiling package for a CTD cast every 12 hours, but videos were recorded only when the camera was stationary at a specific depth between casts. When stationary, the camera was triggered to take a 60-second video when flow was < 1 cm/s, using infrared lighting to avoid modifying zooplankton behavior. The video camera recorded swimming in the X (left, right) and Z (up, down) directions, observing true vertical motion and projected horizontal motion. Videos were recorded at an average frame rate of 20 frames per second. The exact difference in time between frames was used when converting speeds from pixels per frames to mm per second. Each frame was 650 x 876 pixels, and each pixel was 0.088 mm^2, corresponding to a 57.2 x 77.1 mm field of view.

2.2 Video processing

2.2.1 Region of interest isolation

Zooplankton and other particles appeared in videos as grayscale images against a dark background. Regions of interest enclosing plankton from each frame were identified using the Python package **OpenCV** (version 4.7.0) (Bradski 2000). OpenCV-fitted contours and rotated bounding boxes were used to calculate width, height, and area metrics for each region of interest. The nominal "length" of each region of interest was defined as the longer of its width and height measurements. Position, defined as the optical centroid of the zooplankter outline, and size metrics were saved for each region of interest that were potentially zooplankton (areas larger than 30 pixels) within each frame.

2.2.2 Swimming speed calculation

Zooplankton positions were assembled into swimming trajectories using the Matlab software **Tracker3D** (Chan and Grünbaum 2010). A smoothing spline with knots placed every three frames was applied to remove frame rate noise in swimming trajectories caused by bit-flipping during pixelization. Small particles in videos were used to reconstruct a background flow field with particle image velocimetry, using the Python package **OpenPIV** (version 0.23.9) (Liberzon et al. 2021). To prevent confounding of flow estimates by moving zooplankton, regions of interest >30 pixels were masked so only small particles remained. A few small particles (<5%) visually appeared to deviate from the overall flow. The particle image velocimetry algorithm mitigated effects of these participles on flow estimates by masking out grids that failed a series of variance tests. (see Text S1 for additional particle image velocimetry parameterization). A smoothing spline with knots placed every 15 frames was applied to smooth

the high signal/noise ratios that could occur when there were few small particles in a grid, reflecting the relatively slow timescale of flow fluctuations.

After calculating the zooplankton swimming velocities and the flow field separately, the background flow was subtracted from the instantaneous velocities of each swimming track to obtain zooplankters' movement velocities relative to ambient water. A final smoothing spline with knots every three frames was applied to filter out potential error accumulated while taking numerical derivatives of zooplankton and small particle positions to calculate velocities. Speeds were converted to physical units (mm/s) using the difference between frame timestamps and pixel positions of the optical centroids.

2.2.3 Taxonomic identification

Each zooplankton region of interest was assigned a taxonomic identification using a machine learning image classification algorithm. The algorithm was generated using a pre-trained convolutional neural network 50 layers deep (ResNet-50) with **PyTorch**, an open-source, Python-based machine learning framework. The algorithm was trained on 18 broad taxonomic groups or classes – Amphipod, Blob, Chaetognath, *Clione*, Copepod, Diatom, Egg, Euphausiid-Decapod, Filament, Fish Larva, Jellyfish, Larvacean, *Limacina*, *Noctiluca*, Ostracod, Siphonophore, and Snow – and returned a testing accuracy of 97.67% (Fig. S3). The resulting model was applied using a Python-based classifier, to assign labels to a larger library of uncategorized images. The images from this library were sorted into their respective taxonomic folders, enabling us to isolate classes of interest (copepods and amphipods) for this study. Machine learning image classification and tracking algorithms were coupled along the swimming trajectories of individual organisms, reducing the errors associated with ambiguous

individual views in some regions of interest and other classification errors, improving the overall accuracy of the identification (see Text S2 for additional details).

Only zooplankton paths identified as either copepod or amphipod were analyzed in this study. Swimming paths were also sorted into size bins of the organism (1-2 mm, 2-3 mm, 3-4 mm, and >4 mm). The maximum observed body length along the swimming path was used to assign size because it was assumed that the region of interest with the longest length best approximated the zooplankter's true length. In our study, identification to species was not possible for copepods and amphipods, so maximum observed body length was the best available criterion to differentiate individuals within the two classes.

2.2.4 Water chemistry and video matching

The Oceanic Remote Chemical Analyzer mooring conducted a CTD profile at least twice a day at 00:00 and 12:00 PST, recording a range of oceanographic variables including temperature, fluorescence, depth, salinity, and dissolved oxygen (Dunne et al. 2002). The oxygen sensors were annually calibrated by their manufacturer, Sea-Bird Scientific. Readings were taken four times a second, corresponding to depth increments of 0.1 m. Between CTD casts, the Oceanic Remote Chemical Analyzer package was held stationary at depths chosen based on the profiles to ensure videos were recorded under a range of environmental conditions (e.g., within or outside of hypoxic layers). To determine the conditions under which each zooplankton trajectory was observed, each video was matched to the corresponding depth in the nearest prior CTD cast. If there was no CTD cast within 24 hours prior to the video being recorded, the video was removed from analysis.

2.3 Behavioral analysis

The relationships between oxygen concentrations and swimming metrics were assessed using single variable analyses, where videos were binned into two groups (hypoxic or normoxic) using a dissolved oxygen threshold of 2 mg/L. Potential interactions among multiple environmental factors were assessed using a multivariate analysis that included dissolved oxygen, temperature, depth, salinity, and maximum length as continuous variables and time of day (day/night) as a categorical variable to predict swimming behaviors for copepods and amphipods (see supplemental materials Fig. S10-13, Text S3-S6).

2.3.1 Average speeds

Previous studies report three distinct behaviors in copepod swimming paths, classified by speed relative to ambient water: "drifting" (≤ 5 mm/s), "cruising" (> 5 mm/s and < 100 mm/s), and "jumping" (≥100 mm/s) (Svetlichny et al. 2020; Svetlichny et al. 2022). A mean cruising speed was calculated for each copepod path from the instantaneous cruising speeds. Copepod paths were grouped into oxygen concentration (hypoxic/normoxic) and size bins (1-2mm, 2-3mm, 3-4mm, and >4mm). Mean (± standard error) cruising speed was calculated for each group. Cruising speeds were log-transformed and a 2-way ANOVA was used to test for significant effects of oxygen concentration, size, and the interaction of oxygen and size on speed. A Tukey pairwise comparison of size and oxygen was generated using the R package **emmeans** (version 1.7.3) (Lenth 2021).

Previous literature reports that amphipods usually exhibit two different swimming behaviors: "hovering" (≤ 10 mm/s) or "darting" (> 10 mm/s) (von Westernhagen et al. 1979). For each amphipod path, a mean darting speed was calculated from the instantaneous darting

speeds. Amphipod paths were grouped into oxygen concentration and size bins. Mean darting speed was calculated for each group, darting speeds were log transformed and a 2-way ANOVA and a Tukey pairwise comparison were used to test for significant effects of oxygen concentration, size, and the interaction of oxygen and size on speed.

2.3.2 Frequency of swimming states

For each copepod or amphipod path, the fraction of frames classified as "jumping" and "drifting" or "hovering" were used as behavioral frequency metrics. Mean (± standard error) frequencies were calculated for each oxygen concentration and size bin. Frequency data were zero-inflated and were not normally distributed. To test the effect of oxygen concentration (hypoxic and normoxic) and size (1-2mm, 2-3mm, 3-4mm, and >4mm) on jumping, drifting, and darting frequencies, generalized linear models using a quasibinomial distribution were generated using the *R* package **lme4** (version 1.1-34) (Bates et al. 2015). Nested models were generated using different combinations of oxygen environment and size, with both variables treated as factors, and the best model was identified using an F-test. A Tukey pairwise comparison of size and oxygen was generated using the *R* package **emmeans**.

2.3.3 Zooplankton abundance

To estimate relative copepod or amphipod abundance when videos were collected, the total number of observations of copepods or amphipods was normalized by the total number of frames. This metric of zooplankton abundance factors out current and swimming speeds because, on average, faster moving zooplankton enter the field of view at a higher rate but remain in view for a proportionately shorter time. Mean (± standard error) zooplankton abundance was

calculated for each oxygen concentration and size bin. A Tweedie distribution—a log-normal distribution commonly used to model biomass and abundance—was used to test for significant effects of oxygen concentration, size, and the interaction of oxygen and size on abundance using the *R* package **glmmTMB** (version 1.1.8) (Foster and Bravington, 2013). Nested models were generated using different combinations of oxygen environment and size, and the best model was identified using AIC values. A Tukey pairwise comparison of size and oxygen was generated using the *R* package **emmeans**.

2.3.4 Markov chains

A discrete-time Markov chain is a stochastic process in which the next step of a Markov chain is independent of the past and only relies upon the most recent state. To calculate Markov chains, each instantaneous speed was assigned a categorical value (for copepods: "drift", "cruise", or "jump"; for amphipods: "hover", "dart"). To quantify transitions between behaviors across frames, discrete-time Markov chains were used to calculate the probability of transitioning from each of the predefined swimming states (*i*) to the same or a different swimming state (*j*). The number of occurrences for each of the possible transitions was totaled and divided by the number of transition "opportunities" (the number of times the frame started in swimming state *i*). Transition probabilities were organized in a transition probability matrix (Figure S4). A Markov chain was calculated for each oxygen environment.

2.3.5 Hidden Markov models

To estimate changes in swimming behaviors without using predefined speed thresholds, hidden Markov models were used to model inferred behavioral states using instantaneous speeds.

Instantaneous speeds were log-transformed and hidden Markov models were generated using the Python package **hmmlearn** (version 0.2.8) (Lebedev 2016). Hidden Markov models were generated using 100 different starting points and 100 iterations. Hidden Markov models were generated for all copepod/amphipod paths, and for copepod/amphipod paths binned by size. The best hidden Markov model was determined using AIC values. A three-state hidden Markov model was selected for copepods and a two-state hidden Markov model for amphipods. Mean (± standard deviation) swimming speed was calculated and back-transformed for each swimming component estimate within each hidden Markov model.

3. Results

3.1 Environmental conditions

The analyses included 187 videos recorded between 1 August and 31 September 2018. Videos were recorded at depths ranging from 10 to 100 m, temperatures ranging from 9.7 to 10.9 °C, and dissolved oxygen concentrations ranging from 1.3 to 3.4 mg/L. Variability in the dissolved oxygen profiles over the field season is shown in Fig. S5. Of the 187 videos included in our analysis, 80 were recorded under hypoxic conditions and 107 were recorded under normoxic conditions. While Oceanic Remote Chemical Analyzer moorings do not measure pH, carbonate chemistry data are collected annually in April, July, and September in Hood Canal on cruises funded by the Washington Ocean Acidification Center. This dataset shows that dissolved oxygen and pH are tightly correlated in Hood Canal (R^2 = 0.92), especially at low concentrations of dissolved oxygen (Fig S6). For this reason, our subsequent interpretations assumed zooplankton experiencing hypoxic conditions were simultaneously experiencing acidified conditions.

3.2 Copepods

Video analysis of the 80 videos from hypoxic conditions yielded a total 554 copepod paths totaling 22,615 copepod localizations. Analysis of the 107 videos from normoxic conditions yielded 499 copepod paths totaling 18,434 copepod localizations (Table S1)**.** The majority of copepod paths had a maximum observed body length of 1-2 mm (hypoxic: $n = 222$, normoxic: $n = 182$) or 2-3 mm (hypoxic: $n = 262$, normoxic: $n = 234$).

3.2.1 Average cruising speed

Average copepod cruising speed (instantaneous speed between 5-100 mm/s) was significantly slower in hypoxic environments than normoxic environments (2-way ANOVA; $F = 73.32$, $p < 0.0001$) (Fig. 1, Table S2). Copepods 1-2 mm and 2-3 mm in length were, respectively, 28% and 26% slower in hypoxic conditions than normoxic conditions. Neither size or a size*oxygen interaction had a significant effect on average cruising speeds.

3.2.2 Jumping and drifting frequency

Copepods exhibited less frequent jumping behaviors in hypoxic environments than normoxic environments (Fig. 2a, Table S3). The best fit generalized linear model indicated that oxygen concentration ($F_{3,151} = 12.12$, $p = 0.0005$), but not size ($F_{3,151} = 1.18$, $p = 0.317$), had a significant effect on the jumping frequency of copepods. Copepods 1-2 mm, 2-3 mm, and 3-4 mm in length were, respectively, 68%, 47%, and 23% less likely to exhibit a jumping behavior in hypoxic conditions relative to normoxic conditions. Conversely, copepods >4 mm in length were

114% more likely to exhibit a jumping behavior in hypoxic conditions relative to normoxic conditions.

Copepods exhibited more frequent drifting behavior in hypoxic environments than normoxic environments (Fig. 2b, Table S3). The best fit generalized linear model indicated that both oxygen concentration and copepod size had a significant effect on the overall drifting frequency of copepods ($F_{3,151}$ =6.88, p = 0.0001). Copepods 1-2 and 2-3 mm in length showed a 67% and 110% increase in drifting frequency in hypoxic environments relative to normoxic environments. While there were fewer individuals, copepods 3-4 and > 4 mm in length showed a 137% and 166% increase in drifting frequency in hypoxic environments.

3.2.3 Copepod abundance

Copepod abundances varied with oxygen concentration and size (Tweedie; oxygen: p = 0.037, size: $p < 0.0001$) (Fig. 3, Table S4). Copepod abundances were significantly higher in hypoxic environments, except for copepods 3-4 mm in length. On average, the abundance of copepods 1-2, 2-3, and >4 mm in length were, respectively, 56%, 59%, and 42% higher in hypoxic conditions than normoxic conditions. Conversely, the abundance of copepods 3-4 mm in length was 19% lower in hypoxic conditions. The copepod species that were likely present during imaging was determined from a zooplankton net tow collected from Hoodsport in September 2018 (Fig. S7).

3.2.4 Markov chains

In both oxygen environments, the most likely outcome from an initial cruising state was remaining in the cruising state (0.93), indicating that multiple changes per frame interval were

rare and the timestep between transitions was appropriate. Of the nine different transition probabilities, five changed more than 5% between hypoxic and normoxic environments (Fig. 4, yellow highlights). Transition probabilities associated with cruising behaviors were generally the same for copepods in hypoxic and normoxic environments (cruise-cruise, cruise-drift, cruise-jump, and jump-cruise), suggesting that cruising behavior had the same duration in both environments. However, there was a shift towards drifting in hypoxic environments. Copepods were more likely to remain in the drifting state, more likely to transition into drifting from jumping, and less likely to transition from drifting into cruising or jumping in hypoxic environments compared to normoxic environments.

3.2.5 Hidden Markov models

Modeled speed components were slower in hypoxic environments than normoxic environments. For copepods of all sizes, component 1 was 21% slower, component 2 was 22% slower, and component 3 was 18% slower in hypoxic relative to normoxic environments (Fig. 5, Table S5).

3.3 Amphipods

Video analysis of the 80 hypoxic videos yielded 146 amphipod paths totaling 4,193 amphipod localizations. Analysis of the 107 normoxic videos yielded 546 amphipod paths totaling 16,380 amphipod localizations (Table S6)**.** Most amphipods had a maximum observed body length of 2-3 (hypoxic: $n = 33$, normoxic: $n = 178$) or 3-4 (hypoxic: $n = 70$, normoxic: $n = 278$) mm, with most of the paths recorded in normoxic environments.

3.3.1 Average darting speed

Average darting speed (instantaneous speed > 10 mm/s) was significantly faster for larger amphipods (2-way ANOVA; F =10.339, $p < 0.0001$), but did not significantly vary between oxygen environments (2-way ANOVA; F =1.625, $p = 0.203$) (Fig. S8, Table S7). On average, amphipods > 4 mm swam 23% faster than 2-3 mm amphipods.

3.3.2 Frequency of hovering

Amphipods did not exhibit more frequent hovering behaviors in hypoxic relative to normoxic environments. Generalized linear model results indicated that neither amphipod length nor oxygen environment was a significant predictor of hovering frequency (Fig. S9, Table S8).

3.3.3 Amphipod abundance

Amphipod abundances were significantly lower in hypoxic environments. Amphipod abundances varied with oxygen concentration and size (Tweedie; oxygen: $p < 0.0001$, size: $p < 0.0001$) (Fig. 6, Table S9). On average, the abundance of amphipods 3-4 mm in length was 71% lower in hypoxic conditions versus normoxic conditions.

3.3.4 Markov chains

Of the four different transition probabilities, two had a percent change larger than 5% between hypoxic and normoxic environments (Fig. 7, highlighted in yellow). Generally, transition probabilities associated with darting behaviors were the same for all amphipods in hypoxic and normoxic environments. However, amphipods were in the hovering state for shorter

durations in hypoxic environments, consistent with the hypothesis that amphipod are leaving hypoxic areas faster.

3.3.5 Hidden Markov models

Model results did not show consistent trends across size, but overall amphipods were modeled to swim faster in hypoxic environments. For amphipods of all sizes, component 1 was 31% faster and component 2 was 13% faster in hypoxic environments. Model estimates from amphipods in hypoxic environments (especially amphipods 1-2 mm in length) are limited by the low number of recorded paths (Fig. 8, Table S10).

4. Discussion

Zooplankton are critical links in marine food webs and are thought to be informative indicators of ecosystem change (Richardson 2008; Mackas and Beaugrand 2010; Di Lorenzo and Ohman 2013). Zooplankton behaviors can alter vertical population distributions and trophic interactions, but it is difficult to assess these ecosystem impacts because methods for quantifying in situ zooplankton behaviors have been almost nonexistent. A primary goal of this study was to develop a novel methodology that combined three emerging technologies – in situ imaging, video-based tracking, and machine learning classification of individual zooplankton – to quantify in situ zooplankton abundances and behaviors. Our in situ video observations revealed significant changes in copepod swimming behaviors and amphipod abundances in response to hypoxic and acidified waters.

4.1 Copepod responses to environmental stress

Copepods in their natural environment significantly changed swimming speed when exposed to hypoxic and acidified conditions. All three characteristic copepod swimming behaviors (passive "drifting" (≤ 5 mm/s), "cruising" (> 5 mm/s and < 100 mm/s), and fast "jumping" (≥100 mm/s)) were altered in stressful conditions. Overall, within hypoxic and acidified conditions, copepods showed a 24% decrease in cruising speeds, a 53% decrease in the amount of time spent jumping, and a 95% increase in the amount of time spent drifting. Behavioral transition probabilities changed by as much as 25%. Consistent with previous laboratory observations that found swimming speed decreased in low oxygen conditions (Svetlichny et al 1998; Svetlichny et al 2000; Wyeth et al 2022), our results show that behavior changes similarly in the natural environment.

Different swimming behaviors incur significantly different metabolic costs. For example, the respiration rate of the cycloid copepod *Thermocyclops oithonoides* was almost nine times higher when jumping relative to its immobilized basal rate (Svetlichny et al 2022). Decreases in swimming speed, and in the amount of time spent in more metabolically costly swimming states such as cruising and jumping, are therefore likely to increase an individual's tolerance of oxygen stress by decreasing its metabolic demand (Svetlichny and Hubareva 2005; Svetlichny et al 2022). Slower swimming also affects trophic interactions with both higher and lower trophic levels by decreasing encounter rates (Van Duren and Videler 1996; Visser 2007). Because copepod swimming behavior trades off feeding, finding mates, and avoiding predation (Uchima and Hirano 1988; Tiselius and Jonsson 1990; Van Duren and Videler 1996), the changes we observed in swimming speed and transition probabilities may have profound effects on individual fitness and predator-prey interactions.

In the system we studied, temperature and oxygen were correlated, and temperature varied relatively little (9.7 to 10.9 °C), so we focused on oxygen as the primary explanatory environmental variable in our statistical analyses. However, temperature also strongly regulates metabolic demand (Roman et al 2019). While species vary, copepods' respiration rate is an approximately exponential function of temperature (Ikeda 1970; Svetlichny et al 2022). In stratified coastal systems, temperature and oxygen concentrations are typically higher in surface waters. In this study, the reduction of stress in normoxic conditions paired with the potential for increased feeding on phytoplankton near the surface may offset some of the increased metabolic costs associated with exposure to increased temperatures. Incorporating a broader range of temperatures into future in situ analyses will be an important next step.

Our video observations indicate that copepod abundance increased in hypoxic and acidified conditions. We hypothesized that copepod abundances would decrease in stressful water because previous work suggested that copepod distributions shift upwards when hypoxic bottom waters are present (Keister et al. 2000; Auel and Verheye 2007; Roman et al. 2012). However, mechanisms exist that could explain either increases or decreases in abundance within hypoxic conditions. In addition to the direct effects of low oxygen on copepods, which may cause decreases in abundance through mortality or avoidance, indirect effects such as changes in predator-prey interactions are also important in shaping copepod population distributions. When predators are present, hypoxic waters may serve as a refuge for zooplankton from more oxygen-sensitive predators (Taylor and Rand 2003; Ludsin et al. 2009) or may induce diel vertical migration in copepods (Bollens and Frost 1989), both of which may result in increased abundances within stressful waters. Increased drifting may reflect a behavioral strategy for using the hypoxic layer as refuge or a response to mitigate oxygen stress, potentially causing the

observed abundance increase. The presence of predators may also result in copepods suppressing swimming behaviors to make themselves less conspicuous and reduce predator-prey encounters (Buskey et al. 2012).

Our classification algorithm did not differentiate between calanoid and cyclopoid copepods, or among the diverse species within those orders. Copepods' swimming behaviors vary widely across species, feeding strategies, and sex (Greene 1988; Tiselius and Jonsson 1990; Kiørboe 2008). Calanoid copepods are generally cruise feeders while cyclopoid copepods are typically ambush predators (Tiselius and Jonsson 1990). However, even among calanoids there is significant variation in foraging strategies, ranging from stationary to continuous cruising (Greene 1988). Cyclopoid copepods are typically smaller in size, so maximum observed body length may be a rough proxy for differences in swimming behaviors across different orders. Copepod length had a significant effect on drifting frequency, with copepods in the 3-4 mm length bin being significantly more likely to transition into drifting than smaller copepods. While distinguishing taxa by size or identifying species with machine learning remains challenging, our study showed that, even at a coarse level, there are identifiable behavioral responses to hypoxia and acidification. Image classification algorithms and in situ imagery are rapidly improving, and there is reason to expect that more detailed analyses will be possible in the near future.

4.2 Amphipod responses to environmental stress

We observed an apparent 66% reduction in the abundance of amphipods within stressful waters. This could be due to avoidance of chemically stressful waters, to increased mortality rates, or to a combination of the two. Few previous studies have quantified the effects of hypoxia and acidification on amphipod distributions. However, consistent with our video-based

observations, Keister et al. 2020's net tow data showed that the gammarid amphipod *Cyphocaris challengeri* was less common at hypoxic stations relative to normoxic stations in Hood Canal. The penaeid shrimp *Metapenaeus ensis* (Wu et al. 2002) and the European brown shrimp *Crangon crangon* (Hagerman and Uglow 1979) were also reported to actively avoid hypoxic waters. Lower abundances of amphipods within stressful waters likely suggest lower availability to predators.

Globally, amphipods rank third in abundance behind copepods and euphausiids (Bowman 1960) and play important roles in marine food webs, particularly in polar systems where they are a key trophic link between mesozooplankton and higher trophic levels such as planktivorous fishes, seabirds, and marine mammals (Dalpadado et al. 2001; Węsławski and Legeżyńska 2002; Kraft et al. 2012). In Puget Sound, amphipods are an important source of food for numerous species of forage fish such as Pacific sand lance, surf smelt and three spine stickleback (Simenstad et al. 1988; Penttila 2007). Changes we observed in amphipod abundances may have cascading effects through the marine food web, potentially affecting the populations and vertical distributions of both their prey and their predators.

It is interesting, in view of the changes in amphipod abundances, that we did not observe significant changes in swimming speed in response to hypoxic and acidified conditions. Previous work from the Eastern Tropical North Pacific oxygen minimum zone has shown that metabolism is suppressed in hyperiid amphipods when exposed to hypoxia and low temperature (Elder and Seibel 2014). For amphipods, hovering may lead to sinking because they are relatively dense and rely on fast swimming to maintain their position in the water column. Because amphipods need to be darting to stay suspended, it is possible that darting individuals are better represented in the water column, as frequently hovering individuals disproportionately sink. Darting might be more

costly in stressful waters, and it is possible that decreased darting behaviors in hypoxic and acidified waters was one mechanism underlying the decreased amphipod abundances we observed in hypoxic and acidified conditions.

4.3 Modeled behaviors

Hidden Markov models, which do not require predefined swimming states (Patterson et al. 2008), identified changes in zooplankton swimming behaviors in response to environmental stress. The swimming speed components generated autonomously by our hidden Markov models were reasonably consistent with the mean speeds of behaviors we took from the literature. For copepods, "drifting" was defined as speeds < 5 mm/s and the 1st modeled speed components in normoxic conditions ranged from 4-7 mm/s. "Cruising" was defined as speeds > 5 mm/s and < 100 mm/s and the 2nd modeled speed components in normoxic conditions ranged from 14-17 mm/s. "Jumping" was defined as speeds >100 mm/s and the 3rd modeled speed components in normoxic conditions ranged from 42-50 mm/s. For amphipods, "hovering" was defined as speeds < 10 mm/s and the 1st modeled speed components in normoxic conditions ranged from 10-14 mm/s. "Darting" was defined as speeds > 10 mm/s and the 2nd modeled speed components in normoxic conditions ranged from 42-50 mm/s. Hidden Markov model estimates were impressively similar to our pre-defined parameters, highlighting how models may help automate data analysis in the future.

4.4 Conclusions

Environmental stressors, such as changes in dissolved oxygen and pH, are increasing in persistence and extent in coastal waters around the world. To adequately adapt and respond to

changing ocean conditions, we need an improved understanding of the lethal and sublethal effects of environmental stress on zooplankton. In this study, we developed a novel methodology combining in situ videos, particle tracking technology, and machine learning classification of zooplankton to quantify in situ zooplankton swimming and used it to ask whether zooplankton behaviorally respond to environmental stress.

Our in situ observations of zooplankton swimming behaviors showed that copepods exhibited significantly slower "cruising" speeds, were less likely to exhibit a fast "jumping" behavior, and remained longer in the passive "drifting" state than copepods in non-stressful conditions. Amphipods showed significantly decreased abundances within stressful conditions but, perhaps because of small sample sizes in stressful waters, we observed no consistent changes in amphipod swimming speed or transition probabilities.

The identification of video-based statistics quantifying changes in zooplankton population dynamics shows great promise as a diagnostic tool of ecological stress. Our results suggest that in situ changes in abundance, swimming speed, and transition probabilities might be useful in identifying and explaining potential shifts in population distributions and trophic dynamics. With these methodological advances, in situ video analyses is likely to be a cost-effective tool for coastal managers to monitor environmental change and predict trophic impacts.

Acknowledgements

The authors gratefully acknowledge Chris MacGregor for assisting with software development and ZooCAM operation. John Mickett deployed and maintained the Oceanic Remote Chemical Analyzer platform and Jan Newton provided the Oceanic Remote Chemical Analyzer mooring platform. Andrew Nutzhorn assisted developing the image library. Sandeep Jilla and Michael

Stanley developed the zooplankton identification algorithm and classifier. We thank the captain, ship and science crew of the R/V Rachel Carson. This work was funded by NSF Grant OCE-1657992 to J.E.K and D.G.

Literature Cited

Auel, H., and Verheye, H. M. 2007. Hypoxia tolerance in the copepod *Calanoides carinatus* and the effect of an intermediate oxygen minimum layer on copepod vertical distribution in the northern Benguela Current upwelling system and the Angola-Benguela Front. Journal of Experimental Marine Biology and Ecology **352**: 234–243. https://doi.org/10.1016/j.jembe.2007.07.020

Bates, D., Mächler, M., Bolker, B., and Walker, S. 2015. Fitting linear mixed-effects models using lem4. J Stat Softw **67**: 1−48.

Bollens, S. M., and Frost, B. W. 1989. Predator-induced diel vertical migration in a planktonic copepod. Journal of Plankton Research **11**: 1047–1065. https://academic.oup.com/plankt/article-abstract/11/5/1047/1537724

Bowman, T. E. 1960. The pelagic amphipod genus *Parathemisto* (Hyperiidea: Hyperiidae) in the North Pacific and adjacent Arctic Ocean. Proceedings of the United States National Museum **112**: 343–392. https://doi.org/10.1038/103074a0

Bradski, G. 2000. The OpenCV Library. Dr. Dobb's Journal of Software Tools **120**: 122-125.

Buskey, E. J., Lenz, P. H., and Hartline, D. K. 2012. Sensory perception, neurobiology, and behavioral adaptations for predator avoidance in planktonic copepods. Adaptive Behavior 20: 57–66. https://doi.org/10.1177/1059712311426801

Breitburg, D., and others. 2018. Declining oxygen in the global ocean and coastal waters. Science **359:** 1-11. https://doi.org/10.1126/science.aam7240

Campbell, R. W., Roberts, P. L., and Jaffe, J. 2020. The Prince William Sound Plankton Camera: a profiling in situ observatory of plankton and particulates. ICES Journal of Marine Science **77**: 1440-1445. https://doi.org/10.1093/icesjms/fsaa029

Chan, K. Y. K., and Grünbaum, D. 2010. Temperature and diet modified swimming behaviors of larval sand dollars. Marine Ecology Progress Series **415**: 49–59. https://doi.org/10.3354/meps08744

Cowen, R. K., and Guigand, C. M. 2008. In situ ichthyoplankton imaging system (ISIIS): System design and preliminary results. Limnology and Oceanography: Methods **6**: 126–132. https://doi.org/10.4319/lom.2008.6.126

Dalpadado, P., Borkner, N., Bogstad, B., and Mehl, S. 2001. Distribution of *Themisto* (Amphipoda) spp. in the Barents Sea and predator-prey interactions. ICES Journal of Marine Science **58**: 876–895. https://doi.org/10.1006/jmsc.2001.1078

Di Lorenzo, E., and Ohman, M. D. 2013. A double-integration hypothesis to explain ocean ecosystem response to climate forcing. Proceedings of the National Academy of Sciences of the United States of America **110**: 2496–2499. https://doi.org/10.1073/pnas.1218022110

Doney, S. C. 2010. The growing human footprint on the planet. Science **328**: 1512–1516. https://doi.org/10.1126/science.1185198

Dunne, J. P., Devol, A. H., and Emerson, S. 2002. The Oceanic Remote Chemical/Optical Analyzer (ORCA)-An Autonomous Moored Profiler. Journal of Atmospheric and Oceanic Technology **19**: 1709–1721. https://doi.org/https://doi.org/10.1175/1520-0426

Elder, L. E., and Seibel, B. A. 2014. Ecophysiological implications of vertical migration into oxygen minimum zones for the hyperiid amphipod *Phronima sedentaria*. Journal of Plankton Research **37**: 897–911. https://doi.org/10.1093/plankt/fbv066

Ellen, J. S., Graff, C. A., and Ohman, M. D. 2019. Improving plankton image classification using context metadata. Limnology and Oceanography: Methods **17**: 439–461. https://doi.org/10.1002/lom3.10324

Feely, R. A., and others. 2010. The combined effects of ocean acidification, mixing, and respiration on pH and carbonate saturation in an urbanized estuary. Estuarine, Coastal and Shelf Science **88**: 442–449. https://doi.org/10.1016/j.ecss.2010.05.004

Foster, S. D. and Bravington, M. V. 2013. A Poisson-Gamma model for analysis of ecological non-negative continuous data. Environmental and Ecological Statistics **20**: 533–552. https://doi.org/10.1007/s10651-012-0233-0

Frost, B. W. 1972. Effects of size and concentration of food particles on the feeding behavior of the marine planktonic copepod *Calanus pacificus*. Limnology and Oceanography **17**: 805–815.

Greene, C. H. 1988. Foraging tactics and prey-selection patterns of omnivorous and carnivorous calanoid copepods. Hydrobiologia **167/168**: 295–302. https://doi.org/10.1007/BF00026317

Hagerman, L., and Uglow, R. F. 1979. Heart and scaphognathite activity in the shrimp *palaemon adspersus rathke*. Ophelia **18**: 89–96. https://doi.org/10.1080/00785326.1979.10425492

Ikeda, T. 1970. Relationship between respiration rate and body size in marine plankton animals as a function of the temperature of habitat. Bull. Fac. Fish. Hokkaido Univ **21**: 91–112.

IPCC. 2023. Climate Change 2023: Synthesis Report. Contribution of Working Groups I, II and III to the Sixth Assessment Report of the Intergovernmental Panel on Climate Change [Core Writing Team, H. Lee and J. Romero (eds.)]. IPCC, Geneva, Switzerland, pp. 35-115, doi: 10.59327/IPCC/AR6-9789291691647

Keister, J. E., Houde, E. D., and Breitburg, D. L. 2000. Effects of bottom-layer hypoxia on abundances and depth distributions of organisms in Patuxent River, Chesapeake Bay. Marine Ecology Progress Series **205**: 43–59.

Keister, J. E., Winans, A. K., and Herrmann, B. E. L. 2020. Zooplankton community response to seasonal hypoxia: A test of three hypotheses. Diversity **12**: 1-16. https://doi.org/10.3390/d12010021

Kiørboe, T. 2008. Optimal swimming strategies in mate-searching pelagic copepods. Oecologia **155**: 179–192. https://doi.org/10.1007/s00442-007-0893-x

Kiørboe, T., Jiang, H., Gonçalves, R. J., Nielsen, L. T., and Wadhwa, N. 2014. Flow disturbances generated by feeding and swimming zooplankton. Proceedings of the National Academy of Sciences of the United States of America **111**: 11738–11743. https://doi.org/10.1073/pnas.1405260111

Kraft, A., Bauerfeind, E., Nöthig, E. M., and Bathmann, U. V. 2012. Size structure and life cycle patterns of dominant pelagic amphipods collected as swimmers in sediment traps in the eastern Fram Strait. Journal of Marine Systems **95**: 1–15. https://doi.org/10.1016/j.jmarsys.2011.12.006

Lard, M., Bäckman, J., Yakovleva, M., Danielsson, B., and Hansson, L. A. 2010. Tracking the small with the smallest - using nanotechnology in tracking zooplankton. PLoS ONE **5**: e13516. https://doi.org/10.1371/journal.pone.0013516

Lebedev, S. 2016. Hidden Markov Models in Python, with scikit-learn like API. https://github.com/hmmlearn/hmmlearn.

Lenth R. V. 2021. Emmeans: estimated marginal means, aka least-squares means. R package version 1.7.2. https:// CRAN.R-project.org/package=emmeans

Li, Y., and others. 2021. Toward in situ zooplankton detection with a densely connected YOLOV3 model. Applied Ocean Research **114**: 102783. https://doi.org/10.1016/j.apor.2021.102783

Liberzon A., Käufer T., Bauer A., Vennemann P., and Zimmer E. 2021 Open-PIV python package. https ://doi.org/10.5281/zenod o.593157

Ludsin, S. A., Zhang, X., Brandt, S. B., Roman, M. R., Boicourt, W. C., Mason, D. M., and Costantini, M. 2009. Hypoxia-avoidance by planktivorous fish in Chesapeake Bay: Implications for food web interactions and fish recruitment. Journal of Experimental Marine Biology and Ecology **381**: 121–131. https://doi.org/10.1016/j.jembe.2009.07.016

Maboloc, E. A., Batzel, G., Grünbaum, D., and Chan, K. Y. K. 2020. Vertical distribution of echinoid larvae in pH stratified water columns. Marine Biology **167**: 1–9. https://doi.org/10.1007/s00227-019-3629-7

Mackas, D. L., and Beaugrand, G. 2010. Comparisons of zooplankton time series. Journal of Marine Systems **79**: 286–304. https://doi.org/10.1016/j.jmarsys.2008.11.030

Melzner, F., and others. 2013. Future ocean acidification will be amplified by hypoxia in coastal habitats. Marine Biology **160**: 1875–1888. https://doi.org/10.1007/s00227-012-1954-1

Newton, J., and others. 2007. Hypoxia in Hood Canal: An overview of status and contributing factors. Proceedings of the 2007 Georgia Basin Puget Sound Research Conference. www.hoodcanal.washington.edu.

Ohman, M. D., and others 2019. Zooglider: An autonomous vehicle for optical and acoustic sensing of zooplankton. Limnology and Oceanography: Methods **17**: 69–86. https://doi.org/10.1002/lom3.10301

Orenstein, E. C., and others. 2020. The Scripps Plankton Camera system: A framework and platform for in situ microscopy. Limnology and Oceanography: Methods **18**: 681–695. https://doi.org/10.1002/lom3.10394

Park, S., Ahn, I. Y., Sin, E., Shim, J. H., and Kim, T. 2020. Ocean freshening and acidification differentially influence mortality and behavior of the Antarctic amphipod *Gondogeneia antarctica*. Marine Environmental Research **154**: 104847. https://doi.org/10.1016/j.marenvres.2019.104847

Patterson, T. A., Thomas, L., Wilcox, C., Ovaskainen, O., and Matthiopoulos, J. 2008. State-space models of individual animal movement. Trends in Ecology and Evolution **23**: 87–94. https://doi.org/10.1016/j.tree.2007.10.009

Penttila, D. 2007. Marine Forage Fishes in Puget Sound. Prepared for the Puget Sound Nearshore Partnership.

Richardson, A. J. 2008. In hot water: Zooplankton and climate change. ICES Journal of Marine Science **65**: 279–295. https://doi.org/10.1093/icesjms/fsn028

Roman, M. R., Brandt, S. B., Houde, E. D., and Pierson, J. J. 2019. Interactive effects of Hypoxia and temperature on coastal pelagic zooplankton and fish. Frontiers in Marine Science **6**: 1–18. https://doi.org/10.3389/fmars.2019.00139

Roman, M. R., Pierson, J. J., Kimmel, D., and Boicourt, W. C. 2012. Impacts of Hypoxia on Zooplankton Spatial Distributions in the Northern Gulf of Mexico. Estuaries and Coasts **35**: 1261–1269. https://doi.org/10.1007/s12237-012-9531-x

Simenstad, C. A., and others. 1988. Assemblage Structure, Microhabitat Distribution, and Food Web Linkages of Epibenthic Crustaceans in Padilla Bay National Estuarine Research Reserve, Washington. In NOAA Technical Report Series (Issue January).

Svetlichny, L., Larsen, P. S., and Kiørboe, T. 2020. Kinematic and Dynamic Scaling of Copepod Swimming. Fluids **5**: 1-28. https://doi.org/10.3390/fluids5020068

Svetlichny, L., Rudi Strickler, J., and Obertegger, U. 2022. Swimming and respiration in cyclopoid copepods *Thermocyclops oithonoides* and *Oithona davisae* and calanoid copepod *Paracalanus parvus*. Journal of Experimental Zoology Part A: Ecological and Integrative Physiology **337**: 835–851. https://doi.org/10.1002/jez.2643

Svetlichny, L. S., and Hubareva, E. S. 2005. The energetics of *Calanus euxinus*: Locomotion, filtration of food and specific dynamic action. Journal of Plankton Research **27**: 671–682. https://doi.org/10.1093/plankt/fbi041

Svetlichny, L. S., Hubareva, E. S., and Arashkevich, E. 1998. Physiological and behavioural response to hypoxia in active and diapausing stage V copepodites of *Calanus euxinus*. Special Issues Advances in Limnology **52**: 507–519.

Svetlichny, L. S., Hubareva, E. S., Erkan, F., and Gucu, A. C. 2000. Physiological and behavioral aspects of *Calanus euxinus* females (Copepoda: Calanoida) during vertical migration across temperature and oxygen gradients. Marine Biology **137**: 963–971. https://doi.org/10.1007/s002270000405

Taylor, J. C., and Rand, P. S. 2003. Spatial overlap and distribution of anchovies (Anchoa spp.) and copepods in a shallow stratified estuary. Aquatic Living Resources, 16: 191–196. https://doi.org/10.1016/S0990-7440(03)00012-3

Tiselius, P., and Jonsson, P. 1990. Foraging behaviour of six calanoid copepods: observations and hydrodynamic analysis. Marine Ecology Progress Series **66**: 23–33. https://doi.org/10.3354/meps066023

Uchima, M., and Hirano, R. 1988. Swimming behavior of the marine copepod *Oithona davisae*: internal control and search for environment. Marine Biology **99**: 47–56. https://doi.org/10.1007/BF00644976

Van Duren, L. A., and Videler, J. J. 1996. The trade-off between feeding, mate seeking and predator avoidance in copepods: Behavioural responses to chemical cues. Journal of Plankton Research **18**: 805–818. https://doi.org/10.1093/plankt/18.5.805

Visser, A. W. 2007. Motility of zooplankton: Fitness, foraging and predation. Journal of Plankton Research **29**: 447–461. https://doi.org/10.1093/plankt/fbm029

von Westernhagen, H., Rosenthal, H., Kerr, S., and Fürstenberg, G. 1979. Factors influencing predation of *Hyperoche medusarum* (Hyperiida: Amphipoda) on larvae of the Pacific herring *Clupea harengus pallasi*. Marine Biology **51**: 195–201. https://doi.org/10.1007/BF00386798

Węsławski, J. M., and Legeżyńska, J. 2002. Life cycles of some Arctic amphipods. Polish Polar Research **23**: 253–264.

Wu, R. S. S., Lam, P. K. S., and Wan, K. L. 2002. Tolerance to, and avoidance of, hypoxia by the penaeid shrimp (*Metapenaeus ensis*). Environmental Pollution **118**: 351–355. https://doi.org/10.1016/S0269-7491(01)00298-6

Wyeth, A. C., Grünbaum, D., and Keister, J. E. 2022. Effects of hypoxia and acidification on *Calanus pacificus*: behavioral changes in response to stressful environments. Marine Ecology Progress Series **697**: 15–29. https://doi.org/10.3354/meps14142

Figures

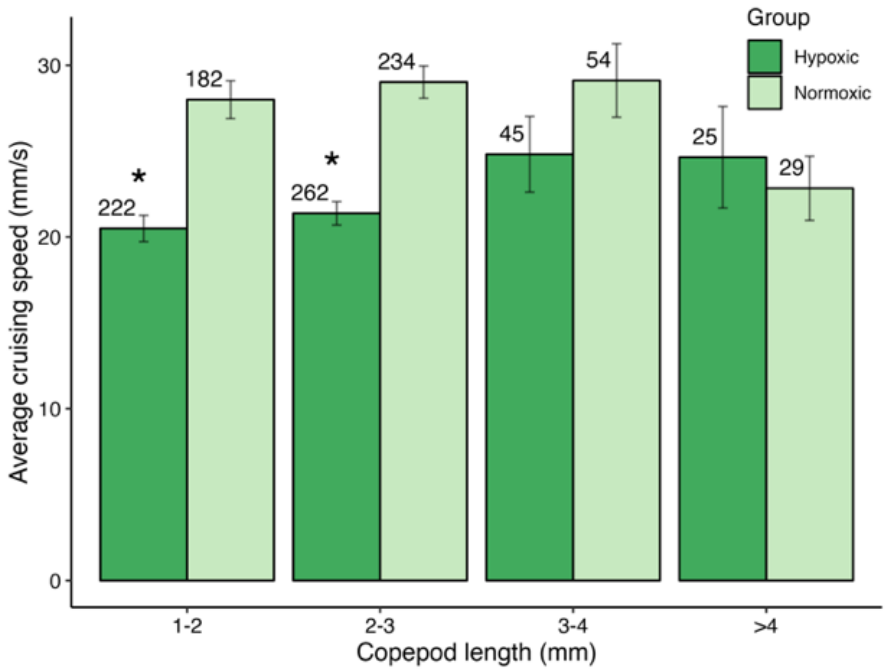

Figure 1. Mean (±SE) copepod "cruising" speed between hypoxic and normoxic environments for copepods 1-2, 2-3, 3-4, or >4 mm in length. There were significant differences between environments ($p < 0.0001$) but not sizes. The number of recorded copepod paths is printed above each bar. * Indicates a significant ($p < 0.05$) difference in pairwise comparisons between oxygen conditions within size bins.

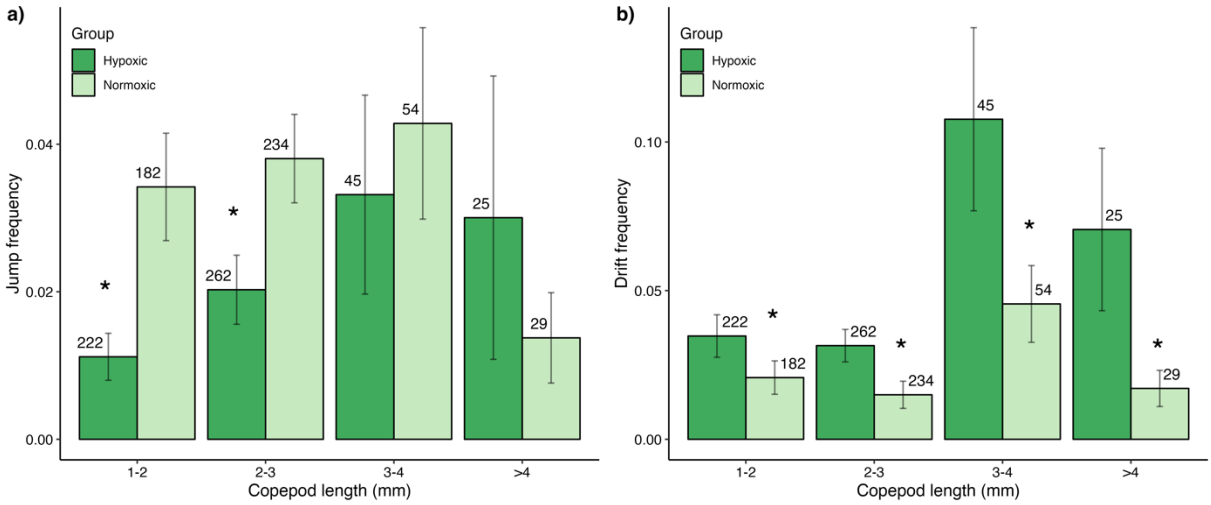

Figure 2. Mean (±SE) frequency of copepod behaviors in hypoxic and normoxic environments for copepods 1-2, 2-3, 3-4, or >4 mm in length. The number of recorded copepod paths are the same in both plots and are printed above each bar in (a). (a) Copepod jumping (>100 mm/s) frequency was significantly different between environments ($F_{3,151} = 12.12$, $p = 0.0005$) but not between sizes. (b) Copepod drifting (<5 mm/s) frequency was significantly different between environments and size ($F_{3,151} = 6.88$, $p = 0.0001$). * Indicates a significant ($p < 0.05$) difference in pairwise comparisons between oxygen conditions within the size bin.

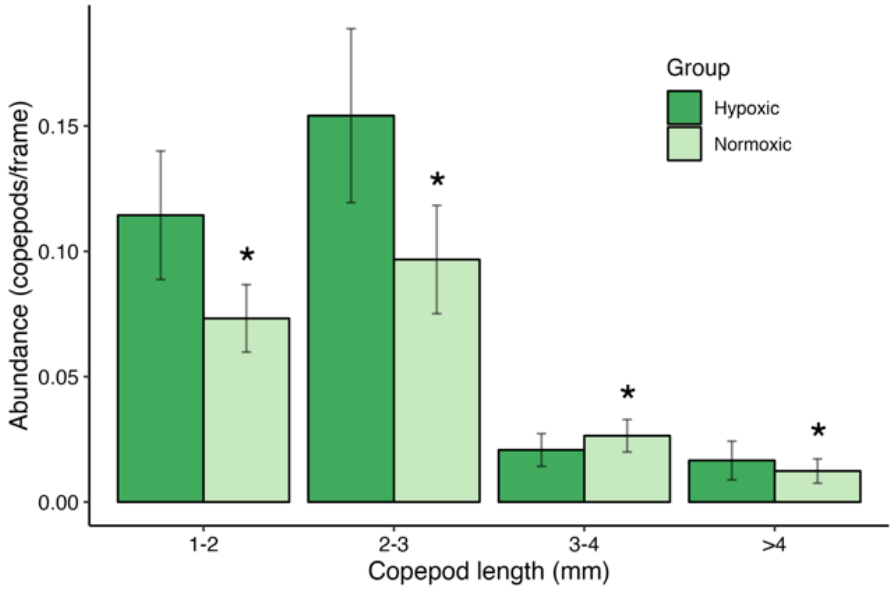

Figure 3. Mean (±SE) relative copepod abundances (copepods per frame) between hypoxic and normoxic environments for copepods 1-2, 2-3, 3-4, or >4 mm in length. Differences were significant between oxygen concentrations ($p = 0.037$) and sizes ($p < 0.0001$). * Indicates a significant ($p < 0.05$) difference in pairwise comparisons between oxygen conditions within the size bin.

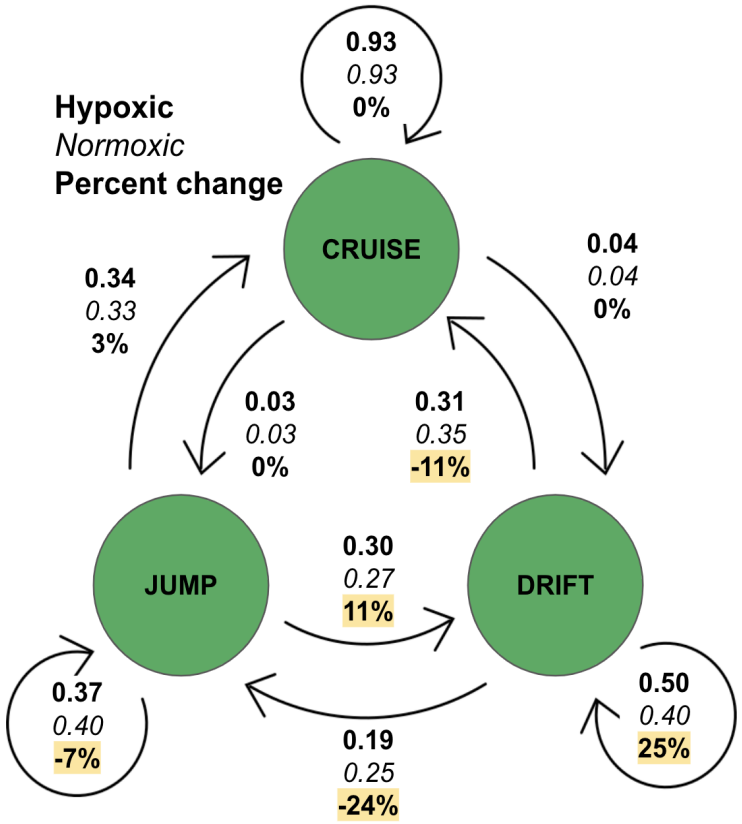

Figure 4. Markov chain probabilities for copepod transition probabilities between the three predefined swimming states: "drifting," "cruising," and "jumping." Transition probabilities in hypoxic environments are listed in bold and transition probabilities in normoxic environments are listed in italics. The percent change is listed underneath the transition probabilities and is highlighted if the percent change between environments is larger than 5%. A positive percent change means the transition was more likely to occur in hypoxic environments; a negative percent change means the transition was less likely to occur in hypoxic environments.

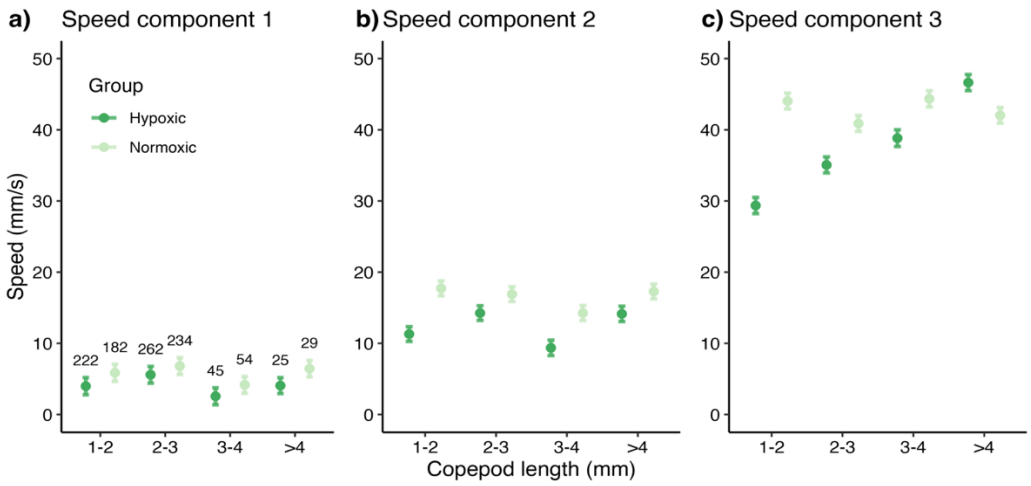

Figure 5. Mean (± SD) swimming speed for the three speed components determined by hidden Markov models for copepods in hypoxic and normoxic environments and 1-2, 2-3, 3-4, or >4 mm in length. The number of recorded copepod paths (same in all plots) are printed above each bar in (a).

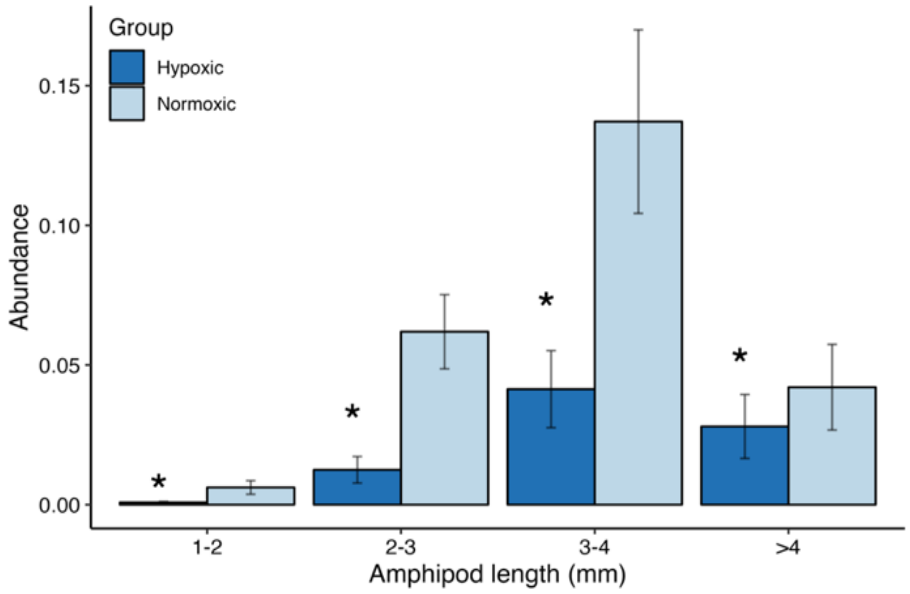

Figure 6. Mean (±SE) amphipod abundances (amphipods per frame) between hypoxic and normoxic environments for amphipods 1-2, 2-3, 3-4, or >4 mm in length. There were significant differences between oxygen environments ($p < 0.0001$) and size ($p < 0.0001$). * Indicates a significant ($p < 0.05$) difference in pairwise comparisons between oxygen conditions within each size bin.

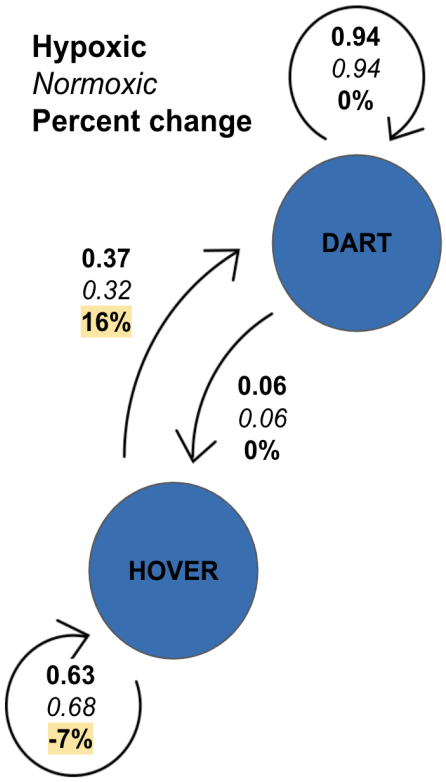

Figure 7. Markov chain for amphipod transition probabilities between the two predefined swimming states: "hovering" and "darting." Transition probabilities in hypoxic environments are listed in bold and transition probabilities in normoxic environments are listed in italics. The percent change is listed underneath the transition probabilities and is highlighted if the percent change between environments is larger than 5%. A positive percent change means the transition was more likely to occur in hypoxic environments; a negative percent change means the transition was less likely to occur in hypoxic environments.

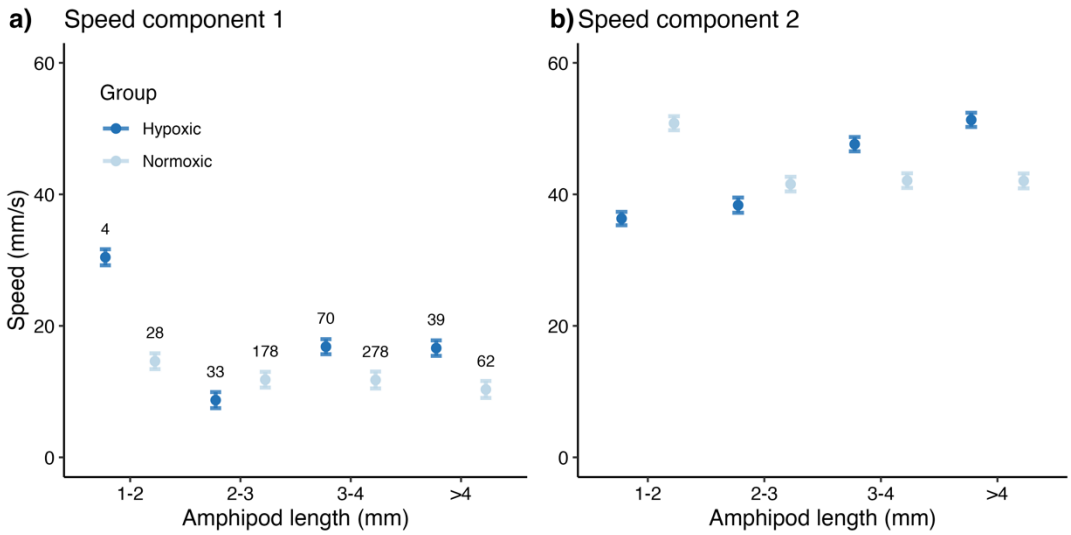

Figure 8. Mean (± SD) swimming speeds for the two speed components determined by hidden Markov models for amphipods in hypoxic and normoxic environments and 1-2, 2-3, 3-4, or >4 mm in length. The number of recorded amphipod paths (same in both plots) are printed above each bar in (a).

Chapter 3: Tidal exchange of zooplankton between intertidal eelgrass beds and pelagic waters

Wyeth, A.C., Keister J.E., Grünbaum, D., Yang, S., Burnett, N., Bolhmann, H.

Abstract

Eelgrass beds are important habitats, providing food and protection for juveniles of many species of fish. Successful foraging within beds is critical for juvenile fish to survive an important life history bottleneck and reach adulthood. Intertidal eelgrasses are tightly interconnected with neighboring pelagic environments through tides, which may transport pelagic species into nearshore environments. Despite the potential importance of pelagic zooplankton in juvenile fish diets, surprisingly little work has been done to estimate the transport of pelagic zooplankton into shallow subtidal habitats. Our study aimed to quantify abundances and variability of pelagic prey within eelgrass beds and quantify the potential role of eelgrass beds as sinks of pelagic zooplankton over the tidal cycle, for example through predation by juvenile fish. We conducted zooplankton net tows over 10 days along two transects within Padilla Bay National Estuary Research Reserve. Each transect included a station located offshore, within the tidal channel, and over the eelgrass bed. We measured high abundances of pelagic zooplankton within intertidal eelgrasses and found that 78% of the total number of unique species and lifestages recorded at the offshore stations were also present at the eelgrass stations. However, on average, pelagic species found only in deeper water offshore of eelgrass beds were significantly larger than species recorded at both stations. Over our 10-day sampling period, we recorded high spatial and temporal variability in zooplankton populations and found

that copepod abundances increased with both temperature and turbidity. To adequately protect coastal systems, managers need an improved understanding of the mechanisms that support the significant ecological and economic services these habitats provide. Future sampling efforts will need to account for the spatial and temporal heterogeneity we recorded to adequately assess changes in zooplankton dynamics in coastal systems.

1. Introduction

Eelgrasses are habitat-forming angiosperms that alter water flow, stabilize sediment, sequester carbon, and support diverse trophic structures. Eelgrass beds are known to serve ecosystem functions such as providing food and protection for juvenile fish and many other marine species (Thayer et al. 1975, Adams 1976). These functions are increasingly important in the context of declining populations of economically important fish species along the West Coast of North America (Noakes et al. 2000). For example, many juvenile anadromous fish feed and gain energy within eelgrass beds during their transition from estuaries to the open ocean, a life stage known to be associated with high rates of natural mortality (Bax 1983). Research has shown that growth rates increase with food availability (Neilson 1992) and that larger fish are less vulnerable to predation and have higher energy reserves to survive periods of limited food (Parker 1971). This indicates that successful foraging is critical to surviving this important life history bottleneck (Illing 2018). The need for a better understanding of the importance of feeding during juvenile stages has therefore focused attention on prey availability within critical habitats such as eelgrass beds.

Juvenile fish typically feed on a wide range of zooplankton, epifaunal invertebrates (such as harpacticoid copepods, amphipods, and polychaetes), and terrestrial insects that are commonly

found in eelgrass beds (Jackson et al. 2001, Kennedy et al. 2018). Preferred diets of fish vary among species, life stages, and locations (Bollens et al. 2010) and some species are plastic in diet when preferred prey are unavailable (Preikshot et al. 2010). Gut analyses from juvenile fish in and around eelgrass beds show that eelgrass-associated prey species are important dietary components, and considerable research has gone into quantifying those benthic and epibenthic invertebrate prey (Howard 1985, Simenstad 1988, Kennedy et al. 2018). However, gut analyses show pelagic zooplankton can also comprise significant components of juvenile fish diets, especially during the critical transition from estuarine to open waters (Adams 1976, Fulton 1985). Little is known about the abundance and distribution of pelagic zooplankton within eelgrass beds, the mechanisms which cause them to be present in these shallow intertidal environments, or their potential for enhancing the growth and survival of juvenile fish.

Intertidal eelgrasses are highly interconnected to neighboring pelagic environments through tides. Pelagic zooplankton, notably calanoid copepods, occur in high abundances in deeper waters offshore, and have high concentrations of essential fatty acids, making them excellent prey (Lee 1970, Saito 2000). Daily tides may transport pelagic species into nearshore environments and the tidal transport of pelagic zooplankton to eelgrass beds could be an important contribution to the productivity of the beds as nurseries for juvenile fish.

Climate change paired with increased anthropogenic pressure to coastal systems is driving environmental changes such as increases in temperature and turbidity in nearshore waters (Orth et al. 2006). To understand and predict how pelagic zooplankton might supplement eelgrass prey availability in the future, it is important to understand how environmental parameters currently impact zooplankton communities. Estuarine zooplankton communities have been shown to vary with a range of environmental parameters, including temperature and salinity

(Tackx et al. 2004, Chaalali et al. 2013). In intertidal systems, salinity is typically an important driver in shaping zooplankton community composition (Bollens et al. 2014). Additionally, evidence suggests that warmer waters decrease pelagic zooplankton abundances and shift community composition (Woodworth-Jefcoats 2017, Möllmann 2000, Möllmann 2005, Richardson 2008). As environmental parameters in coastal systems continue to change, it will be important to quantify the impacts of these changes on the influx of zooplankton into eelgrass beds.

Padilla Bay National Estuarine Research Reserve (NERR) in Washington State contains one of the largest eelgrass meadows in the U.S. and is one of many reserves hosting eelgrasses that provide habitat and food for numerous ecologically important species (Bulthuis 2010). Padilla Bay is a meso-tidal estuary with mixed semidiurnal tides and a mean tidal range of 1.6 m. Freshwater input is relatively low, with a maximum daily discharge that is less than 1% of the average tidal exchange to the bay. For this reason, tidal flushing is the main driver controlling water characteristics within Padilla Bay (Bulthuis 2010). It follows that pelagic prey may play an important role within Padilla Bay's nearshore ecosystem. However, very little is known about the influence of pelagic species within the bay.

The goal of this study was to contribute to a better understanding of pelagic zooplankton availability within Padilla Bay's eelgrasses by quantifying abundances and variability of offshore zooplankton in shallow subtidal eelgrass habitats, and by quantifying the role of eelgrass beds as potential sinks of pelagic zooplankton over the tidal cycle. Our hypotheses were: 1) flood tides transport offshore, pelagic zooplankton species into channels and over shallow subtidal eelgrass beds; 2) abundance and community composition of pelagic zooplankton in nearshore systems varies with temperature and salinity and; 3) over tidal cycles, eelgrass beds act as sinks of

pelagic species, possibly through consumption by juvenile fish. An improved understanding of the patterns of transport of pelagic species into intertidal habitats would help inform management goals aimed at maintaining eelgrass beds as productive nurseries for economically important fisheries throughout the Pacific Northwest.

2. Methods

2.1 Field Collections

Zooplankton net tow samples were collected over 10 days in June 2023 along two transects (Ploeg and Bayview) within Padilla Bay National Estuary Research Reserve (Fig. 1). Each transect consisted of three stations: a deep station outside of the bed, a station within a channel to the bed, and a shallower station over the eelgrass bed. A tidal replicate consisted of four samples (in chronological order): a sample from the deep station collected during low tide, a sample from the channel station collected during the flooding tide, a sample from the eelgrass station during high tide, and a sample from the channel station collected during the ebbing tide (Table S1 & S2). Eight tidal replicates were collected in duplicate along each of the two transects totaling 128 zooplankton samples. All samples were collected during the daytime.

During the sampling period, there was a mixed semidiurnal tide with a larger tidal cycle during the day and a much smaller tidal cycle overnight. Assuming that minimal exchange happened over the smaller 1-2 ft tide, and to allow for maximum time for predation to take place over the beds, samples were collected during the larger flooding and ebbing tides (Fig 2). Tidal heights for all the sampling days can be found in supplemental materials (Fig. S1). To sample the same period of the tidal cycle in each tidal replicate, stations were sampled at specific tidal heights to quantify the relative flux of pelagic zooplankton into and out of eelgrass beds over the

tidal cycle. Deep stations were sampled around a 0 ft tidal height, channel stations (both flooding and ebbing) were sampled around a 2.5 ft tidal height, and eelgrass stations were sampled around a 7 ft tidal height.

Zooplankton samples were collected using a 50-cm diameter, 200-µm mesh single ring net. At deep stations, the net was pulled vertically from 1 m off the bottom to the surface targeting a rate of 30 m/min. To sample within the eelgrass beds, the net was slowly lowered to the bottom of the water column and, after 30 seconds for disturbed water to be replaced by flow, pulled vertically to the surface targeting a rate of 30 m/min. Multiple net tows were collected at eelgrass stations and preserved in aggregate to increase the biomass collected in shallow waters. At channel stations, vertical tows were not possible due to strong currents, so samples were collected using oblique tows pulled from approximately 1 m from the bottom to the surface. The target depth was estimated using the amount of line out and the wire angle. A TSK flow meter was used to measure the volume of water filtered for vertical tows and a Sea-Gear MF315 flow meter was used for oblique tows. The median volume of water filtered in deep stations was 3.0 m^3. In channel stations during flooding tide the medium volume was 3.9 m^3 and during ebbing tide the medium volume was 4.8 m^3. In eelgrass stations the medium volume sampled was 1.8 m^3. All samples were preserved in 5% buffered formalin in seawater and returned to the laboratory for analysis.

Environmental data were provided by the National Estuary Research Reserve's System Wide Monitoring Program. The program consists of an array of standardized instrumentation and data collection protocols that enable collection of near real-time data that are comparable across national reserves. Data were collected every 15 minutes by two water quality moorings located at the Bayview and Ploeg channel stations and a weather station located at the southern end of

Padilla Bay. The moorings collected data such as temperature, salinity, depth, and turbidity while the weather station collected wind speed and wind direction data. Because of the location of the moorings, environmental data were only available for the two channel stations.

2.2 Laboratory Analysis

Zooplankton samples were examined under a dissecting microscope for taxonomic composition, abundance, and size measurements using morphological characteristics. Rare and large organisms (> 5 mm) were removed from the whole sample for identification. Then, three small aliquots were taken from the whole sample using a Stempel pipette. The volume of the small aliquot was determined by the volume required to quantitatively sample ~200-250 copepods. A larger aliquot (10 times the volume of the smaller aliquots) was taken to quantify rarer and mid-sized species that may have been undersampled in the smaller aliquots. Organisms in the subsamples were counted, identified, and staged as follows.

Among copepods, all adults were identified to species and sex. All C1-C5 copepodite stages were grouped. Cyclopoid copepodites were identified to species. For larger calanoid species (with adult females > 2 mm), copepodites were identified to species. For smaller calanoid species (adult females < 2 mm), copepodites were not speciated and were classed as either a "small" (< 0.5mm) or "medium" (≥ 0.5mm) calanoid copepodite. All copepod nauplii stages were grouped and not speciated. Harpacticoids were grouped and were not speciated or staged. Select non-copepod groups were also counted: amphipods, barnacle cyprid larvae and nauplii, bivalve veligers, *Caprellidae*, chaetognaths, crab megalops and zoeae, ctenophores, echinoderm pluteus larvae, euphausiid furcilia and nauplii, cladocera (*Evadne* and *Podon*), fish eggs,

gastropod adults and veligers, *Obelia* medusae, *Oikopleura*, Oweniidae larvae, polychaete larvae, and shrimp.

The density of organisms (number of individuals m^{-3}) was calculated from sample counts using the volume of water filtered by each net tow. We used zooplankton density (number normalized by filtered volume) as a metric for abundance. To assess repeatability of plankton sampling and counting protocols, the replicate samples from eight back-to-back net tows were quantified. Based on the consistency of these results, subsequent counting was done for only a single replicate tow (Fig. S2).

2.3 Statistical Analyses

2.3.1 Potential transport of offshore zooplankton to eelgrass beds

We addressed the hypothesis that flood tides transport offshore, pelagic zooplankton species into channels and over shallow subtidal eelgrass beds by comparing zooplankton communities collected offshore and above eelgrasses at high tide. To do this, we calculated the mean (± 1 standard error) abundance of each unique species and lifestage combination for the deep and eelgrass stations. A 2-way ANOVA was performed to compare the effect of species/lifestage and station on copepod and non-copepod abundances. Abundances were log10(X+0.001) transformed to mitigate distorting the relationship between zeros and small values in the dataset (McCune and Grace 2002). Visual inspection of residual plots did not reveal any deviations from normality or homoscedasticity. A Tukey pairwise comparison of species/lifestage and station was generated using the R package **emmeans** (version 1.7.3) (Lenth 2021).

In addition to comparing the abundances of individual zooplankton species in the deep and eelgrass stations, we also compared the number of species and the average length of species that were sampled at each station. The mean (± 1 standard error) number of copepod species/life stages observed at each station was calculated, and an ANOVA was used to test for significant effects of the station on the number of species/life stages. Copepod species/lifestages that were observed only at deep stations were grouped separately from species that were observed at both deep and eelgrass stations, and the mean (± 1 standard error) length of each group (deep-only, deep & eelgrass) was calculated. Data on typical average lengths of the copepod species and lifestages collected were obtained from monthly samples collected throughout Puget Sound as part of another study (the Puget Sound Zooplankton Monitoring Program). The mean length of the copepods in these two groups were statistically compared using a non-parametric Kruskal-Wallis test.

To compare how the relative abundance of copepods at deep and eelgrass stations varied with size, we plotted the response ratio of each copepod species against size. The response ratio was determined by calculating the log response ratio (LRR) (Eq. 1) for each species/lifestage combination using the R package **metafor** (version 4.6-0) (Viechtbauer 2010). A small number was added to the mean abundances to put all the samples within the valid domain of a log-transformation. A small value of 0.001 was chosen to be in the same order of magnitude as the lowest observed non-zero abundances.

(1) $$LRR = \ln((\bar{x}_{eel} + 0.001) / (\bar{x}_{deep} + 0.001))$$

Log response ratios for each copepod species/stage were plotted against the average length of the species/stage. Mixed-effects models were used to determine the effect of copepod length and transect (Bayview, Ploeg) on the response ratios.

2.3.2 Variability in offshore zooplankton populations

To identify potential differences in zooplankton community composition between transects and among tidal phases we calculated zooplankton community ordinations. First, zooplankton abundances were converted to proportions and arcsin square root transformed. Then the relative distance of samples based on the zooplankton assemblages were represented in two-dimensional spaces using a Non-metric Multidimensional Scaling (NMDS) analysis using a Bray-Curtis similarity index and the **vegan** package in R (version) (Oksanen et al. 2024). A Permutational Analysis of Variance (PERMANOVA) was generated to determine the effect of tide and transect on community composition. The significance of permutational variance components was tested using 999 permutations. Zooplankton species and environmental parameters that were significantly correlated with an NMDS axis were calculated using the R package **vegan** (version 2.6-6.1) (Oksanen et al. 2024).

In addition to testing for variation through space, we also tested for correlations between zooplankton abundances in the channels and environmental parameters. Multiple linear regressions were used to test the effects of different environmental metrics on average copepod and non-copepod abundances, using the R package **lme4** (version 1.1-35.5) (Bates et al. 2015). Abundances were log(X+0.001) transformed to prevent distorting the relationship between zeros and small values in the dataset (McCune and Grace 2002). Nested models were generated using different combinations of temperature, salinity, depth, turbidity, wind speed, and wind direction as continuous variables and transect and tidal phase as factors. Wind speed and wind direction showed multicollinearity ($r = 0.72$), as did temperature and depth ($r = 0.68$). The best models were identified using AIC values. A visual inspection of residual plots did not reveal any

deviations from normality or homoscedasticity. Model predictions and confidence intervals were back transformed and plotted over raw abundance data.

2.3.3 Eelgrass beds as potential sinks of offshore zooplankton

We addressed the hypothesis that, over tidal cycles, eelgrass beds act as sinks of pelagic species, by comparing abundances of pelagic communities in channels during ebb tides relative to flood tides. To do this, we calculated the mean (± 1 standard error) abundance of each species/lifestage collected at channel samples during each tidal phase (flooding or ebbing). A 2-way ANOVA was performed to compare the effect of tidal phase and species on copepod and non-copepod species abundances. An additional 2-way ANOVA was performed to compare the effect of transect and tidal phase on total copepod abundances. Abundances were log10(X+0.001) transformed and visual inspection of residual plots did not reveal any deviations from normality or homoscedasticity. Tukey pairwise comparisons of species/lifestage and tidal phase as well as transect and tidal phase were generated using the R package **emmeans**.

To compare how the relative abundance of copepods during flooding and ebbing tides varied among species, we calculated the log response ratio (Eq. 1) for each species/lifestage combination using the R package **metafor** (version 4.6-0) (Viechtbauer 2010). A small number was added to the mean abundance since log-transformations of zero are not defined. A small value of 0.001 was chosen so as to be in the same order of magnitude as the lowest observed non-zero abundances. Mixed-effects models were used to determine the effect of tidal phase and transect (Bayview, Ploeg) on log response ratios.

3. Results

3.1 Potential transport of offshore zooplankton to eelgrass beds

We observed high abundances of pelagic zooplankton in intertidal habitats. A total of 42 copepod species/lifestage combinations were recorded cumulatively on the two transects (Bayview and Ploeg) (Table 1, Fig. S3- S4). On the Bayview transect, the average abundance of *Acartia longiremis* females, *Pseudocalanus moultoni* females, and *Pseudocalanus* males was significantly higher at the deep station relative to the eelgrass station and the average abundance of *Acartia hudsonica* males, harpacticoids, and *Oithona similis* copepodites was significantly higher in the eelgrass station relative to the deep station. On the Ploeg transect, the average abundance of *Calanus* copepodites, *Centropages abdominalis* females, *Paracalanus* females, *Paracalanus* males, and *Pseudocalanus moultoni* females was significantly higher in the deep station and the average abundance of *Acartia hudsonica* females, *Acartia hudsonica* males, and harpacticoids was significantly higher in the eelgrass station (Table 1).

A total of 26 non-copepod species/lifestage combinations were recorded cumulatively on the two transects (Table S3). On the Bayview transect, the average abundance of chaetognaths was significantly higher at the deep station relative to the eelgrass station and on the Ploeg transect, the average abundances of crab zoeae, *Evadne*, and *Podon* was higher at the deep station while the average abundances of barnacle nauplii, bivalve veligers, gastropod veligers, and *Oikopleura* was higher at the eelgrass station.

There was no significant difference between the number of species/lifestage combinations identified at deep stations and eelgrass stations on either transect (ANOVA, $p = 0.072$) (Fig. 3a). Copepod species/stage combinations that were recorded only at the deep stations were significantly longer than copepods found at both deep and eelgrass stations

(Kruskal-Wallis, $p < 0.0001$) (Fig. 3b). On the Bayview transect, no copepod species/lifestages were recorded only at the eelgrass station. On the Ploeg transect, male *Eurytemora* were recorded only at the eelgrass station in low abundances (not shown in Fig. 3b but included in statistical analyses). All the non-copepod species/lifestage combinations were found at both the deep and eelgrass stations.

A log response ratio > 0 indicates higher copepod abundances within eelgrass beds, a log response ratio < 0 indicates higher copepod abundances at deep stations, and 95% confidence intervals that cross 0 indicate similar abundances at both sites (Fig. 4). A total of 25 species/lifestage combinations had confidence intervals that crossed zero. Species such as *Aetideus armatus, Calanus pacificus, Calanus marshallae, Centropages abdominalis, Epilabidocera longipedata, Metridia pacifica, Microcalanus, Oncaeidae, Oithona atlantica,* and *Pseudocalanus* had log response ratios < 0. Harpacticoids, *Acartia hudsonica,* and *Eurytemora* had log response ratios > 0. Mixed-effect model results indicated that average copepod length, but not transect, was a significant predictor of the log response ratio of copepod abundances (length: p = 0.01, transect: p = 0.63), with the log response ratio decreasing with increasing copepod length (Fig. 4).

3.2 Variability in offshore zooplankton populations

3.2.1 Zooplankton variation across tidal replicates

Overall, there was no significant difference in total copepod abundance between flooding and ebbing tides (p-value = 0.98). Abundances of different lifestages also showed no significant differences between flooding and ebbing tides (adult females: p-value = 0.40, adult males: p-value = 0.81, copepodites: p-value = 0.52) (Fig. S5). We observed large inter-tidal variability on

both transects in total copepod abundance (Fig. 5) and relative copepod abundances (Fig. S6). The only significant difference in total copepod abundances observed was higher copepod abundances in Ploeg ebbing tide than Bayview ebbing tide (p-value = 0.035) (Fig. S7). There was no significant difference in total non-copepod abundance between flooding and ebbing tides (p-value = 0.80) (Fig. S8).

3.2.2 Zooplankton variation across sampling transects

There were distinctly different zooplankton community compositions between sampling transects. Ordinations comparing zooplankton assemblages between transects at channel stations and deep stations resulted in two-dimensional ordinations that fit the data well (final stresses of 0.13 and 0.06, respectively) (Fig. 6). Sampling transect (Bayview, Ploeg) was a significant predictor of zooplankton community composition (PERMANOVA, channel sites: p-value = 0.002, deep sites: p-value = 0.01). Zooplankton species/lifestages that were significantly correlated with an NMDS axis (p-value < 0.01) are plotted. An ordination comparing zooplankton assemblages between transects and tidal phases at the channel stations showed no significant effect of tidal phases (Fig. S9). At the channel stations, no environmental parameters were significantly correlated with an NMDS axis (Table S4).

3.2.3 Zooplankton variation with environmental parameters

In addition to differing between transects, we found that copepod abundances varied with temperature and turbidity. The best linear model included transect, water temperature, turbidity, and wind direction as predictors of total copepod abundance. However, only transect (p-value = 0.044), temperature (p-value = 0.035), and turbidity (p-value = 0.017) were significant. Total

copepod abundances were significantly higher on the Ploeg transect and abundances increased with increasing temperature and turbidity (Fig. 7). At a turbidity reading of 4 NTU on the Ploeg transect, copepod abundances were predicted to be 64% higher in waters with a temperature of 18 °C versus 14 °C (3748 versus 2282 ind/m3, respectively). At a water temperature of 15 °C on the Ploeg transect, copepod abundances were predicted to be 67% higher in waters with turbidity readings of 4 NTU versus 2 NTU (4180 versus 2502 ind/m3, respectively). For non-copepod species, the best linear model included transect and turbidity. However, only turbidity (*p*-value = 0.002) was a significant predictor of non-copepod abundance (Fig. S10).

3.3 Eelgrass beds as potential sinks of offshore zooplankton

Samples collected from the channel stations during flooding and ebbing tides were quantitatively compared to assess whether pelagic species had higher abundances going into or coming out of the eelgrass beds over the tidal cycle. A total of 33 copepod species/lifestage combinations were recorded at the channel stations on the two transects (Bayview and Ploeg) (Table 2, Fig. S11 & S12). On the Bayview transect, the average abundance of *Acartia longiremis* females was significantly higher within flooding tides than ebbing tides. On the Ploeg transect the average abundance of *Acartia longiremis* males, *Calanus* copepedites, and *Pseudocalanus newmani* females was significantly higher within ebbing tides than flooding tides (Table 2). A total of 21 non-copepod species/lifestage combinations were recorded on the two transects (Bayview and Ploeg) (Table S5). On the Bayview transect, the average abundance of *Evande* and *Polychaete* larvae was significantly higher within flooding tides than ebbing tides. On the Ploeg transect, the average abundance of shrimp zoea was significantly higher within ebbing tides than flooding tides.

A log response ratio > 0 indicates higher relative abundances within ebbing tides, a log response ratio < 0 indicates higher copepod relative abundances within flooding tides and 95% confidence intervals that cross 0 indicate similar abundances at both sites (Fig. 8). On average, species such as *Calanus marshallae* copepodites, *Eucalanus bungii* copepodites, *Eurytemora* copepodites, and *Oncaedae* copepodites had log response ratios < 0 while *Centropages abdominalis* males, *Oncaedae* males, *Pseudocalanus newmani* females, and *Tortanus discaudatus* adults had log response ratios > 0 (Fig. 8). Trends for a given species/lifestage combination sometimes differed across the two sites.

On average, non-copepod species such as amphipods, *Euphausiid* nauplii, and *Polychaeta* had positive log response ratios while *Caprellidae*, crab megalopae, *Euphausiid* nauplii, fish eggs, and *Oweniidae* larva had negative log response ratios (Fig. 9).

4. Discussion

In this study, we aimed to quantify abundances and variability of pelagic prey within Padilla Bay National Estuary Research Reserve's eelgrass beds and quantify the role of eelgrass beds as potential sinks of pelagic zooplankton over the tidal cycle, potentially due to predation by juvenile fish. Our analysis of zooplankton samples on two transects (Bayview and Ploeg) within Padilla Bay revealed high but variable abundances of pelagic zooplankton within intertidal eelgrasses and found systematic variation of zooplankton populations with certain environmental parameters.

4.1 Potential transport of offshore zooplankton to eelgrass beds

Many pelagic species recorded in Padilla Bay were found at both the deep and eelgrass stations. Around 78% of the unique species/lifestage combinations recorded at the deep stations were also recorded at the eelgrass stations, and 29% of the species/lifestage combinations had 95% confidence intervals for LRR that crossed zero, indicating copepods had relatively similar abundances at the two stations. The pelagic species with the highest abundances in the eelgrass beds were *Acartia hudsonica*, unspeciated calanoid copepodites, *Acartia longiremis*, *Oithona similis*, *Pseudocalanus* ssp., *Paracalnus* ssp., *Centropoges abdominalis*, *Ditrichocorycaeus anglicus*, and *Epilabidocera longipedata*. Genera such as *Paracalanus*, *Acartia*, and *Centropages* have been recorded in other eelgrass systems and were consumed by juvenile fish in laboratory studies (Fulton 1985). Because pelagic species are not typically able to survive exposure during low tides, the high abundances of pelagic species within intertidal eelgrasses suggests transport of these species from deep to intertidal waters over the previous tidal cycle.

However, not all pelagic species recorded at the deep stations were also recorded at the eelgrass stations. Pelagic copepods recorded only at the deep stations were significantly longer than pelagic copepods recorded at both stations. We speculate that the mechanisms preventing these species from entering the eelgrass beds occurred before reaching the tidal channels. The relationship between tidal transport and length could result from differences in species' swimming behaviors. Many of the species we recorded at deep stations undergo a behavior called diel vertical migration (Palomares-García et al. 2013; Daase et al. 2016), and generally the strength of migrations increases with copepod size (Ohman & Romagnan 2016). It is possible that larger copepods were deeper in the water column during daytime flooding tides and therefore less likely to be horizontally advected with the tides. If this is the case, we might expect

to see higher concentrations of larger pelagic species in the eelgrass beds during nighttime high tides.

The higher abundances of smaller pelagic species has trophic implications for nearshore food webs. Larger calanoid copepods are known for their large lipid sacs, making them energy-rich prey (Saito 2000). If larger pelagic species are less abundant or absent in eelgrass beds, it raises questions about the nutritional quality of pelagic species in nearshore systems compared to in deeper waters and whether the higher abundance of smaller species can compensate for their lower lipid content (Ljungström et al. 2020). While we tried to sample the eelgrass beds as early into the flooding tide as possible, the boat could not travel over the eelgrass beds with less than two meters of water. Therefore, we cannot rule out that larger species were preferentially removed from the water column during flooding tides through mechanisms such as predation. However, if this were the case we would have expected to observe these species in the channels during flooding tides, which we did not.

4.2 Variability in offshore zooplankton populations

We observed large spatial variability, with significant differences in the zooplankton abundances and community composition between the two sampling transects. We observed significantly higher total copepod abundances at Ploeg than at Bayview. Model estimates from LiveOcean (MacCready et al. 2021) indicate that, during flooding tides, water may enter Padilla Bay through Guemes Channel and then flow northward from the Bayview transect toward the Ploeg transect. We speculate that higher abundances on the Ploeg transect could be explained by the accumulation of pelagic species in front of Samish Island by tidal currents. In addition to differences driven by circulation, Bayview and Ploeg differ in parameters such as water currents,

residence times, depth, density of eelgrass, and other environmental variables. These differences can structure habitat use and therefore predator-prey interactions (Jackson et al. 2001), which could also drive changes in zooplankton populations even over small spatial scales.

Along with differences in abundance, we observed significant differences in zooplankton community composition between the two sampling transects. Interestingly, some of the same species that were significant in structuring community differences between the Bayview and Ploeg transects at the channel stations were also significant in structuring differences between the two transects at the deep stations. Generally, the species associated with Bayview were more nearshore-oriented species (*Acartia hudsonica*, harpacticoids, crab zoea, and barnacle nauplii), while the species associated with Ploeg were more pelagic (*Acartia longiremis*). To our knowledge, there has been little work looking at current dynamics within Padilla Bay (Bulthuis 2010). However, it is possible that the northern and southern parts of Padilla Bay are flooded by water from different sources (possibly from the North in Ploeg and from the West in Bayview), potentially containing different zooplankton communities. An alternative hypothesis is that one water mass enters Padilla Bay but is modified as it moves through the estuary during flooding tides, resulting in differences between the two transects.

In addition to spatial variability, we also observed large variability in zooplankton abundances between consecutive tidal cycles. Copepod abundances varied by up to a factor of two between consecutive days. Large variation across consecutive tides makes it hard to detect significant changes in copepod abundances over the tidal cycle. Zooplankton are known in many contexts to be "patchy," meaning that they often exhibit large variability over small spatial and temporal scales in the ocean. The formation of zooplankton patches requires an aggregation mechanism, which could include physical mechanisms such as convergent currents (Woodson

and Litvin 2015), biological mechanisms such as swimming behaviors (Folt and Burns 1999, Chen at al. 2021), or a combination of the two. While the focus of numerous research studies, zooplankton patch dynamics are still poorly understood, especially in coastal systems with strong tidal influences (Mahara et al. 2021). Our study highlights that sampling protocols will likely require multiple sites with several sampling times per tidal cycle to document patterns of variability.

Finally, our models showed that total copepod abundances increased with both turbidity and temperature. Turbidity can alter predator-prey interactions by altering the optical properties of the water (Aksnes et al. 2004) and decreasing foraging efficiency of predators such as visually-feeding fish (Lunt & Smee 2020). Additionally, diel vertically migrating copepods such as *Paracalanus* and *Acartia* have been shown to form aggregations within a couple centimeters of the bottom during the day (Fulton 1984; Metillo et al. 2019) where they may be able to avoid net tows. In cases when high turbidity is due to resuspended sediment, diel vertically migrating copepods are likely also displaced higher in the water column (Chazarreta et al. 2015). Temperature can alter population dynamics by increasing individuals' metabolic demands, potentially resulting in changes in swimming behaviors, such as decreased swimming speeds, decreasing interactions with predators. (Hirche 1987, Zhao et al. 2020). Over shorter time periods, temperature could be acting as a proxy for other processes impacting copepod abundances, such as the source of water flooding into the eelgrass beds or the residence time of the water above eelgrasses. Both temperature and turbidity are changing with climate change and human impacts (Orth et al. 2006). An improved understanding of the relationship between these parameters and zooplankton dynamics will inform how to manage nearshore foodwebs under future conditions.

4.3 Eelgrass beds as potential sinks of offshore zooplankton

Few studies have tried to quantify changes in pelagic zooplankton abundances within intertidal areas. Of the handful of studies that have, a few reported evidence of predation over the tidal cycle (Kimmerer & McKinnon 1989; Mazumder et al. 2009), but most did not find significant changes over the tidal cycle and observed large variability between tides (Houser & Dennis 1996; Rawlinson et al. 2005; Lehman et al. 2010). While some studies occurred over longer timescales and variability was attributed to seasonal changes, others found highly variable zooplankton densities over a 48-hour period with copepod abundances changing by an order of magnitude over a day (Houser & Dennis 1996). We hypothesized that predation over eelgrass beds is a dominant determinant of zooplankton abundances at the Padilla Bay eelgrass beds. To test this hypothesis, we compared the abundances of pelagic communities in channels during ebb tides relative to flood tides. Pelagic zooplankton were more abundant during flooding tides in some tidal cycles and during ebbing tides in others. If there were reductions over the tidal cycle, differences were likely masked by the large inter-tidal and inter-channel variability we observed over the 10-day sampling period.

We found that prey were intermittently present at high densities, but we could not document significant reductions consistent with predation. While reductions were statistically undetectable, the high abundances of pelagic species within eelgrass beds may still be ecologically important to fish. Studies have shown that fish foraging success is a function of prey abundance, with foraging success increasing with abundances (Noda et al. 1992). Zooplankton abundances and community compositions were markedly different between the two transects, and another explanation for this is that fish populations, and therefore predation pressure, differed across the two transects. Several species of economically important fish, such as salmon

have been in sharp decline along the West Coast (Noakes et al. 2000). Additional research monitoring the presence and diet composition of juvenile fish utilizing different habitats within Padilla Bay would help identify the characteristics that are important in shaping productive foraging habitats.

4.4 Conclusions

Estuaries and coastal systems such as eelgrass beds provide critical habitats for juvenile fish and numerous other ecologically important species. Reserves such as the Padilla Bay National Estuarine Research Reserve are tasked with monitoring and protecting coastal systems from human impact and further degradation. To adequately protect coastal systems, managers need an improved understanding of the mechanisms that support the important ecological and economic services these habitats provide. Our research aimed to improve our understanding of the mechanistic drivers shaping pelagic prey availability within eelgrass beds. We found evidence of transport of pelagic species into intertidal habitats and measured large spatial and temporal variability, as well as changes in zooplankton populations with temperature and turbidity. Future sampling efforts within coastal reserves will need to account for the spatial and temporal heterogeneity we recorded to adequately assess changes in zooplankton dynamics.

Literature Cited

Adams, S. M. (1976). Feeding Ecology of Eelgrass Fish Communities. Transactions of the American Fisheries Society, 105(4), 514–519.

Aksnes, D. L., Nejstgaard, J., Sædberg, E., & Sørnes, T. (2004). Optical control of fish and zooplankton populations. Limnology and Oceanography, 49(1), 233–238. https://doi.org/10.4319/lo.2004.49.1.0233

Bates, D., Mächler, M., Bolker, B., and Walker, S. 2015. Fitting linear mixed-effects models using lem4. J Stat Softw 67: 1−48.

Bax, N. J. (1983). Early marine mortality of marked juvenile chum salmon (Oncorhynchus keta) released into Hood Canal, Puget Sound, Washington, in 1980. Canadian Journal of Fisheries and Aquatic Sciences, 40(4), 426–435. https://doi.org/10.1139/f83-061

Bollens, S. M., Breckenridge, J. K., Cordell, J. R., Simenstad, C. A., & Kalata, O. (2014). Zooplankton of tidal marsh channels in relation to environmental variables in the upper San Francisco Estuary. Aquatic Biology, 21(3), 205–219. https://doi.org/10.3354/ab00589

Bollens, S. M., vanden Hooff, R., Butler, M., Cordell, J. R., & Frost, B. W. (2010). Feeding ecology of juvenile pacific salmon (oncorhynchus spp.) in a northeast pacific fjord: Diet, availability of zooplankton, selectivity for prey, and potential competition for prey resources. Fishery Bulletin, 108(4), 393–407.

Bulthuis, D. A. (2010). The Ecology of Padilla Bay Washington: An Estuarine Profile of a National Estuarine Research Reserve. In Washington State Department of Ecology.

Chaalali, A., Chevillot, X., Beaugrand, G., David, V., Luczak, C., Boët, P., Sottolichio, A., & Sautour, B. (2013). Changes in the distribution of copepods in the Gironde estuary: A warming and marinisation consequence? Estuarine, Coastal and Shelf Science, 134, 150–161. https://doi.org/10.1016/j.ecss.2012.12.004

Chazarreta, J., Hoffmeyer, M. S., Cuadrado, D. G., & Berasategui, A. A. (2015). Tidal effects on short-term mesozooplankton distribution in small channels of a temperate-turbid estuary, Southwestern Atlantic. Brazilian Journal of Oceanography, 63(2), 83–92. https://doi.org/10.1590/S1679-87592015076806302

Chen, B., Masunaga, E., Smith, S. L., & Yamazaki, H. (2021). Diel vertical migration promotes zooplankton horizontal patchiness. Journal of Oceanography, 77(1), 123–135. https://doi.org/10.1007/s10872-020-00564-4

Daase, M., Hop, H., & Falk-Petersen, S. (2016). Small-scale diel vertical migration of zooplankton in the High Arctic. Polar Biology, 39(7), 1213–1223. https://doi.org/10.1007/s00300-015-1840-7

Davenport, J., Barnett, P. R. O., & McAllen, R. J. (1997). Environmental Tolerances of Three Species of the Harpacticoid Copepod Genus Tigriopus. Journal of the Marine Biological Association of the United Kingdom, 1997, 3–16.

Folt, C. L., & Burns, C. W. (1999). Biological drivers of zooplankton patchiness Box 1. Why is scale important? (Vol. 14, Issue 8).

Fulton, R. S. (1985). Predator-Prey Relationships in an Estuarine Littoral Copepod Community. Ecology, 66(1), 21–29.

Fulton, R. S. I. (1984). Distribution and Community Structure of Estuarine Copepods. Estuaries, 7(1), 38–50.

Gao, Y., Jiang, Z., Du, M., Fang, J., Jiang, W., & Fang, J. (2019). Photosynthetic and metabolic responses of eelgrass Zostera marina L. to short-term high-temperature exposure. Journal of Oceanology and Limnology, 37(1), 199–209. https://doi.org/10.1007/s00343-019-7319-6

Hirche, H. J. (1987). Temperature and plankton II. Effect on respiration and swimming activity in copepods from the Greenland Sea. Marine Biology, 94(1), 347–356. https://doi.org/10.1007/BF00392894

Houser, D. S., & Dennis, A. M. (1996). Zooplankton Dynamics in an Intertidal Salt-Marsh Basin. Estuaries, 19(3), 659–673.

Howard, R. K., & Koehn, J. D. (1985). Population dynamics and feeding ecology of pipefish (Syngnathidae) associated with eelgrass beds of western port, victoria. Marine and Freshwater Research, 36(3), 361–370. https://doi.org/10.1071/MF9850361

Illing, B., Moyano, M., Berg, J., Hufnagl, M., & Peck, M. A. (2018). Behavioral and physiological responses to prey match-mismatch in larval herring. Estuarine, Coastal and Shelf Science, 201, 82–94. https://doi.org/10.1016/j.ecss.2016.01.003

Jackson, E. L., Rowden, A. A., Attrill, M. J., Bossey, S. J., & Jones, M. B. (2001). The Importance of Seagrass Beds as a Habitat for Fishery Species. Oceanography and Marine Biology: An Annual Review, 39, 269–303.

Kennedy, L. A., Juanes, F., & El-Sabaawi, R. (2018). Eelgrass as Valuable Nearshore Foraging Habitat for Juvenile Pacific Salmon in the Early Marine Period. Marine and Coastal Fisheries, 10(2), 190–203. https://doi.org/10.1002/mcf2.10018

Kimmerer, W. J., & McKinnon, A. D. (1989). Zooplankton in a marine bay. III. Evidence for influence of vertebrate predation on distributions of two common copepods. Marine Ecology Progress Series, 53, 21–35.

Lee, R. F., Nevenzel, J. C., & Paffenhöfer, G. (1970). Wax Esters in Marine Copepods. Science, 167(3924), 1510–1511.

Lehman, P. W., Mayr, S., Mecum, L., & Enright, C. (2010). The freshwater tidal wetland Liberty Island, CA was both a source and sink of inorganic and organic material to the San Francisco Estuary. Aquatic Ecology, 44(2), 359–372. https://doi.org/10.1007/s10452-009-9295-y

Lenth R. V. 2021. Emmeans: estimated marginal means, aka least-squares means. R package version 1.7.2. https:// CRAN.R-project.org/package=emmeans

Ljungström, G., Claireaux, M., Fiksen, Ø., & Jørgensen, C. (2020). Body size adaptation under climate change: Zooplankton community more important than temperature or food abundance in model of a zooplanktivorous fish. Marine Ecology Progress Series, 636, 1–18. https://doi.org/10.3354/meps13241

Lunt, J., & Smee, D. L. (2020). Turbidity alters estuarine biodiversity and species composition. ICES Journal of Marine Science, 77(1), 379–387. https://doi.org/10.1093/icesjms/fsz214

MacCready, P., McCabe, R. M., Siedlecki, S. A., Lorenz, M., Giddings, S. N., Bos, J., Albertson, S., Banas, N. S., & Garnier, S. (2021). Estuarine Circulation, Mixing, and Residence Times in the Salish Sea. Journal of Geophysical Research: Oceans, 126(2). https://doi.org/10.1029/2020JC016738

Mahara, N., Pakhomov, E. A., Dosser, H. V., & Hunt, B. P. V. (2021). How zooplankton communities are shaped in a complex and dynamic coastal system with strong tidal influence. Estuarine, Coastal and Shelf Science, 249. https://doi.org/10.1016/j.ecss.2020.107103

Mazumder, D., Saintilan, N., & Williams, R. J. (2009). Zooplankton inputs and outputs in the saltmarsh at Towra Point, Australia. Wetlands Ecology and Management, 17, 225–230. https://doi.org/10.1007/s11273-008-9102-x

McCune, B. & Grace, J.B. (2002) Analysis of Ecological Communities. MjM Software Design, Gleneden Beach, OR, USA

Metillo, E. B., Nishikawa, J., Ross, O. B. H., Yoshida, T., Md. Yusoff, F., Kuppan, P., Ohtsuka, S., Mulyadi, Sekiguchi, H., Toda, T., & Nishida, S. (2019). Diel patterns of Zooplankton community structure in nearshore waters of different substrates off Tinggi and Sibu Islands, Malaysia, with special reference to Copepods. Aquatic Ecosystem Health and Management, 22(1), 86–102. https://doi.org/10.1080/14634988.2018.1505139

Mochida, K., Hano, T., Onduka, T., Ito, K., & Yoshida, G. (2019). Physiological responses of eelgrass (Zostera marina) to ambient stresses such as herbicide, insufficient light, and high water temperature. Aquatic Toxicology, 208(July 2018), 20–28. https://doi.org/10.1016/j.aquatox.2018.12.018

Nielsen, J. L. (1992). Microhabitat-specific foraging behavior, diet, and growth of juvenile coho salmon. Transactions of the American Fisheries Society, 121, 617–634. https://doi.org/10.1577/1548-8659(1992)121<0617:mfbdag>2.3.co;2

Noakes, D. J., Beamish, R. J., & Kent, M. L. (2000). On the decline of Pacific salmon and speculative links to salmon farming in British Columbia. Aquaculture, 183(3–4), 363–386. https://doi.org/10.1016/S0044-8486(99)00294-X

Noda, M., Kawabata, K., Gushima, K., & Kakuda, S. (1992). Importance of zooplankton patches in foraging ecology of the planktivorous reef fish *Chromis chrysurus* (Pomacentridae) at Kuchinoerabu Island, Japan. Marine Ecology Progress Series, 87, 251–263.

Ohman, M. D., & Romagnan, J. B. (2016). Nonlinear effects of body size and optical attenuation on Diel Vertical Migration by zooplankton. Limnology and Oceanography, 61(2), 765–770. https://doi.org/10.1002/lno.10251

Oksanen J, Simpson G, Blanchet F, Kindt R, Legendre P, Minchin P, O'Hara R, Solymos P, Stevens M, Szoecs E, Wagner H, Barbour M, Bedward M, Bolker B, Borcard D, Carvalho G, Chirico M, De Caceres M, Durand S, Evangelista H, FitzJohn R, Friendly M, Furneaux B, Hannigan G, Hill M, Lahti L, McGlinn D, Ouellette M, Ribeiro Cunha E, Smith T, Stier A, Ter Braak C, Weedon J (2024). _vegan: Community Ecology Package_. R package version 2.6-6.1, <https://CRAN.R-project.org/package=vegan>.

Orth, R. J., Carruthers, T. J. B., Dennison, W. C., Duarte, C. M., Fourqurean, J. W., Heck, K. L., Hughes, A. R., Kendrick, G. A., Kenworthy, W. J., Olyarnik, S., Short, F. T., Waycott, M., & Williams, S. L. (2006). A global crisis for seagrass ecosystems. BioScience, 56(12), 987–996. https://doi.org/10.1641/0006-3568(2006)56[987:AGCFSE]2.0.CO;2

Palomares-García, R. J., Gómez-Gutiérrez, J., & Robinson, C. J. (2013). Winter and summer vertical distribution of epipelagic copepods in the Gulf of California. Journal of Plankton Research, 35(5), 1009–1026. https://doi.org/10.1093/plankt/fbt052

Parker, R. R. (1971). Size Selective Predation Among Juvenile Salmonid Fishes in a British Columbia Inlet. Journal of the Fisheries Research Board of Canada, 28(10), 1503–1510. https://doi.org/10.1139/f71-231

Preikshot, D. B., Beamish, R. J., & Sweeting, R. M. (2010). Changes in the Diet Composition of Juvenile Sockeye Salmon in the Strait of Georgia from the 1960s to the Present. North Pacific Anadromous Fish Commission, 1285(October). https://doi.org/10.13140/RG.2.2.22410.88001

Puget Sound Zooplankton Monitoring Program, University of Washington, Chan Laboratory, https://karenchanlab.org/pszmp/

Rawlinson, K. A., Davenport, J., & Barnes, D. K. A. (2005). Tidal exchange of zooplankton between Lough Hyne and the adjacent coast. Estuarine, Coastal and Shelf Science, 62(1–2), 205–215. https://doi.org/10.1016/j.ecss.2004.08.018

Richardson, A. J. (2008). In hot water: Zooplankton and climate change. ICES Journal of Marine Science, 65(3), 279–295. https://doi.org/10.1093/icesjms/fsn028

Saito, H., & Kotani, Y. (2000). Lipids of four boreal species of calanoid copepods: Origin of monoene fats of marine animals at higher trophic levels in the grazing food chain in the subarctic ocean ecosystem. Marine Chemistry, 71(1–2), 69–82. https://doi.org/10.1016/S0304-4203(00)00041-4

Simenstad, C. A., Cordell, J. R., Wissmar, R. C., Fresh, K. L., Schroder, S. L., Carr, M., Sanborn, G., & Burg, M. (1988). Assemblage Structure, Microhabitat Distribution, and Food Web Linkages of Epibenthic Crustaceans in Padilla Bay National Estuarine Research Reserve, Washington. In NOAA Technical Report Series (Issue January).

Tackx, M. L. M., De Pauw, N., Van Mieghem, R., Azémar, F., Hannouti, A., Van Damme, S., Fiers, F., Daro, N., & Meire, P. (2004). Zooplankton in the Scheide estuary, Belgium and the Netherlands. Spatial and temporal patterns. Journal of Plankton Research, 26(2), 133–141. https://doi.org/10.1093/plankt/fbh016

Thayer, G. W., Wolfe, D. A., & Williams, R. B. (1975). The impact of man of seagrass systems. American Scientist, 63(3), 288–296. https://doi.org/10.1007/BF01060519

Viechtbauer W (2010). “Conducting meta-analyses in R with the metafor package.” Journal of Statistical Software, 36(3), 1–48. doi:10.18637/jss.v036.i03.

Woodson, C. B., & Litvin, S. Y. (2015). Ocean fronts drive marine fishery production and biogeochemical cycling. Proceedings of the National Academy of Sciences of the United States of America, 112(6), 1710–1715. https://doi.org/10.1073/pnas.1417143112

Zerebecki, R. A., & Sorte, C. J. B. (2011). Temperature tolerance and stress proteins as mechanisms of invasive species success. PLoS ONE, 6(4). https://doi.org/10.1371/journal.pone.0014806

Zhao, Q., Liu, S., & Niu, X. (2020). Effect of water temperature on the dynamic behavior of phytoplankton–zooplankton model. Applied Mathematics and Computation, 378, 125211. https://doi.org/10.1016/j.amc.2020.125211

Tables

Table 1. Abundances (individuals / m^3) (± SE) of copepod species recorded at the deep and eelgrass stations on the two sampling transects. Abundances are in bold if there was a significance difference ($p > 0.05$) between deep and eelgrass abundances on that transect.

		Bayview		**Ploeg**	
Taxa	**Lifestage**	**Deep**	**Eelgrass**	**Deep**	**Eelgrass**
Acartia hudsonica	Female, Adult	299 ± 149.6	379 ± 64.2	**125 ± 73.1**	**854 ± 163.4**
	Male, Adult	**242 ± 112.2**	**471 ± 62.7**	**122 ± 65.6**	**912 ± 178.5**
Acartia longiremis	Female, Adult	**110 ± 28.8**	**45 ± 16.0**	238 ± 79.3	89 ± 24.8
	Male, Adult	144 ± 28.9	163 ± 41.0	366 ± 79.5	164 ± 32.2
Aetideus armatus	Copepodite	0 ± 0	0 ± 0	1.1 ± 1.1	0 ± 0
Bradyidius saanichi	Copepodite	1 ± 0.7	0 ± 0	0 ± 0	0 ± 0
Calanoida (medium)	Copepodite	1377 ± 152.9	2089 ± 291.7	2262 ± 562.7	2285 ± 280.5
Calanoida (small)	Copepodite	182 ± 46.4	303 ± 53.7	286 ± 108.1	208 ± 34.8
Calanus spp.	Copepodite	30 ± 6.5	31 ± 9.4	**40 ± 7.1**	**11 ± 4.5**
Calanus pacificus	Female, Adult	0.7 ± 0.7	0 ± 0	0 ± 0	0 ± 0
	Male, Adult	0 ± 0	1 ± 1.2	1 ± 1.3	0 ± 0
Centropages abdominalis	Copepodite	49 ± 5.0	43 ± 10.0	46 ± 11.8	31 ± 13.4
	Female, Adult	6 ± 1.4	5 ± 1.8	**6 ± 2.1**	**1 ± 0.7**
	Male, Adult	4 ± 1.5	3 ± 1.5	3 ± 1.9	3 ± 1.2
Ditrichocorycaeus anglicus	Copepodite	32 ± 12.2	36 ± 5.1	18 ± 3.3	17 ± 4.0
	Female, Adult	27 ± 10.7	21 ± 7.9	10 ± 3.8	10 ± 5.8
	Male, Adult	23 ± 3.8	42 ± 9.3	12 ± 4.7	17 ± 6.0
Epilabidocera longipedata	Copepodite	27 ± 10.2	35 ± 10.4	50 ± 19.5	48 ± 17
	Female, Adult	0.1 ± 0	0.1 ± 0.1	0 ± 0	0 ± 0
Eurytemora	Female, Adult	1 ± 0.8	6 ± 3.4	1 ± 1.1	5 ± 1.6
	Male, Adult	1 ± 1.2	2 ± 1.6	0 ± 0	7 ± 3.3
Harpacticoida	Unknown	**38 ± 11.3**	**1758 ± 441.2**	**9 ± 5.6**	**625 ± 195.0**
Metridia pacifica	Copepodite	4 ± 1.3	0 ± 0	0 ± 0	0 ± 0
	Female, Adult	0.8 ± 0.6	0 ± 0	0 ± 0	0 ± 0
	Male, Adult	0 ± 0	0 ± 0	0.3 ± 0.2	0 ± 0
Microcalanus spp.	Female, Adult	3 ± 1.1	0 ± 0	0.6 ± 0.6	0 ± 0
Oithona atlantica	Female, Adult	0.6 ± 0.6	0 ± 0	0 ± 0	0 ± 0
Oithona similis	Copepodite	**33 ± 9.7**	**69 ± 23.0**	30 ± 12.6	17 ± 8.5
	Female, Adult	34 ± 8.6	45 ± 13.0	18 ± 6.7	9 ± 5.4
	Male, Adult	9 ± 2.2	14 ± 4.7	1 ± 1.1	1 ± 1.0
Oncaeidae	Copepodite	3 ± 1.1	4 ± 2.9	4 ± 2.3	1 ± 1.0
	Female, Adult	5 ± 3.1	0.6 ± 0.6	0.9 ± 0.6	2 ± 2.0
	Male, Adult	0.7 ± 0.7	3 ± 1.8	0 ± 0	0 ± 0
Paracalanus spp.	Female, Adult	53 ± 11.5	70 ± 14.8	**80 ± 17.7**	**36 ± 14.8**
	Male, Adult	9 ± 3.4	4 ± 3.7	**9 ± 4.9**	**4 ± 2.9**
Pseudocalanus moultoni	Female, Adult	**61 ± 26.0**	**20 ± 7.8**	**7 ± 2.4**	**3 ± 1.5**
Pseudocalanus newmani	Female, Adult	16 ± 3.2	13 ± 5.4	4 ± 1.9	0.7 ± 0.7
Pseudocalanus (large)	Male, Adult	7 ± 3.5	4 ± 2.6	3 ± 2.8	0 ± 0
Pseudocalanus (small)	Male, Adult	**105 ± 25.3**	**25 ± 8.5**	33 ± 7.1	9 ± 3.1
Tortanus discaudatus	Copepodite	4 ± 1.4	10 ± 2.0	6 ± 2.7	7 ± 2.7
	Female, Adult	0.2 ± 0.1	0.2 ± 0.1	0 ± 0	0 ± 0
	Male, Adult	1 ± 0.9	2 ± 0.9	0.3 ± 0.2	2 ± 1.4

Table 2. Abundances (individuals / m^3) (± SE) of copepod species recorded at the channel stations during flooding and ebbing tides on the two sampling transects. Abundances are in bold if there was a significance (p-value < 0.05) difference between flooding and ebbing tides on that transect.

		Bayview		**Ploeg**	
Taxa	**Lifestage**	**Flood (ind / m3)**	**Ebb (ind / m3)**	**Flood (ind / m3)**	**Ebb (ind / m3)**
Acartia hudsonica	Female, Adult	1165 ± 531.3	528 ± 155.5	775 ± 234.6	848 ± 229.8
	Male, Adult	926 ± 456.3	636 ± 256.7	799 ± 270.0	1227 ± 327.1
Acartia longiremis	Female, Adult	**24 ± 8.4**	**10 ± 3.5**	6 ± 26.9	66 ± 16.9
	Male, Adult	57 ± 17.9	43 ± 15.0	**52 ± 18.8**	**91 ± 41.1**
Calanoida (medium)	Copepodite	1703 ± 527.1	1321 ± 259.1	1747 ± 324.9	2517 ± 357.5
Calanoida (small)	Copepodite	301 ± 93.2	168 ± 62.4	238 ± 43.7	305 ± 77.5
Calanus	Copepodite	4 ± 2.7	3 ± 1.3	**3 ± 1.5**	**19 ± 6.8**
Centropages abdominalis	Copepodite	7 ± 2.8	3 ± 1.5	15 ± 4.4	31 ± 8.5
	Female, Adult	0.7 ± 0.7	0.7 ± 0.7	0.6 ± 0.3	1 ± 1.1
	Male, Adult	0 ± 0	0 ± 0	0 ± 0	1 ± 1.1
Ditrichocorycaeus anglicus	Copepodite	18 ± 10.3	8 ± 1.8	14 ± 4.9	29 ± 6.8
	Female, Adult	7 ± 2.6	3 ± 1.8	5 ± 1.8	5 ± 2.0
	Male, Adult	6 ± 2.6	9 ± 4.3	17 ± 5.7	25 ± 5.8
Epilabidocera longipedata	Copepodite	8 ± 5.0	6 ± 1.8	27 ± 8.7	36 ± 9.7
Eucalanus bungii	Copepodite	1 ± 1.0	0 ± 0	0 ± 0	0 ± 0
Eurytemora	Copepodite	11 ± 10.3	0 ± 0	0 ± 0	0 ± 0
	Female, Adult	12 ± 5.5	3 ± 2.0	58 ± 19.2	34 ± 14.9
	Male, Adult	7 ± 2.9	6 ± 4.0	84 ± 36.2	28 ± 6.7
Harpacticoida	Unknown	189 ± 54.7	155 ± 80.5	129 ± 36.1	201 ± 61.7
Oithona similis	Copepodite	11 ± 4.5	22 ± 11.6	9 ± 3.8	22 ± 8.3
	Female, Adult	22 ± 3.9	28 ± 10.0	10 ± 2.7	22 ± 7.3
	Male, Adult	5 ± 2.6	5 ± 1.5	0.9 ± 0.9	4 ± 1.6
Oncaeidae	Copepodite	1 ± 1	1 ± 0.9	0.3 ± 0.3	0 ± 0
	Female, Adult	0 ± 0	0 ± 0	1 ± 0.8	1 ± 1.4
	Male, Adult	0 ± 0	0.4 ± 0.4	0 ± 0	0 ± 0
Paracalanus	Female, Adult	12 ± 3.3	12 ± 3.9	36 ± 10.9	48 ± 18.7
	Male, Adult	0.5 ± 0.5	3 ± 0.9	12 ± 4.9	19 ± 6.4
Pseudocalanus moultoni	Female, Adult	3 ± 1.2	3 ± 2.1	3 ± 2.3	9 ± 4.6
Pseudocalanus newmani	Female, Adult	0 ± 0	1 ± 1.2	**0 ± 0**	**9 ± 3.3**
Pseudocalanus (small)	Male, Adult	4 ± 2.4	3 ± 1.3	10 ± 3.9	35 ± 11.8
Pseudocalanus (large)	Male, Adult	0 ± 0	0 ± 0	2 ± 1.5	2 ± 1.2
Tortanus discaudatus	Copepodite	4 ± 1.4	5 ± 1.9	6 ± 2.4	9 ± 4.2
	Male, Adult	0 ± 0	0 ± 0	0.1 ± 0	0.1 ± 0

Figures

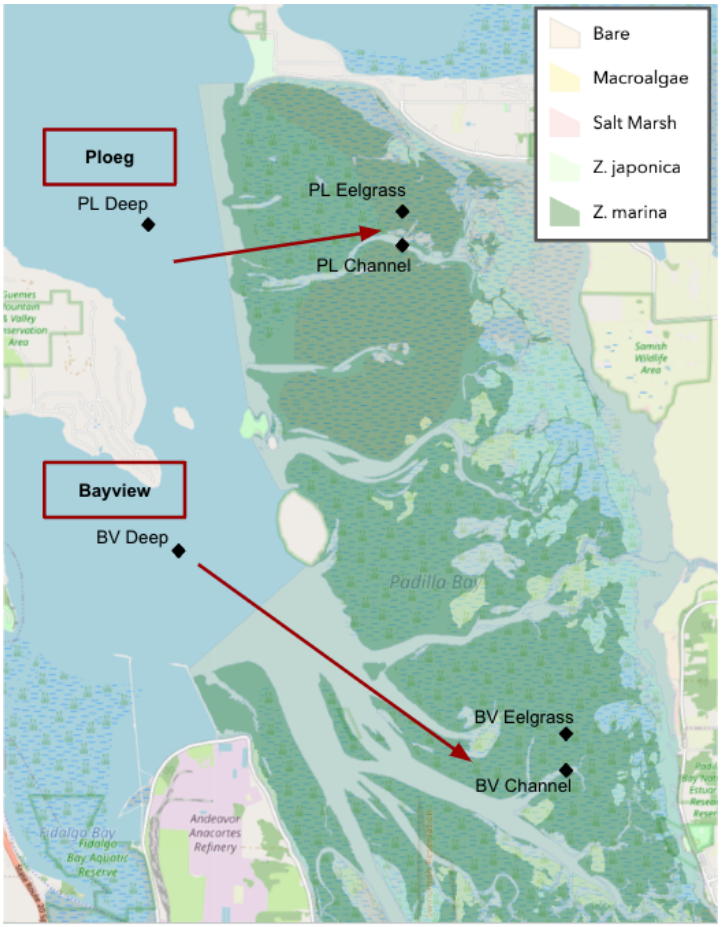

Figure 1. Map of Padilla Bay National Estuarine Research Reserve, Washington. Arrows designate the two sampling transects where zooplankton samples were collected in June 2023. The basemap and habitat layers (colors) were sourced from the Padilla Bay NERR Geospatial Research Database.

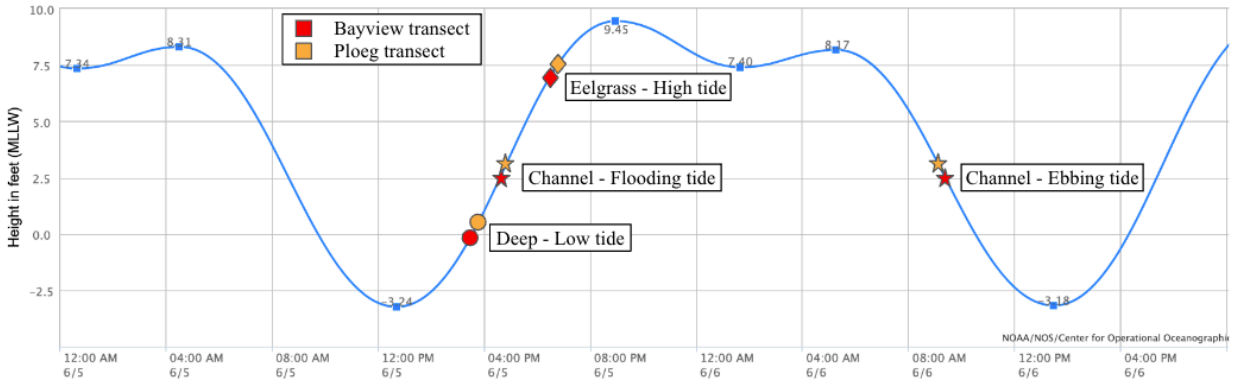

Figure 2. Annotated time series of tidal height over the first day of sampling. This sampling sequence was the same for all tidal replicates. Four samples were collected along the Ploeg (red) and Bayview (orange) transects at three sampling locations (Deep, Channel, and Eelgrass) during flooding and ebbing tides.

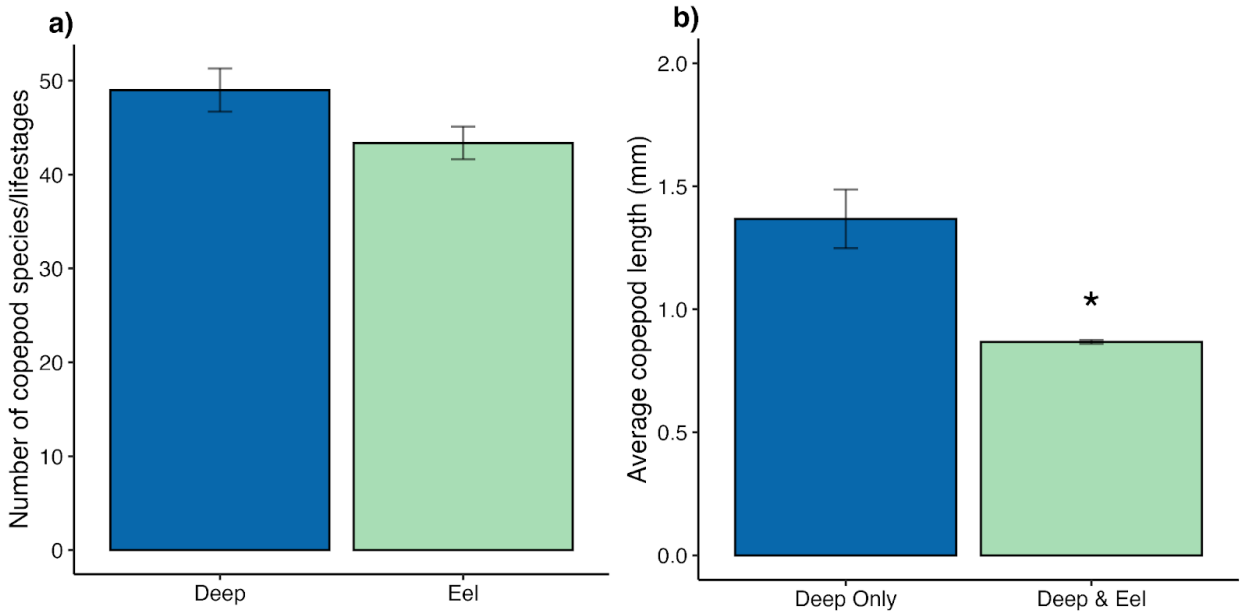

Figure 3. Mean (±SE) (a) number of unique copepod species/lifestage combinations identified at the deep stations and eelgrass stations and (b) length (mm) of copepods identified only at the deep stations versus identified at both stations. * Indicates a significant ($p < 0.05$) difference between stations.

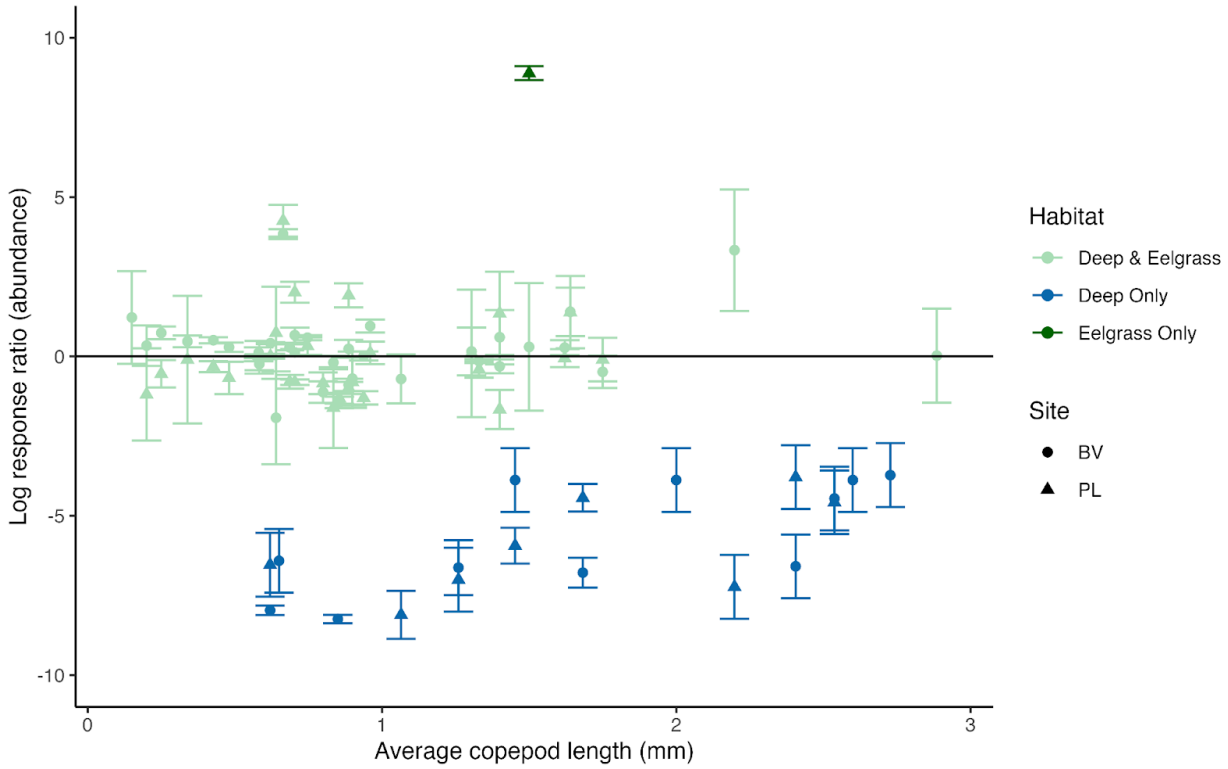

Figure 4. The relative abundance of copepod species/lifestages at eelgrass stations and deep stations (shown as log response ratio ± 95% confidence intervals) versus average copepod length (mm). Each point represents a copepod species/lifestage in either Bayview (circle) or Ploeg (triangle). Log response ratios significantly > 0 indicate that the relative abundance of copepods was higher at the eelgrass stations. Log response ratios significantly < 0 indicate that the relative abundance of copepods was higher at the deep stations. Species that were observed only at the deep station are colored in blue and species that were observed at both the eelgrass and deep stations are colored in green.

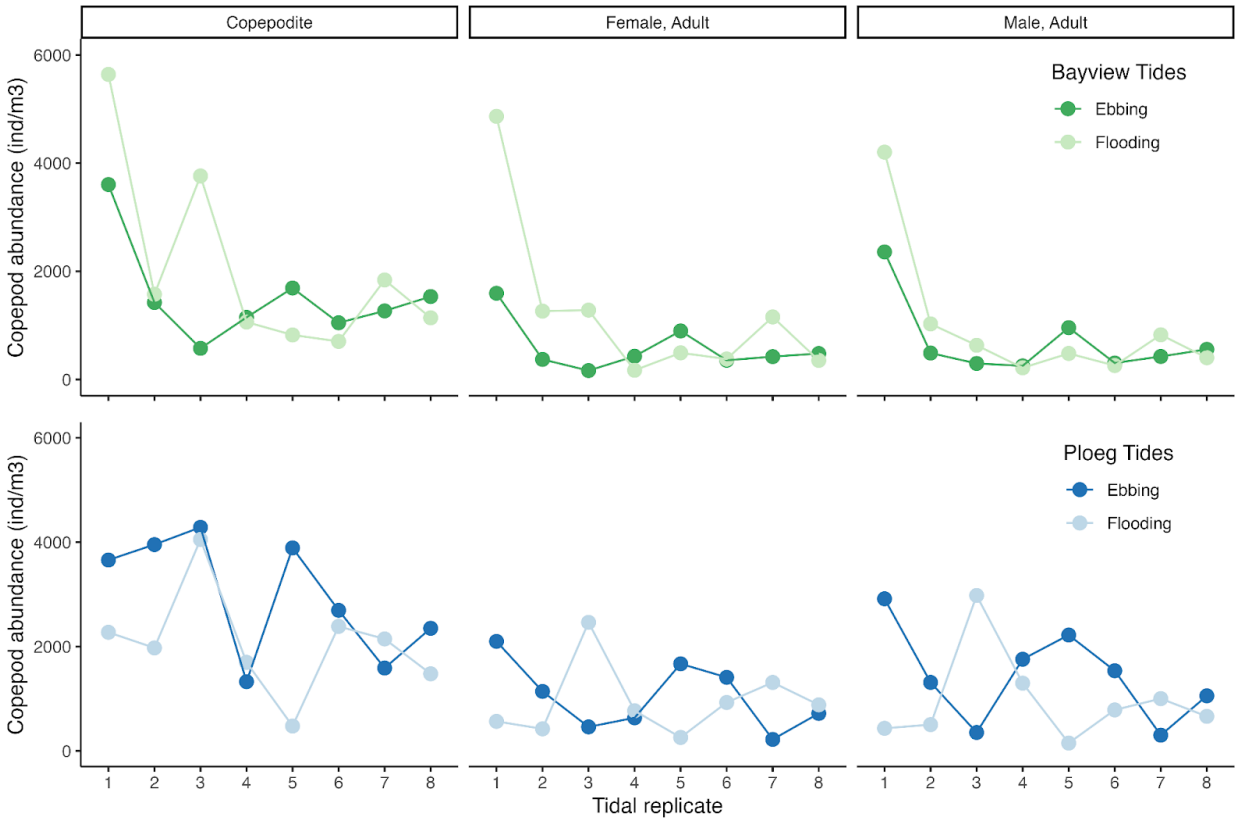

Figure 5. Variability across tidal replicates in the total abundance of copepods grouped by lifestage from samples collected from Bayview (top panel, green) and Ploeg (bottom panel, blue) channel sites during ebbing (dark colors) and flooding (light colors) tides. There were no significant differences between flooding and ebbing tides.

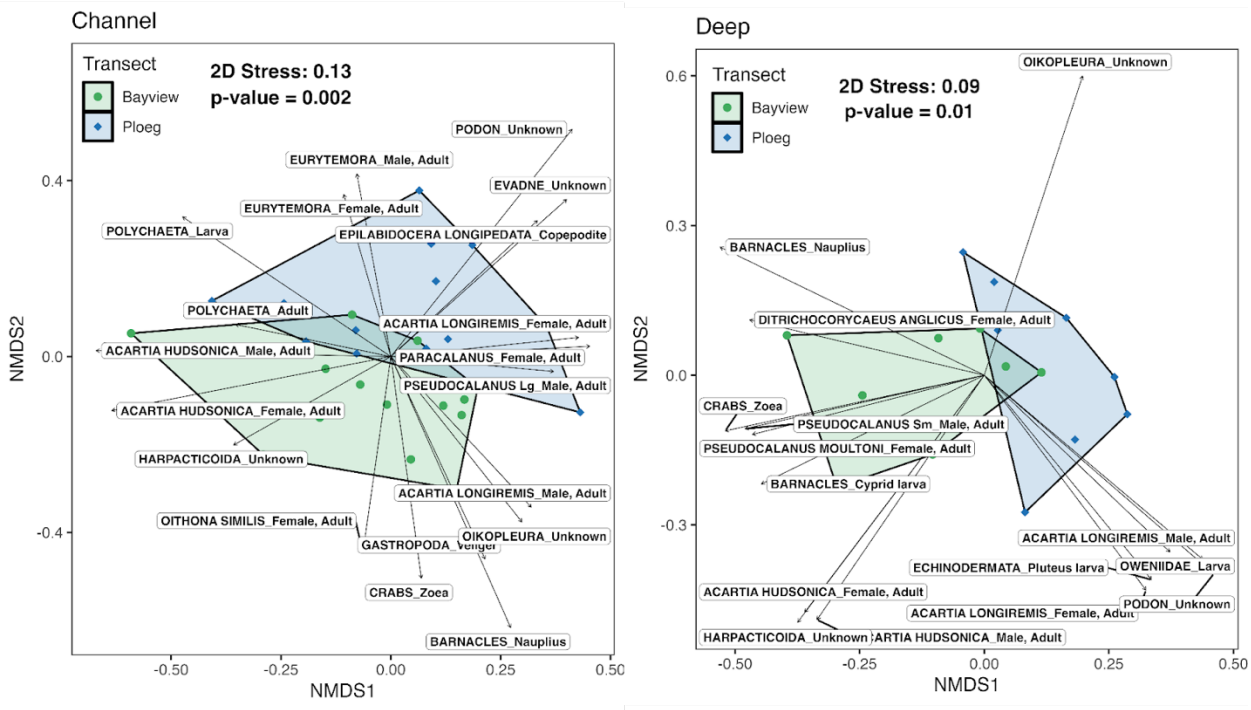

Figure 6. Nonmetric multidimensional scaling ordination of zooplankton species proportions in samples collected from the a) channel stations and b) deep stations on different transects (Bayview = green, Ploeg = blue). Zooplankton species/life stages that were significantly correlated with an NMDS axis (p-value < 0.01) are plotted.

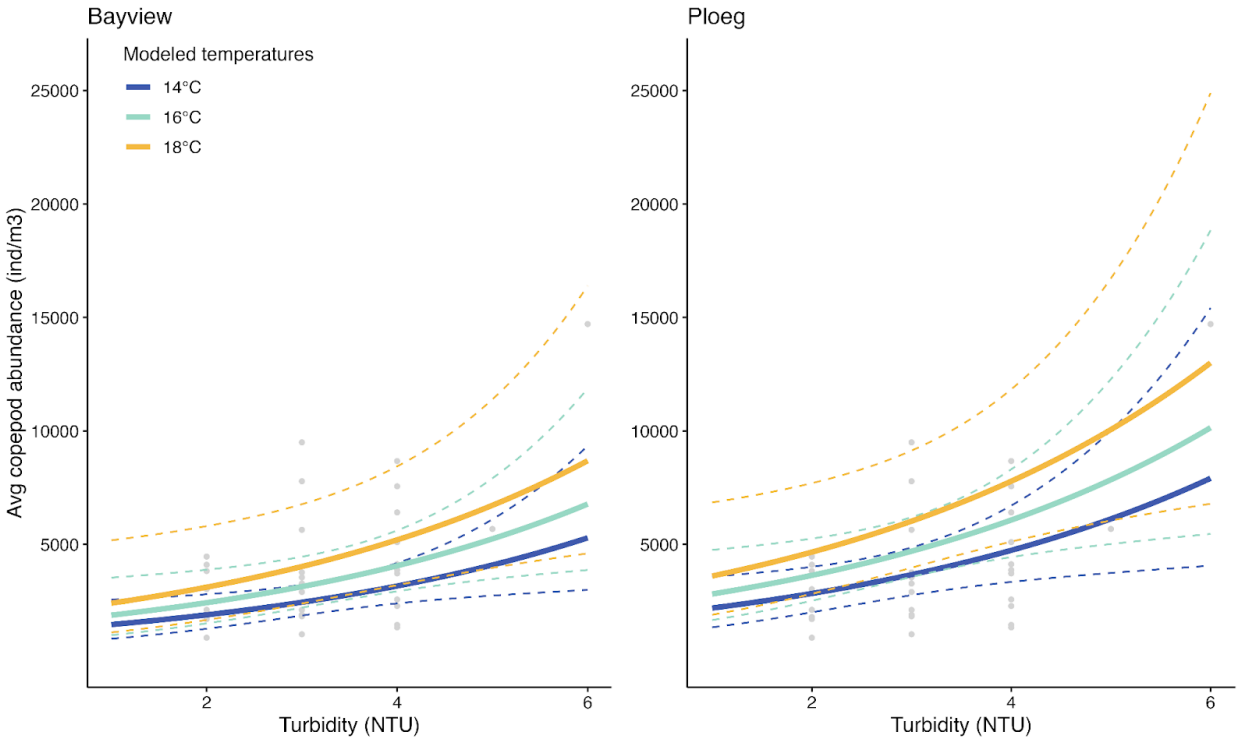

Figure 7. Average copepod abundance (individuals / m^3) against turbidity (NTU). The trendlines (solid line) and confidence intervals (dashed lines) show predicted abundances at a) Bayview and b) Ploeg transects at temperatures of 14 (blue lines), 16 (green lines) and 18 (yellow lines) °C from the best-fit generalized linear model.

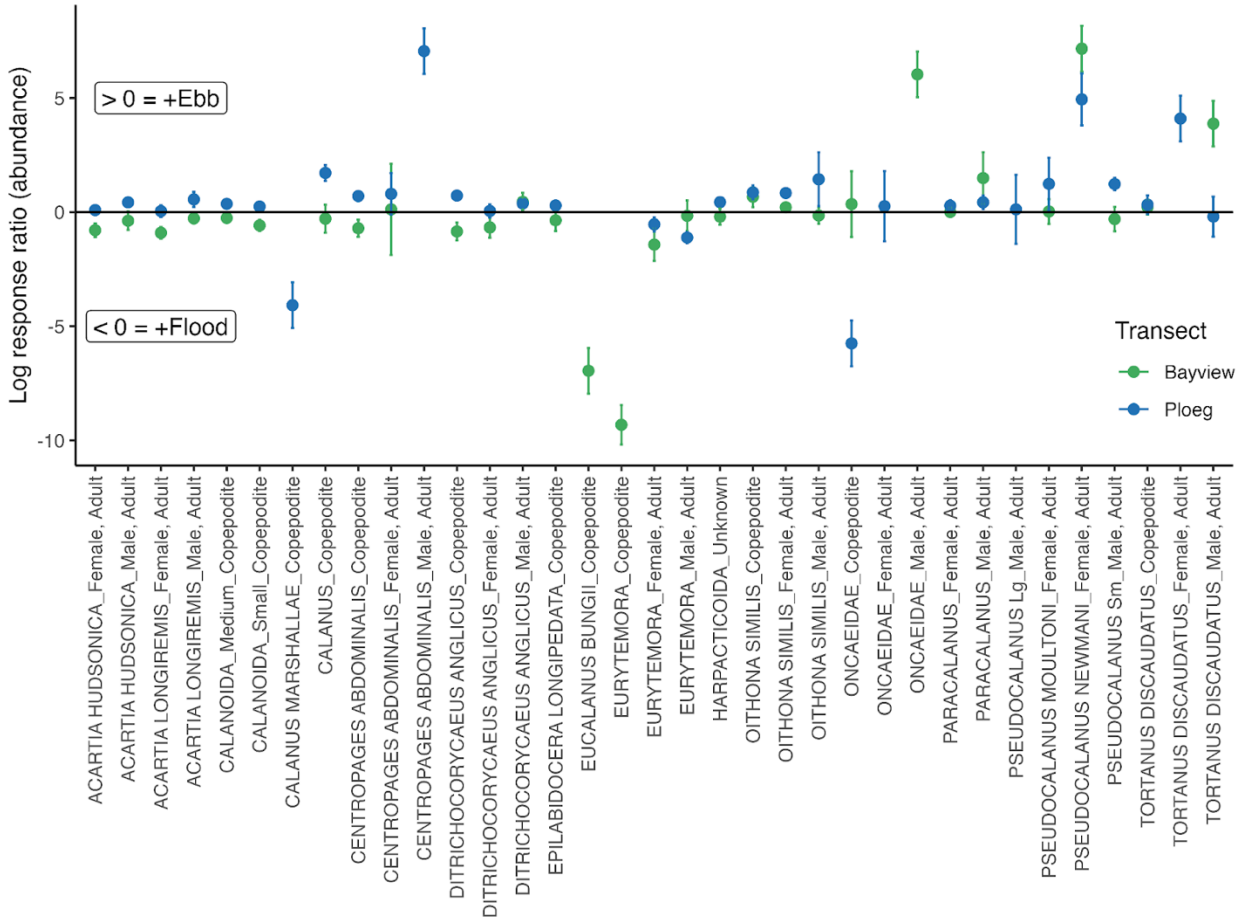

Figure 8. The relative abundance (log response ratio ± 95% confidence intervals) of copepod species/lifestages at channel stations during ebbing and flooding tides. Each point represents a copepod species/lifestage in either Bayview (green) or Ploeg (blue). Log response ratios significantly > 0 indicate that the relative abundance of copepods was higher in ebbing tides. Log response ratios significantly < 0 indicate that the relative abundance of copepods was higher in flooding tides.

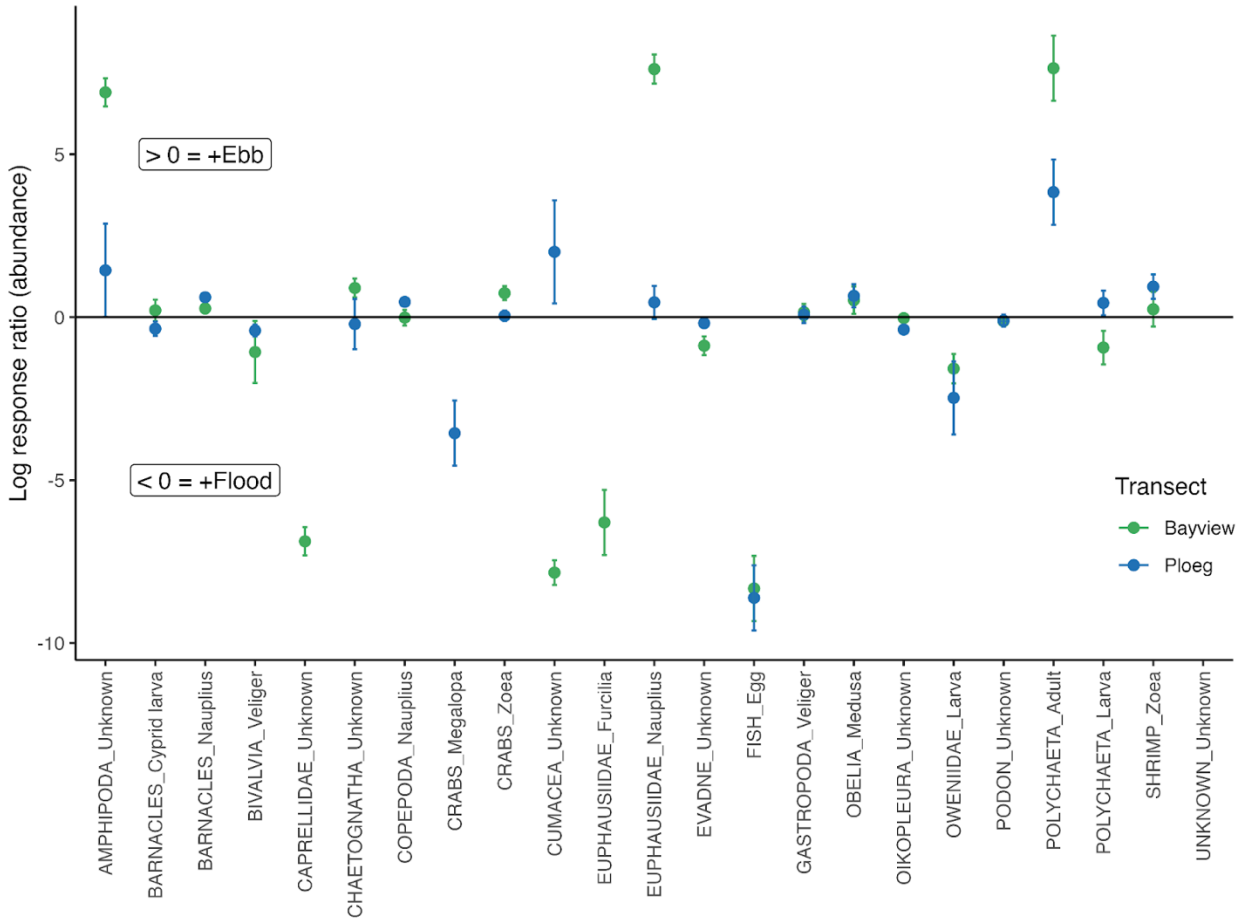

Figure 9. The relative abundance (log response ratio ± 95% confidence intervals) of non-copepod species/lifestages at channel stations during ebbing tide and flooding tide. Each point represents a non-copepod species/lifestage in either Bayview (green) or Ploeg (blue).

Conclusion

The main objectives on my dissertation work were twofold: 1) quantify how environmental changes affect coastal zooplankton populations and the higher trophic levels that rely on them, and 2) develop novel methodologies that facilitate an improved understanding of the role zooplankton play in supporting coastal ecosystems. The different chapters of my dissertation focused on identifying the mechanisms that link the effects of environmental stressors across individual responses to population, community, and ecosystem level scales. Zooplankton are critical links in marine food webs and, through quantifying lethal and sublethal responses to environmental stress, we contributed to an improved understanding of how changing ocean conditions may impact marine food webs.

In Chapter 1, our laboratory experiments demonstrated significant effects of bottom water hypoxia and acidification on behavioral avoidance, swimming statistics, and apparent mortality rates in the copepod, *Calanus pacificus*. Copepods showed strong behavioral responses to hypoxia, and weaker but significant responses to acidification. Current projections predict that copepods will be exposed to greater bottom water hypoxia and acidification in this century. Therefore, the implications of our experiments are important in understanding ecosystems currently stressed by hypoxia and acidification, and for predicting how systems will respond moving into the future. The observed sublethal effects may result in decreased abundances of copepods, changes in predator-prey encounter rates and spatial overlap, and reduced retention in nearshore environments. Sub-lethal effects of hypoxic and, even more so, acidic conditions on copepods are only just starting to be explored in the literature.

Building on Chapter 1, in Chapter 2 we developed a novel methodology combining in situ videos, particle tracking technology, and machine learning classification of zooplankton to

quantify in situ zooplankton swimming and used it to ask whether zooplankton behaviorally respond to environmental stress. Understanding past, present and future dynamics of zooplankton populations is challenging, in large part because traditional methods for quantifying zooplankton distributions are limiting. Our in situ videos revealed that copepods in stressful conditions exhibited significantly slower swimming speeds than copepods in non-stressful conditions. Amphipods showed significantly decreased abundances within stressful conditions, but we observed no consistent changes in amphipod swimming speed or transition probabilities. Observed changes in swimming speeds can help identify the mechanisms driving other in situ observations, such as changes in vertical population distributions, as well as improve our ability to predict stress driven changes in predator-prey interactions. For example, slower swimming speeds may alleviate some of the predation pressure associated with the increased spatial overlap between predators and prey. The identification of video-based statistics quantifying changes in zooplankton population distributions could be used as a diagnostic tool of in situ change and ecological stress.

Pelagic zooplankton, such as copepods, may be an important source of food for juvenile fish in shallow coastal systems, such as eelgrass beds, as they transition from freshwater to the open ocean. Despite the potential importance of offshore zooplankton species in juvenile fish diets, surprisingly little work has been done to estimate the transport of pelagic zooplankton into shallow subtidal and intertidal habitats through tides. In Chapter 3, we found evidence of transport of pelagic species into intertidal habitats and measured large spatial and temporal variability, as well as changes in zooplankton populations with temperature and turbidity. Padilla Bay National Estuary Research Reserve (NERR) in Washington State contains one of the largest eelgrass meadows in the U.S., and is one of many reserves that host eelgrasses, providing habitat

and food for numerous ecologically important species. Important management needs for the Padilla Bay NERR include quantifying factors that contribute to the services these eelgrass beds provide, such as acting as nurseries for important fishes. The large differences in zooplankton community composition and abundances we observed across sampling transects within Padilla Bay highlights the need for sampling programs that can capture variability over small spatial scales to improve our understanding of zooplankton patch dynamics in intertidal environments.

Taken together, the three chapters of my dissertation provide insight into some of the specific mechanisms driving changes in marine zooplankton populations and trophic dynamics due to environmental change. In addition to lethal responses to hypoxia, we observed a range of sub-lethal responses to hypoxia and acidification, both when they are experienced separately in laboratory experiments, and when they are experienced simultaneously in the field. Notably, in both our laboratory experiments and in situ observations, we recorded behavioral avoidance of stressful waters and slower swimming speeds within stressful waters. These behavioral changes may impact vertical population distributions (through modifications to diel vertical migrations and avoidance of stressful bottom waters), horizontal distributions (through changes in retention in nearshore systems and tidal advection), and predator-prey interactions (through changes in swimming speed and spatial overlap, both of which impact encounter rates). While changing zooplankton dynamics has direct implications for pelagic food-webs, our work suggests it will also impact nearshore and intertidal food-webs.

This work was conducted during a time of rapid advancement of in situ zooplankton methodologies and technological capabilities. While laboratory experiments are likely best suited to study single-stress, single-species responses to chemical changes, and zooplankton net tows paired with microscopy likely provide the best taxonomic resolution, in situ observations offer

opportunities to advance our understanding of how simultaneous stressors impact population dynamics. As camera resolution, the taxonomic resolution of machine learning based identification of zooplankton, and data processing capabilities all continue to improve, the amount of in situ zooplankton data we will be able collect and analyze will finally start to catch up with other oceanographic parameters. While we will need new strategies to integrate traditional and novel sampling techniques, it is exciting to think about what possibilities will continue to unfold for zooplankton ecologists.

Appendix A: Chapter 1 Supplemental Materials

Figure S.1: Screenshots of Tracker3D outputs from representative 90-second video clips recorded by the Bottom Camera during a selected hypoxia experiment showing copepod X, Z pixel coordinates (blue lines) and assembled swimming paths (pink lines) after a) 1 minute, b) 8 minutes, and c) 25 minutes of experimental time. The white dashed line shows the location of the halocline. Note that copepods swimming at the bottom of the experimental tanks are not represented clearly in this camera view, motivating the addition of the Base Cameras in 2020.

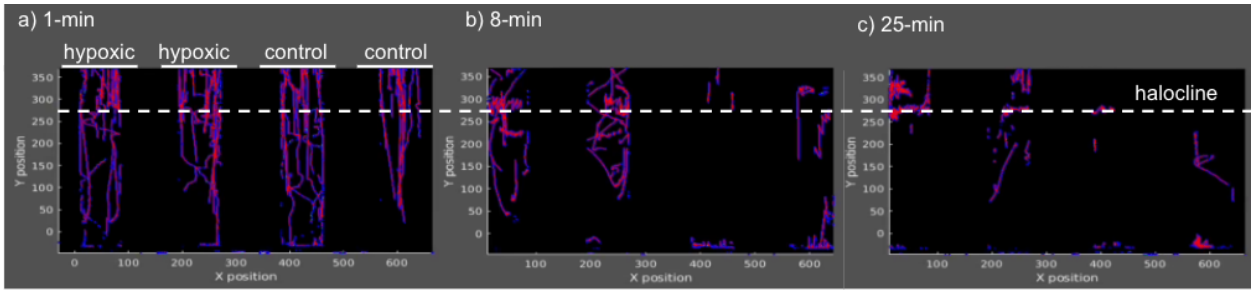

Figure S.2: Hypoxia Experiments–*Raw mean true vertical speeds (VS_{tr}) and projected horizontal speeds (HS_{proj}) (mm/s) from front-facing Bottom Camera (below the halocline and off the bottom) and Surface Camera (above the halocline) (+/-SE) during 2019 and 2020.* Blue lines show swimming speed in control tanks and red lines show swimming speed in treatment tanks. Note the difference in scales between vertical and horizontal speeds. Estimated total speeds (*TS*) are reported in the manuscript and were calculated using raw VS_{tr} and HS_{proj} speeds and the following equations:

(1) $$HSproj = HStr \times (1/2\pi) \times \int_0^{2\pi} |cos(x)|dx = HStr \times (2/\pi)$$

(2) $$TS = \sqrt{(HStr)^2 + (VStr)^2}$$

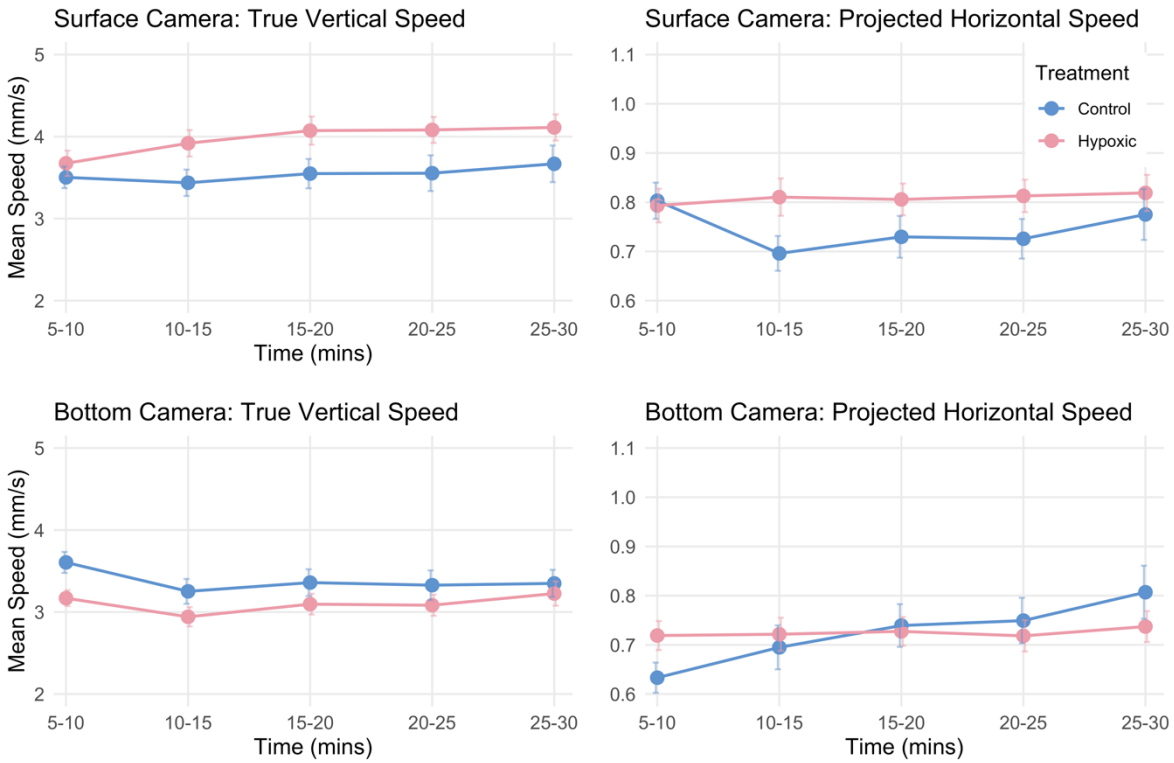

Figure S.3: Acidification Experiments–*Raw mean true vertical speeds (VS_{tr}) and projected horizontal speeds (HS_{proj}) (mm/s) from front-facing Bottom Camera (below the halocline and off the bottom) and Surface Camera (above the halocline) (+/-SE).* Blue lines show swimming speed in control tanks and red lines show swimming speed in treatment tanks. Note the difference in scales between vertical and horizontal speeds. Estimated total speeds (*TS*) are reported in the manuscript and were calculated using raw VS_{tr} and HS_{proj} speeds and the following equations:

(1) $$HSproj = HStr \times (1/2\pi) \times \int_0^{2\pi} |cos(x)|dx = HStr \times (2/\pi)$$

(2) $$TS = \sqrt{(HStr)^2 + (VStr)^2}$$

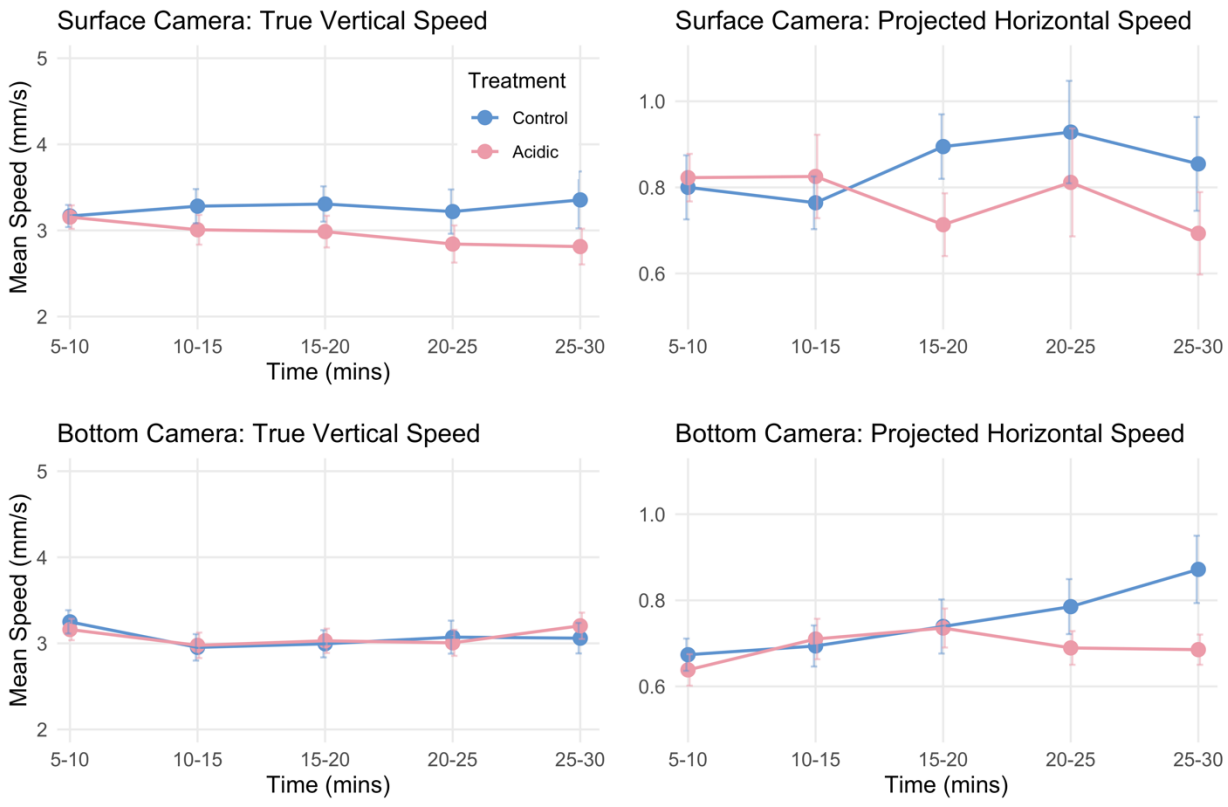

Figure S.4: Hypoxia Experiments - Mean counts of moving copepods per frame (+/- SE) over 5-minute intervals from each of the three camera views. Mean copepod counts per frame were calculated by dividing the total number of copepod localizations in each 5-minute video clip by the number of frames in that video clip. The blue lines show counts in control tanks and the red lines show counts in treatment tanks. The circles with cross marks on the bottom panel show mean moribundity counts taken after 90 minutes. Treatment and control tanks significantly differed from each other in all camera views with a significant interaction between treatment and time in the Bottom Camera (Base Camera: $p = 0.0002$, Bottom Camera: $p < 0.0001$, Surface Camera: $p = 0.001$).

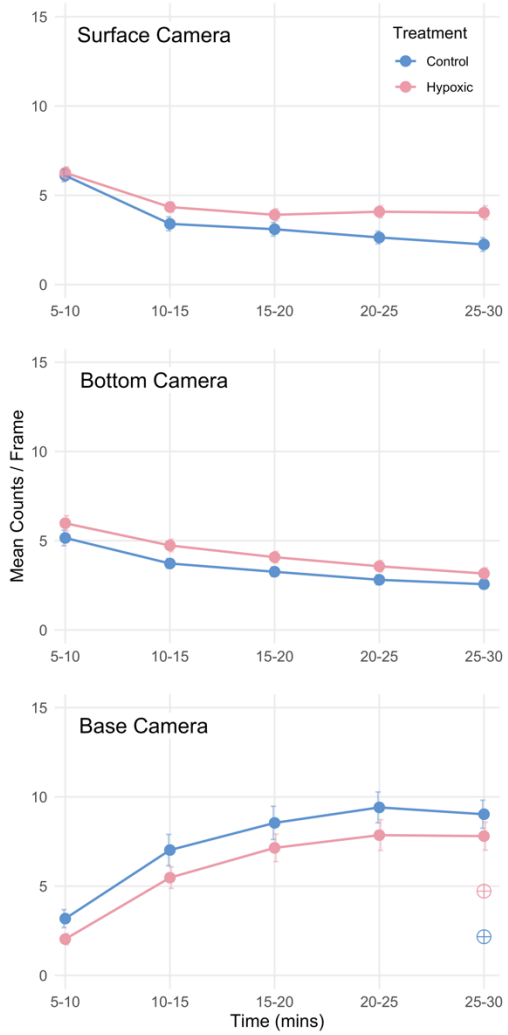

Figure S.5: Acidification Experiments – Mean counts of moving copepods per frame (+/- SE) over 5-minute intervals from each of the three camera views. Mean copepod counts per frame were calculated by dividing the total number of copepod localizations in each 5-minute video clip by the number of frames in that video clip. The blue lines show counts in control tanks and the red lines show counts in treatment tanks. The circles with cross marks on the bottom panel show mean moribundity counts taken after 90 minutes. Treatment and control tanks significantly differed from each other in the Base Camera (p=0.001).

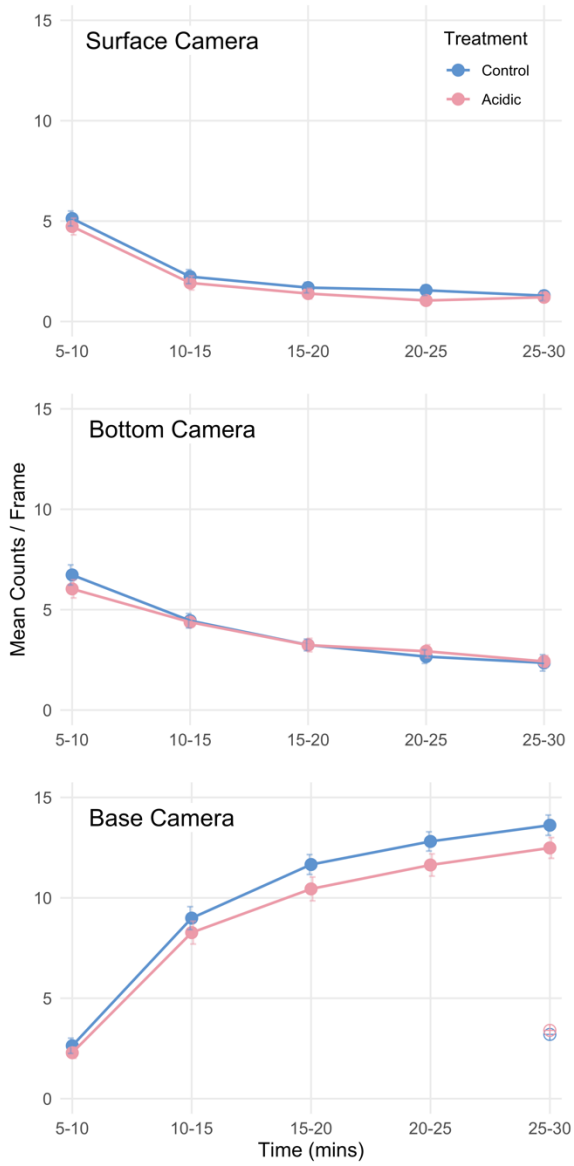

Table S.1: Overview describing the "batches" of copepods collected for 2019 and 2020 hypoxia and acidification experiments. The variation explained by different collection times and locations was incorporated into statistics by including experiment as a random effect in mixed-effects models.

Collection Date	Collection Location	Number of Batches from Collection	Treatment	Notes
28 Aug 2019	Main Basin	1	Hypoxia	
14 Sept 2019	Hood Canal	3	Hypoxia	
7 Oct 2019	Main Basin	3	Hypoxia	
9 June 2020	South Sound	3	Hypoxia	
28 June 2020	South Sound	3	Hypoxia	Dropped from all analyses
11 July 2020	Hood Canal	4	Hypoxia	
16 Aug 2020	Hood Canal	4	Hypoxia	
29 Aug 2020	Main Basin	2	Hypoxia	
15 Sept 2020	Hood Canal	5	pH	
2 Oct 2020	South Sound	1	pH	South Sound dropped from pH post-hoc statistics
7 Oct 2020	Main Basin	4	pH	

Table S.2.1: Mean height models and AIC values used for model selection for hypoxia experiments. Best fit model indicated in bold.

Model	**AIC**
Mean height ~ 1 + (1|experiment)	2685.2
Mean height ~ time + (1|experiment)	2608.9
Mean height ~ treatment + (1|experiment)	2677.2
Mean height ~ time^2 + (1|experiment)	2628.8
Mean height ~ collection site + (1|experiment)	2687.6
Mean height ~ time + time^2 + (1|experiment)	2585.0
Mean height ~ time + treatment + (1|experiment)	2596.5
Mean height ~ time + collection site + (1|experiment)	2611.3
Mean height ~ treatment + collection site + (1|experiment)	2679.6
Mean height ~ time + treatment + time^2 + (1|experiment)	**2570.7**
Mean height ~ time + collection site + time^2 + (1|experiment)	2587.4
Mean height ~ treatment*time + (1|experiment)	2597.1
Mean height ~ treatment*time + collection site + (1|experiment)	2599.6
Mean height ~ treatment*time + time^2 + (1|experiment)	2571.1
Mean height ~ treatment*collection site + (1|experiment)	2681.7
Mean height ~ treatment*collection site + time (1|experiment)	2600.3
Mean height ~ treatment*time + treatment*collection site + (1|experiment)	2600.9

Table S.2.2: Best Fit Model Summary. Asterisk indicates significant P values at alpha = 0.05

Fixed Effects

Parameter	**Estimate**	**SE**	**T**	**P**
Intercept	449.901	38.158	11.790	< 0.0001 *
Time	-114.773	15.455	-7.426	< 0.0001 *
Treatment	35.768	8.681	4.120	< 0.0001 *
$Time^2$	13.778	2.527	5.452	< 0.0001 *

Random Effects

Effects	**Variance**	**SD**
Experiment	13320	115.41
Residual	4023	63.43

Deviance = 2558.7, df = 219

Table S.3.1: Mean height models and AIC values used for model selection for acidification experiments. Best fit model indicated in bold.

Model	**AIC**
Mean height ~ 1 + (1|experiment)	1993.5
Mean height ~ time + (1|experiment)	1993.5
Mean height ~ treatment + (1|experiment)	2178.5
Mean height ~ $time^2$ + (1|experiment)	2050.0
Mean height ~ collection site + (1|experiment)	2177.8
Mean height ~ time + $time^2$ + (1|experiment)	**1909.6**
Mean height ~ time + treatment + (1|experiment)	1994.9
Mean height ~ time + collection site + (1|experiment)	1994.6
Mean height ~ treatment + collection site + (1|experiment)	2179.6
Mean height ~ time + treatment + $time^2$ + (1|experiment)	1910.7
Mean height ~ time + collection site + $time^2$ + (1|experiment)	1910.7
Mean height ~ treatment*time + (1|experiment)	1996.8
Mean height ~ treatment*time + collection site + (1|experiment)	1997.9
Mean height ~ treatment*time + $time^2$ + (1|experiment)	1912.6
Mean height ~ treatment*collection site + (1|experiment)	2180.5
Mean height ~ treatment*collection site + time (1|experiment)	1994.7
Mean height ~ treatment*time + treatment*collection site + (1|experiment)	1996.6

Table S.3.2: Best Fit Model Summary. Asterisk indicates significant P values at alpha = 0.05

Fixed Effects

Parameter	**Estimate**	**SE**	**T**	**P**
Intercept	477.104	21.350	22.35	< 0.0001 *
Time	-178.350	11.965	-14.91	< 0.0001 *
$Time^2$	20.659	1.956	10.56	< 0.0001 *

Random Effects

Effects	**Variance**	**SD**
Experiment	1884	43.40
Residual	1929	43.92

Deviance = 1899.7, df = 175

Table S.4.1: Bottom Camera total swimming speed models and AIC values used for model selection for hypoxia experiments. Best fit model indicated in bold.

Model	**AIC**
Total swimming speed ~ 1 + (1|experiment)	752.3
Total swimming speed ~ time + (1|experiment)	754.2
Total swimming speed ~ treatment + (1|experiment)	727.1
Total swimming speed ~ $time^2$ + (1|experiment)	753.6
Total swimming speed ~ collection site + (1|experiment)	754.5
Total swimming speed ~ time + $time^2$ + (1|experiment)	749.3
Total swimming speed ~ time + treatment + (1|experiment)	728.9
Total swimming speed ~ time + collection site + (1|experiment)	756.4
Total swimming speed ~ treatment + collection site + (1|experiment)	729.3
Total swimming speed ~ time + treatment + $time^2$ + (1|experiment)	723.5
Total swimming speed ~ time + collection site + $time^2$ + (1|experiment)	751.5
Total swimming speed ~ treatment*time + (1|experiment)	729.5
Total swimming speed ~ treatment*time + collection site + (1|experiment)	731.7
Total swimming speed ~ treatment*time + $time^2$ + (1|experiment)	724.0
Total swimming speed ~ treatment*collection site + (1|experiment)	**722.5**
Total swimming speed ~ treatment*collection site + time (1|experiment)	724.4
Total swimming speed ~ treatment*time + treatment*collection site + (1|experiment)	724.8

Table S.4.2: Best Fit Model Summary. Asterisk indicates significant P values at alpha = 0.05

Fixed Effects

Parameter	**Estimate**	**SE**	**T**	**P**
Intercept	3.37790	0.23371	14.453	< 0.0001 *
Treatment	-0.11207	0.06879	-1.629	0.1041
Collection Site (Main Basin)	0.25030	0.37478	0.668	0.5112
Collection Site (South Sound)	0.86529	0.50488	1.714	0.1006
Treatment*Collection Site (Main Basin)	-0.30924	0.11031	-2.803	0.0053 *
Treatment*Collection Site (South Sound)	-0.36935	0.14860	-2.486	0.0133 *

Random Effects

Effects	**Variance**	**SD**
Experiment	0.5748	0.7582
Residual	0.2602	0.5101

Deviance = 706.6, df = 412

Table S.4.3: Pairwise Comparison Summary. Asterisk indicates significant P values at alpha = 0.05

	Estimate	SE	T	P
cont hood.canal - exp hood.canal	0.1121	0.069	1.623	0.5837
cont hood.canal - cont main.basin	-0.2503	0.4042	-0.619	0.9886
cont hood.canal - exp main.basin	0.1710	0.4042	0.423	0.9981
cont hood.canal - cont south.sound	-0.8653	0.5445	-1.589	0.6127
cont hood.canal - exp south.sound	-0.3839	0.5445	-0.705	0.9796
exp hood.canal - cont main.basin	-0.3624	0.4042	-0.896	0.9439
exp hood.canal - exp main.basin	0.0589	0.4042	0.146	1.0000
exp hood.canal - cont south.sound	-0.9774	0.5445	-1.795	0.4863
exp hood.canal - exp south.sound	-0.4959	0.5445	-0.911	0.9402
cont main.basin - exp main.basin	0.4213	0.0866	4.867	<.0001 *
cont main.basin - cont south.sound	-0.615	0.5769	-1.066	0.8902
cont main.basin - exp south.sound	-0.1336	0.5769	-0.232	0.9999
exp main.basin - cont south.sound	-1.0363	0.5769	-1.796	0.4854
exp main.basin - exp south.sound	-0.5549	0.5769	-0.962	0.9257
cont south.sound - exp south.sound	0.4814	0.1322	3.641	0.0041 *

Table S.5.1: Surface Camera total swimming speed models and AIC values used for model selection for hypoxia experiments. Best fit model indicated in bold.

Model	**AIC**
Total swimming speed ~ 1 + (1|experiment)	977.3
Total swimming speed ~ time + (1|experiment)	969.3
Total swimming speed ~ treatment + (1|experiment)	951.0
Total swimming speed ~ $time^2$ + (1|experiment)	970.4
Total swimming speed ~ collection site + (1|experiment)	980.3
Total swimming speed ~ time + $time^2$ + (1|experiment)	970.9
Total swimming speed ~ time + treatment + (1|experiment)	943.5
Total swimming speed ~ time + collection site + (1|experiment)	972.3
Total swimming speed ~ treatment + collection site + (1|experiment)	954.0
Total swimming speed ~ time + treatment + $time^2$ + (1|experiment)	945.2
Total swimming speed ~ time + collection site + $time^2$ + (1|experiment)	974.0
Total swimming speed ~ treatment*time + (1|experiment)	944.7
Total swimming speed ~ treatment*time + collection site + (1|experiment)	947.7
Total swimming speed ~ treatment*time + $time^2$ + (1|experiment)	946.3
Total swimming speed ~ treatment*collection site + (1|experiment)	943.5
Total swimming speed ~ treatment*collection site + time (1|experiment)	**935.7**
Total swimming speed ~ treatment*time + treatment*collection site + (1|experiment)	936.8

Table S.5.2: Best Fit Model Summary. Asterisk indicates significant P values at alpha = 0.05

Fixed Effects

Parameter	**Estimate**	**SE**	**T**	**P**
Intercept	3.29544	0.26236	12.561	< 0.0001 *
Treatment	0.59325	0.09759	6.079	< 0.0001 *
Collection Site (Main Basin)	0.58537	0.40511	1.445	0.162036
Collection Site (South Sound)	0.51511	0.54474	0.946	0.354306
Time	0.07777	0.02473	379.09541	0.001791 *
Treatment*Collection Site (Main Basin)	-0.59537	0.15658	-3.802	0.000167 *
Treatment*Collection Site (South Sound)	-0.06791	0.20832	-0.326	0.744599

Random Effects

Effects	**Variance**	**SD**
Experiment	0.6461	0.8038
Residual	0.4894	0.6996

Deviance = 917.8, df = 391

Table S.5.3: Pairwise Comparison Summary. Asterisk indicates significant P values at alpha = 0.05

	Estimate	SE	T	P
cont hood.canal – exp hood.canal	-0.59325	0.0981	-6.046	<.0001 *
cont hood.canal – cont main.basin	-0.58537	0.4364	-1.341	0.7599
cont hood.canal – exp main.basin	-0.58324	0.4352	-1.340	0.7606
cont hood.canal – cont south.sound	-0.51511	0.5869	-0.878	0.9486
cont hood.canal – exp south.sound	-1.04045	0.5859	-1.776	0.4973
exp hood.canal – cont main.basin	0.00788	0.4357	0.018	1.0000
exp hood.canal – exp main.basin	0.01001	0.4345	0.023	1.0000
exp hood.canal – cont south.sound	0.07814	0.5864	0.133	1.0000
exp hood.canal – exp south.sound	-0.4472	0.5853	-0.764	0.9712
cont main.basin – exp main.basin	0.00212	0.1232	0.017	1.0000
cont main.basin – cont south.sound	0.07026	0.622	0.113	1.0000
cont main.basin – exp south.sound	-0.45508	0.621	-0.733	0.9759
exp main.basin – cont south.sound	0.06813	0.6212	0.110	1.0000
exp main.basin – exp south.sound	-0.4572	0.6201	-0.737	0.9753
cont south.sound – exp south.sound	-0.52534	0.185	-2.839	0.0536 *

Table S.6.1: Base Camera swimming speed models and AIC values used for model selection for hypoxia experiments. Best fit model indicated in bold.

Model	**AIC**
Swimming speed ~ 1 + (1|experiment)	-902.6
Swimming speed ~ time + (1|experiment)	-938.6
Swimming speed ~ treatment + (1|experiment)	-982.5
Swimming speed ~ $time^2$ + (1|experiment)	-930.9
Swimming speed ~ collection site + (1|experiment)	-902.5
Swimming speed ~ time + $time^2$ + (1|experiment)	-943.9
Swimming speed ~ time + treatment + (1|experiment)	-1036.4
Swimming speed ~ time + collection site + (1|experiment)	-938.6
Swimming speed ~ treatment + collection site + (1|experiment)	-983.7
Swimming speed ~ time + treatment + $time^2$ + (1|experiment)	**-1047.0**
Swimming speed ~ time + collection site + $time^2$ + (1|experiment)	-943.9
Swimming speed ~ treatment*time + (1|experiment)	-1035.1
Swimming speed ~ treatment*time + collection site + (1|experiment)	-1036.4
Swimming speed ~ treatment*time + $time^2$ + (1|experiment)	-1045.9
Swimming speed ~ treatment*collection site + (1|experiment)	-989.3
Swimming speed ~ treatment*collection site + time (1|experiment)	-1046.9
Swimming speed ~ treatment*time + treatment*collection site + (1|experiment)	-1045.5

Table S.6.2: Best Fit Model Summary. Asterisk indicates significant P values at alpha = 0.05

Fixed Effects

Parameter	**Estimate**	**SE**	**T**	**P**
Intercept	1.211e-01	8.002e-03	15.129	< 0.0001 *
Time	-2.619e-02	5.093e-03	-5.144	< 0.0001 *
Treatment	-3.308e-02	2.843e-03	-11.637	< 0.0001 *
$Time^2$	3.004e-03	8.326e-04	3.608	0.000386 *

Random Effects

Effects	**Variance**	**SD**
Experiment	0.0002175	0.01475
Residual	0.0004250	0.02062

Deviance = -1059.1, df = 215

Table S.7.1: Bottom Camera total swimming speed models and AIC values used for model selection for acidification experiments. Best fit model indicated in bold.

Model	**AIC**
Total swimming speed ~ 1 + (1|experiment)	168.2
Total swimming speed ~ time + (1|experiment)	169.9
Total swimming speed ~ treatment + (1|experiment)	167.9
Total swimming speed ~ time^2 + (1|experiment)	168.8
Total swimming speed ~ collection site + (1|experiment)	169.4
Total swimming speed ~ time + time^2 + (1|experiment)	162.0
Total swimming speed ~ time + treatment + (1|experiment)	169.5
Total swimming speed ~ time + collection site + (1|experiment)	171.1
Total swimming speed ~ treatment + collection site + (1|experiment)	169.1
Total swimming speed ~ time + treatment + time^2 + (1|experiment)	**161.6**
Total swimming speed ~ time + collection site + time^2 + (1|experiment)	163.3
Total swimming speed ~ treatment*time + (1|experiment)	171.3
Total swimming speed ~ treatment*time + collection site + (1|experiment)	172.6
Total swimming speed ~ treatment*time + time^2 + (1|experiment)	163.4
Total swimming speed ~ treatment*collection site + (1|experiment)	168.0
Total swimming speed ~ treatment*collection site + time (1|experiment)	169.7
Total swimming speed ~ treatment*time + treatment*collection site + (1|experiment)	171.5

Table S.7.2: Best Fit Model Summary. Asterisk indicates significant P values at alpha = 0.05

Fixed Effects

Parameter	**Estimate**	**SE**	**T**	**P**
Intercept	3.68904	0.23661	15.591	< 0.0001 *
Time	-0.27127	0.08982	-3.020	0.00291 *
Treatment	-0.07765	0.04915	-1.580	0.11602
$Time^2$	0.04704	0.01469	3.203	0.00162 *

Random Effects

Effects	**Variance**	**SD**
Experiment	0.3734	0.6110
Residual	0.1087	0.3297

Deviance = 149.6, df = 174

Table S.8.1: Surface Camera total swimming speed models and AIC values used for model selection for acidification experiments. Best fit model indicated in bold.

Model	**AIC**
Total swimming speed ~ 1 + (1|experiment)	352.1
Total swimming speed ~ time + (1|experiment)	353.9
Total swimming speed ~ treatment + (1|experiment)	346.1
Total swimming speed ~ $time^2$ + (1|experiment)	353.9
Total swimming speed ~ collection site + (1|experiment)	354.0
Total swimming speed ~ time + $time^2$ + (1|experiment)	355.9
Total swimming speed ~ time + treatment + (1|experiment)	347.9
Total swimming speed ~ time + collection site + (1|experiment)	355.7
Total swimming speed ~ treatment + collection site + (1|experiment)	348.0
Total swimming speed ~ time + treatment + $time^2$ + (1|experiment)	349.9
Total swimming speed ~ time + collection site + $time^2$ + (1|experiment)	357.7
Total swimming speed ~ treatment*time + (1|experiment)	347.6
Total swimming speed ~ treatment*time + collection site + (1|experiment)	349.4
Total swimming speed ~ treatment*time + $time^2$ + (1|experiment)	349.6
Total swimming speed ~ treatment*collection site + (1|experiment)	**344.6**
Total swimming speed ~ treatment*collection site + time (1|experiment)	346.3
Total swimming speed ~ treatment*time + treatment*collection site + (1|experiment)	345.7

Table S.8.2: Best Fit Model Summary. Asterisk indicates significant P values at alpha = 0.05

Fixed Effects

Parameter	**Estimate**	**SE**	**T**	**P**
Intercept	3.7936	0.2587	14.666	< 0.0001 *
Treatment	-0.5143	0.1382	-3.722	0.000278 *
Collection Site	-0.3754	0.3861	-0.972	0.353089
Treatment*Collection Site	0.4684	0.2005	2.336	0.020803 *

Random Effects

Effects	**Variance**	**SD**
Experiment	0.2854	0.5343
Residual	0.3994	0.6320

Deviance = 332.7, df = 155

Table S.8.3: Pairwise Comparison Summary. Asterisk indicates significant P values at alpha = 0.05

	Estimate	SE	T	P
cont hood.canal - exp hood.canal	0.514	0.139	3.696	0.0017
cont hood.canal - cont main.basin	0.375	0.435	0.864	0.8232
cont hood.canal - exp main.basin	0.421	0.434	0.971	0.7679
exp hood.canal - cont main.basin	-0.139	0.434	-0.32	0.9881
exp hood.canal - exp main.basin	-0.093	0.433	-0.215	0.9963
cont main.basin - exp main.basin	0.046	0.146	0.314	0.9892

Table S.9.1: Base Camera swimming speed models and AIC values used for model selection for acidification experiments. Best fit model indicated in bold.

Model	**AIC**
Swimming speed ~ 1 + (1|experiment)	-945.4
Swimming speed ~ time + (1|experiment)	-978.0
Swimming speed ~ treatment + (1|experiment)	-949.1
Swimming speed ~ $time^2$ + (1|experiment)	-973.1
Swimming speed ~ collection site + (1|experiment)	-945.3
Swimming speed ~ time + $time^2$ + (1|experiment)	-978.3
Swimming speed ~ time + treatment + (1|experiment)	**-983.2**
Swimming speed ~ time + collection site + (1|experiment)	-977.9
Swimming speed ~ treatment + collection site + (1|experiment)	-948.9
Swimming speed ~ time + treatment + $time^2$ + (1|experiment)	-983.7
Swimming speed ~ time + collection site + $time^2$ + (1|experiment)	-978.3
Swimming speed ~ treatment*time + (1|experiment)	-981.4
Swimming speed ~ treatment*time + collection site + (1|experiment)	-981.3
Swimming speed ~ treatment*time + $time^2$ + (1|experiment)	-982.0
Swimming speed ~ treatment*collection site + (1|experiment)	-947.4
Swimming speed ~ treatment*collection site + time (1|experiment)	-981.6
Swimming speed ~ treatment*time + treatment*collection site + (1|experiment)	-979.8

Table S.9.2: Best Fit Model Summary. Asterisk indicates significant P values at alpha = 0.05

Fixed Effects

Parameter	**Estimate**	**SE**	**T**	**P**
Intercept	6.425e-02	4.868e-03	13.199	< 0.0001 *
Time	-4.737e-03	7.467e-04	-6.343	< 0.0001 *
Treatment	-5.716e-03	2.106e-03	-2.714	0.00733 *

Random Effects

Effects	**Variance**	**SD**
Experiment	0.0001473	0.01214
Residual	0.0001984	0.01408

Deviance = -993.2, df = 174

Appendix B: Chapter 2 Supplemental Materials

Methods

Fig. S1. Image of a) the high-resolution camera (black cylinder), constructed by the Jaffe Laboratory for Underwater Imaging (Scripps Institute of Oceanography) and a CTD (white cylinder) before being mounted on the profiling package an Oceanic Remote Chemical Analyzer mooring over the summer of 2018. The camera is rotated to a horizontal orientation after deployment and b) the high-resolution camera before being installed.

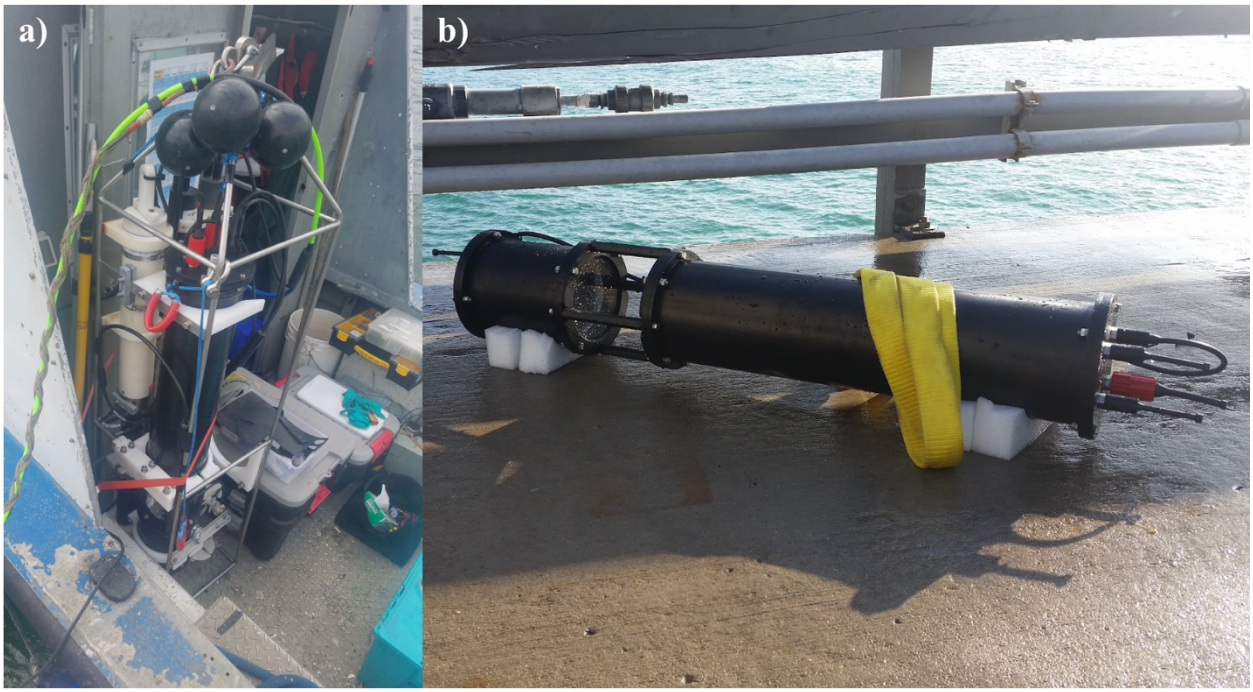

Fig. S2. Puget Sound, Washington, USA, and the Hoodsport Oceanic Remote Chemical Analyzer Mooring location where videos were recorded in 2018.

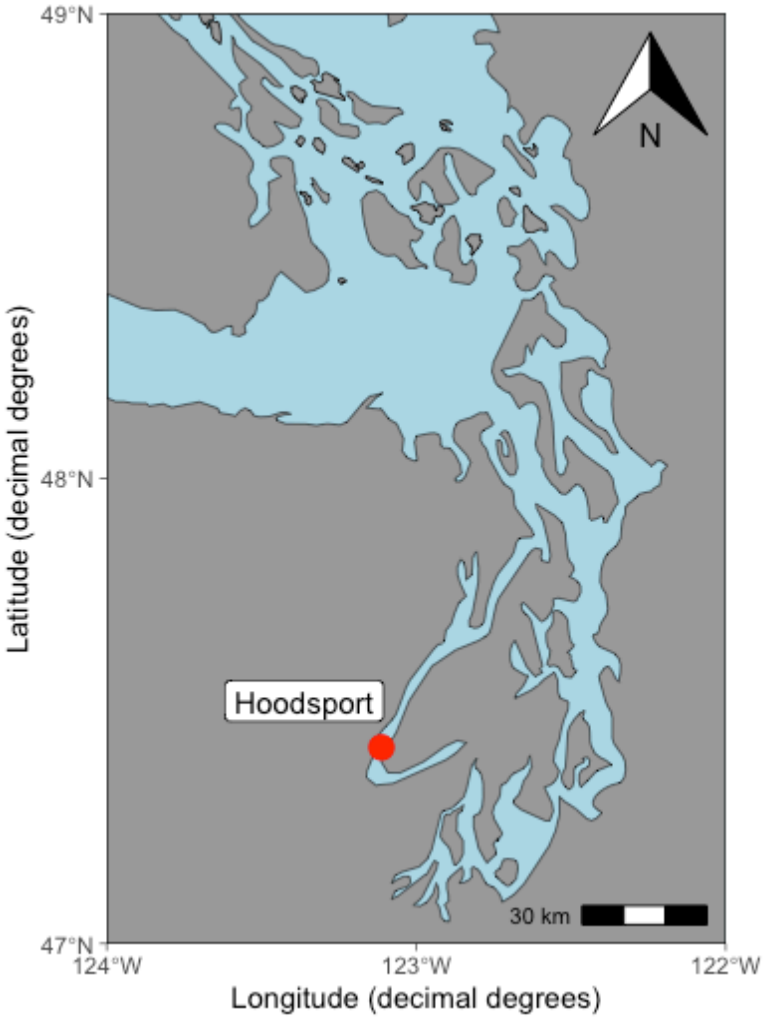

Text S1. Particle image velocimetry flow velocities were calculated for rectangles within a grid of 5 columns and 4 rows. Particle image velocimetry variance was constrained by masking out grids that failed 1 or more of three tests: 1) if the signal to noise ratio was greater than 1.2, 2) if the absolute difference with the local median of surrounding grids was greater than 10 pixels/frame (corresponding to 0.2-0.3 mm/s), or 3) if the grid was outside 1.5 standard deviations of other grids. Masked grids were filled using vales from neighboring grids. If there were more than 12 masked grids, the frame pair was dropped from the analysis. This is a technique for mitigating the small number of motile small particles and other error types.

Fig. S3. Confusion matrix for the zooplankton identification algorithm. The algorithm was trained on 18 broad taxonomic groups or classes: Amphipod, Blob, Chaetognath, *Clione*, Copepod, Diatoms, Eggs, Euphausiid-Decapod, Filaments, Fish Larvae, Jellyfish, Larvacean, *Limacina*, *Noctiluca*, Ostracod, Siphonophore, and Snow. The algorithm returned a testing accuracy of 97.67%

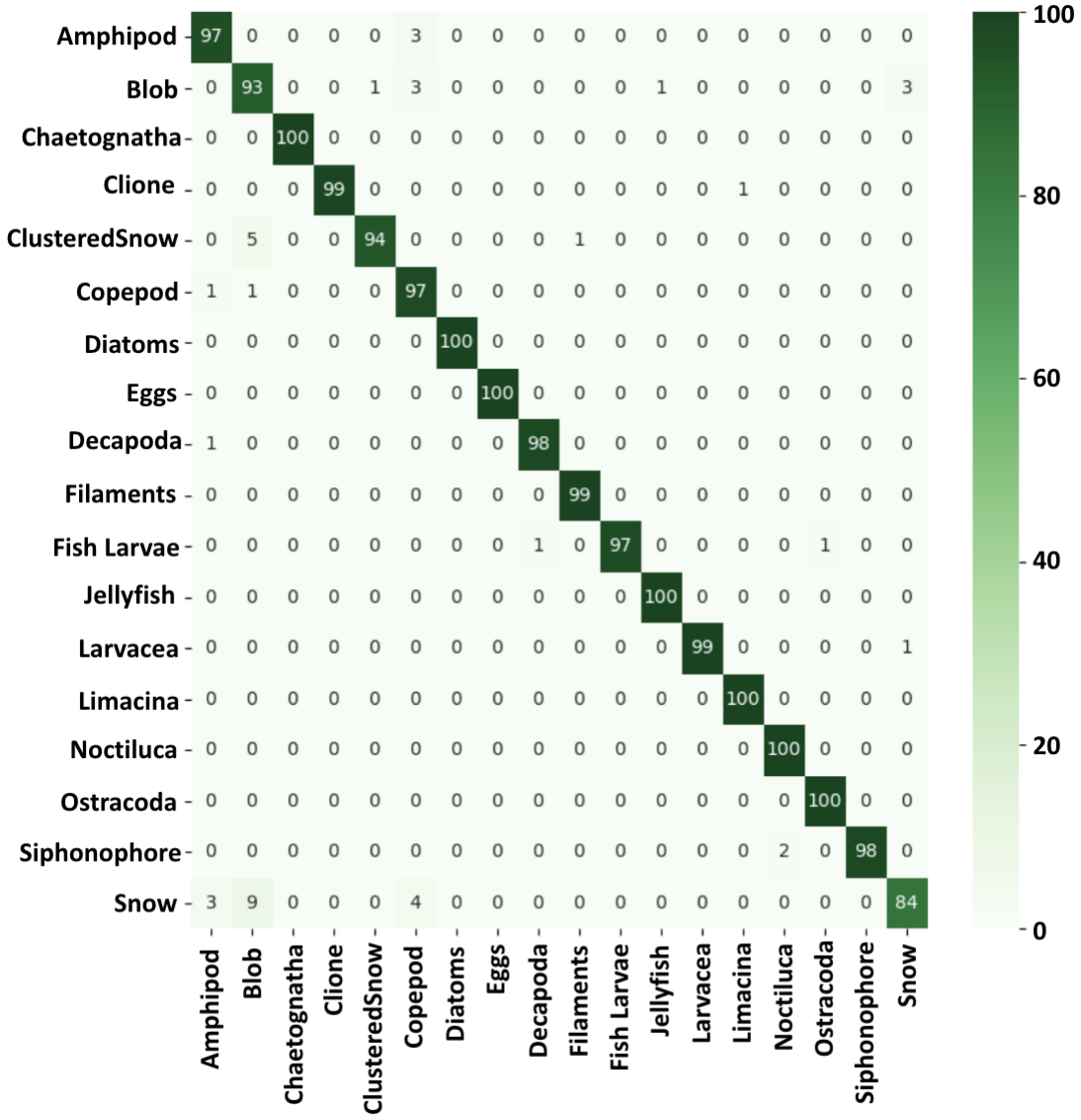

Text S2. A challenge with in situ machine learning image classification of zooplankton is that some orientations of the animal lead to ambiguity or misclassifications. To address this problem, machine learning image classification and tracking algorithms were coupled along the swimming trajectories of individual organisms. As a result, each zooplankton swimming path contained a vector of classifications (typically ~40 frames in length), capturing the individual as it moved and changed orientation relative to the camera. The vector of classifications across each swimming path was typically dominated by one classification, with a small percentage of regions of interest assigned to a different class. For our statistical analyses, the most frequent classification was assigned to the whole path. This integrated video tracking-machine learning image classification reduces the errors associated with ambiguous individual views of some regions of interest and other classification errors, improving the overall accuracy of the identification.

Fig. S4. Schematic representation of a Markov chain transition probabilities for a) copepods and b) amphipods. Each letter is a placeholder for a transition probability. For example, in a), A represents the probability that a copepod which is cruising in frame *i* is still cruising in frame *i*+1, B represents the probability it has shifted to drifting, and C represents the probability it has shifted to jumping. Probabilities of the same color sum to one because a copepod/amphipod must transition into one of the predefined states in the subsequent frame. For example, a copepod that is cruising in frame *i* must transition into the jumping state (C), the drifting state (B) or back into the cruising state (A) in frame *i*+1; therefore A + B + C = 1.

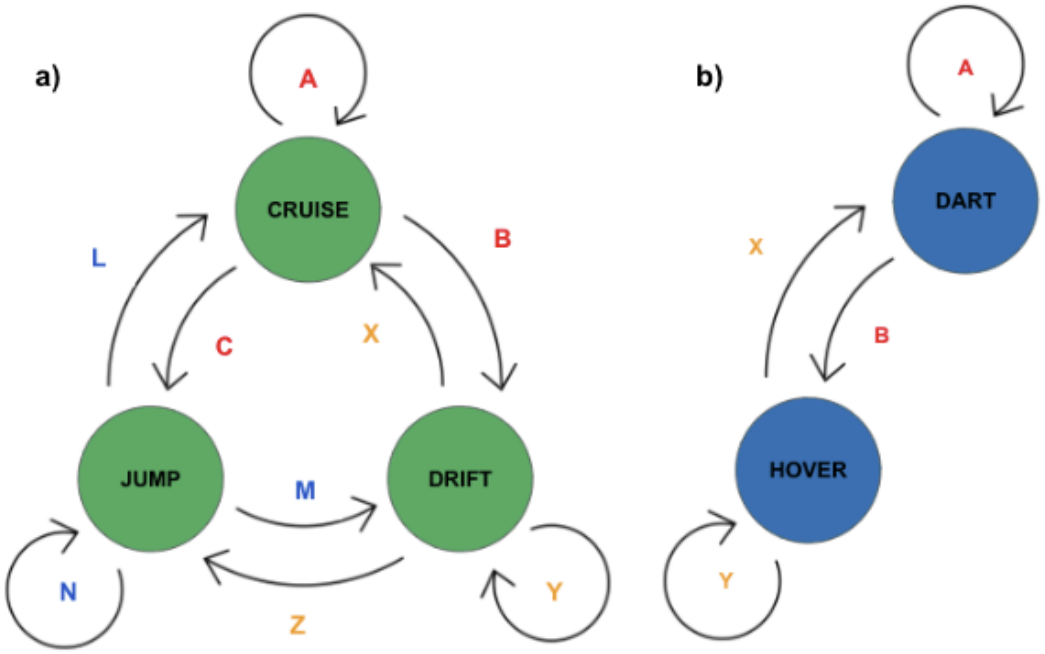

Environmental Conditions

Fig. S5. Dissolved oxygen (mg/L) profiles from the Oceanic Remote Chemical Analyzer (ORCA) mooring in Hood Canal, Washington on three different days over the summer of 2018. Black dashed line marks the hypoxia threshold (2 mg/L). These three dates were chosen to highlight the variability in oxygen profiles common in Hood Canal.

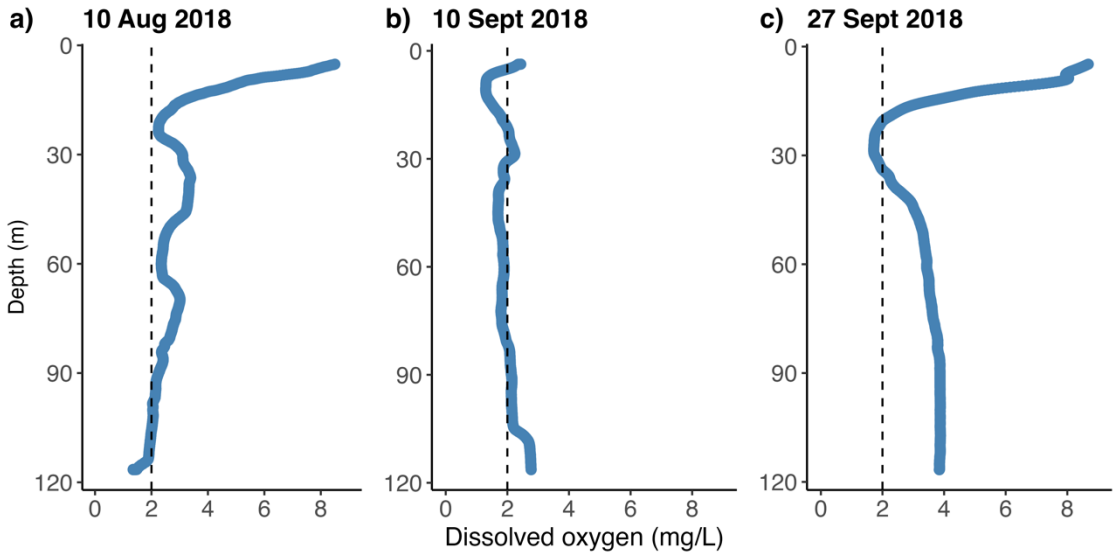

Fig. S6. pH versus dissolved oxygen (mg/L) in Hood Canal, Washington between 2014 and 2022. The red line shows the linear regression line (R^2 = 0.92), and gray shading shows 95% confidence intervals. Data are from bottle samples collected annually in April, July, and September by the Washington Ocean Acidification Center.

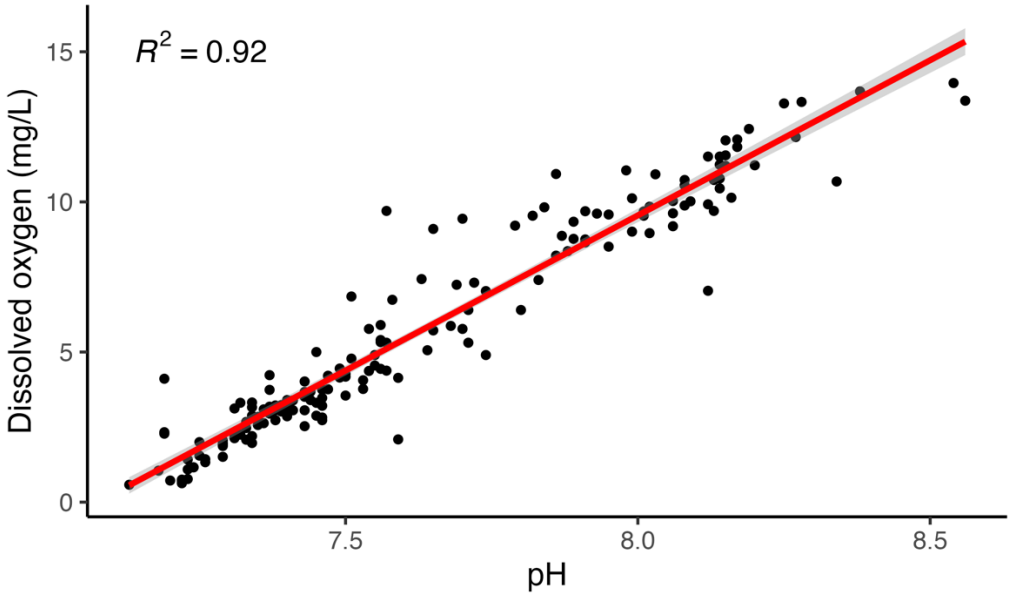

Copepods

Table S1. Mean (±SD) cruising, drifting, and jumping probabilities in copepod paths recorded in hypoxic and normoxic conditions.

Group	Total videos	Total paths	Total localizations	Cruising probability	Drifting probability	Jumping probability
Hypoxic	80	554	22615	0.941 ± 0.129	0.041 ± 0.113	0.018 ± 0.069
Normoxic	107	499	18434	0.944 ± 0.113	0.021 ± 0.074	0.036 ± 0.092

Table S2. Mean (±SE) cruising speed (mm/s) in copepod paths recorded in hypoxic and normoxic environments for all copepods and copepods 1-2, 2-3, 3-4, or >4 mm in length.

Group	Size bin (mm)	Total paths	Cruising speed (mm/s)
Hypoxic	all	554	21.5 ± 0.50
	1-2	222	20.5 ± 0.77
	2-3	262	21.4 ± 0.68
	3-4	45	24.8 ± 2.21
	> 4	25	24.6 ± 2.96
Normoxic	all	499	28.3 ± 0.65
	1-2	182	28.0 ± 1.10
	2-3	234	29.0 ± 0.94
	3-4	54	29.1 ± 2.14
	>4	29	22.8 ± 1.87

Table S3. Mean (±SE) jumping and drifting frequencies in copepod paths recorded in hypoxic and normoxic environments for all copepods and copepods 1-2, 2-3, 3-4, or >4 mm in length.

Group	Size bin (mm)	Total paths	Jumping frequency	Drifting frequency
Hypoxic	all	554	0.018 ± 0.003	0.041 ± 0.005
	1-2	222	0.011 ± 0.003	0.035 ± 0.007
	2-3	262	0.020 ± 0.005	0.032 ± 0.005
	3-4	45	0.033 ± 0.014	0.108 ± 0.031
	> 4	25	0.030 ± 0.019	0.071 ± 0.027
Normoxic	all	499	0.036 ± 0.004	0.021 ± 0.003
	1-2	182	0.034 ± 0.007	0.021 ± 0.006
	2-3	234	0.038 ± 0.006	0.015 ± 0.005
	3-4	54	0.043 ± 0.013	0.046 ± 0.013
	>4	29	0.014 ± 0.006	0.017 ± 0.006

Table S4. Mean (±SE) relative copepod abundances (copepods per frame) between hypoxic and normoxic environments for all copepods and copepods 1-2, 2-3, 3-4, or >4 mm in length.

Group	Total videos	Size bin (mm)	Relative abundance
Hypoxic	80	all	0.077 ± 0.012
		1-2	0.114 ± 0.026
		2-3	0.154 ± 0.035
		3-4	0.021 ± 0.007
		> 4	0.017 ± 0.008
Normoxic	107	all	0.052 ± 0.007
		1-2	0.073 ± 0.014
		2-3	0.010 ± 0.022
		3-4	0.026 ± 0.006
		>4	0.012 ± 0.005

Figure S7. Density (number of individuals per m^3) of copepod species and life stages from Hood Canal, Washington in September 2018. Data are from a zooplankton vertical tow lifted from 10 meters off the bottom using a 60 cm bongo net with 200 um mesh collected by the Washington Ocean Acidification Center.

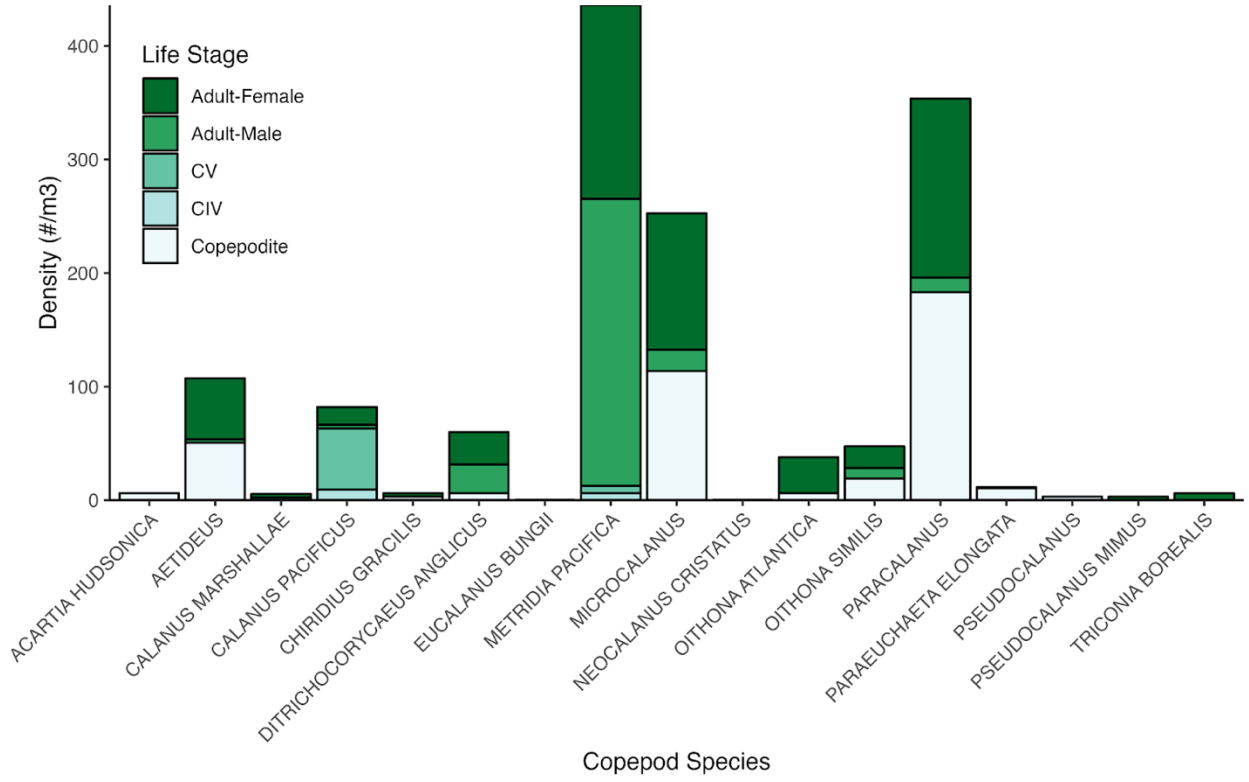

Table S5. Mean (± SD) swimming speeds determined by hidden Markov models for the three hidden swimming states (components 1-3) for copepods in hypoxic and normoxic environments and for lengths of 1-2, 2-3, 3-4, or >4 mm.

Group	Size bin (mm)	Total paths	Component 1 (mm/s)	Component 2 (mm/s)	Component 3 (mm/s)
Hypoxic	all	554	4.706 ± 1.207	13.222 ± 1.0408	34.854 ± 1.139
	1-2	222	3.983 ± 1.214	11.305 ± 1.0408	29.360 ± 1.137
	2-3	262	5.586 ± 1.1885	14.254 ± 1.0315	35.065 ± 1.132
	3-4	45	2.563 ± 1.195	9.365 ± 1.088	38.828 ± 1.1840
	>4	25	4.059 ± 1.125	14.137 ± 1.0814	46.637 ± 1.1441
Normoxic	all	499	5.971 ± 1.205	16.871 ± 1.0465	42.595 ± 1.122
	1-2	182	5.863 ± 1.209	17.730 ± 1.050	44.043 ± 1.120
	2-3	234	6.807 ± 1.196	16.914 ± 1.0389	40.891 ± 1.1206
	3-4	54	4.161 ± 1.182	14.262 ± 1.0565	44.350 ± 1.1481
	>4	29	6.446 ± 1.163	17.291 ± 1.0389	42.029 ± 1.096

Amphipods

Table S6. Mean (±SD) darting and hovering probabilities in amphipod paths recorded in hypoxic and normoxic conditions.

Group	Total videos	Total paths	Total localizations	Darting probability	Hovering probability
Hypoxic	80	146	4193	0.951 ± 0.119	0.049 ± 0.119
Normoxic	107	546	16380	0.934 ± 0.149	0.066 ± 0.149

Table S7. Mean (±SE) darting speed (mm/s) in amphipod paths recorded in hypoxic and normoxic environments for all amphipods and amphipods 1-2, 2-3, 3-4, or >4 mm in length.

Group	Size bin (mm)	Total paths	Darting speed (mm/s)
Hypoxic	all	146	45.8 ± 1.77
	1-2	4	41.7 ± 10.9
	2-3	33	40.1 ± 4.36
	3-4	70	44.7 ± 2.44
	> 4	39	53.1 ± 2.92
Normoxic	all	546	43.9 ± 0.93
	1-2	28	33.6 ± 3.58
	2-3	178	41.5 ± 1.61
	3-4	278	45.2 ± 1.29
	>4	62	49.4 ± 2.80

Fig. S8. Mean (±SE) amphipod darting (instantaneous speed > 10 mm/s) speed between hypoxic and normoxic environments for amphipods 1-2, 2-3, 3-4, or >4 mm in length. Differences were significant between amphipod length ($p < 0.0001$) but not environmental conditions. The number of recorded amphipod paths is printed above each bar.

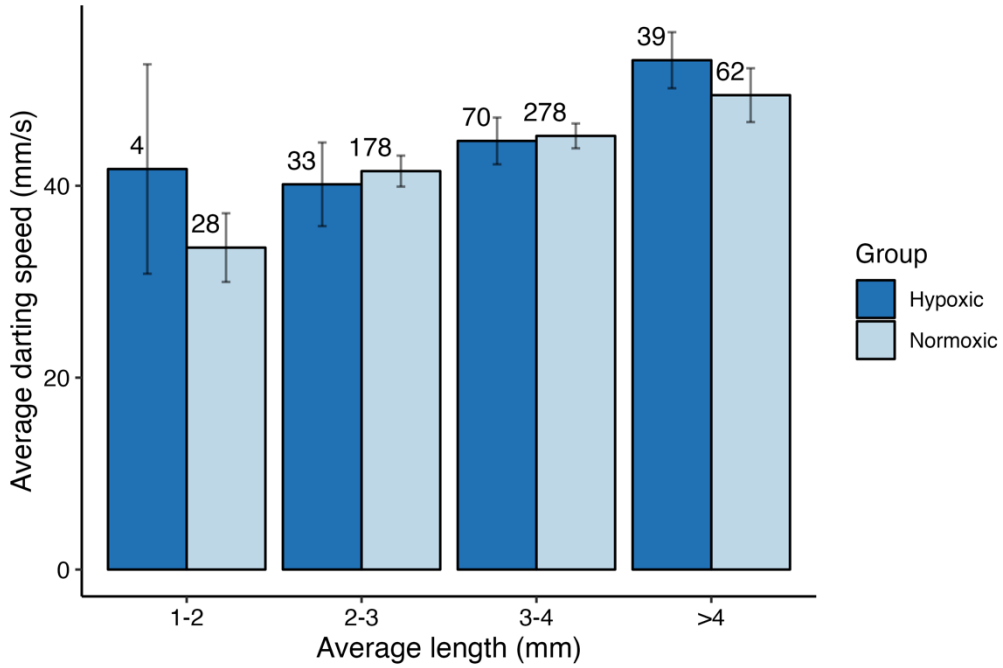

Table S8. Mean (±SE) hovering frequency in amphipod paths recorded in hypoxic and normoxic environments for all amphipods and amphipods 1-2, 2-3, 3-4, or >4 mm in length.

Group	Size bin (mm)	Total paths	Hovering frequency
Hypoxic	all	146	0.049 ± 0.010
	1-2	4	0 ± 0
	2-3	33	0.088 ± 0.034
	3-4	70	0.043 ± 0.011
	> 4	39	0.033 ± 0.011
Normoxic	all	546	0.066 ± 0.006
	1-2	28	0.117 ± 0.038
	2-3	178	0.070 ± 0.012
	3-4	278	0.061 ± 0.008
	>4	62	0.056 ± 0.016

Fig. S9. Mean (±SE) hovering frequency in amphipod paths recorded in hypoxic and normoxic environments for amphipods 1-2, 2-3, 3-4, or >4 mm in length. The number of recorded amphipod paths are printed above each bar. There were no significant differences between environments.

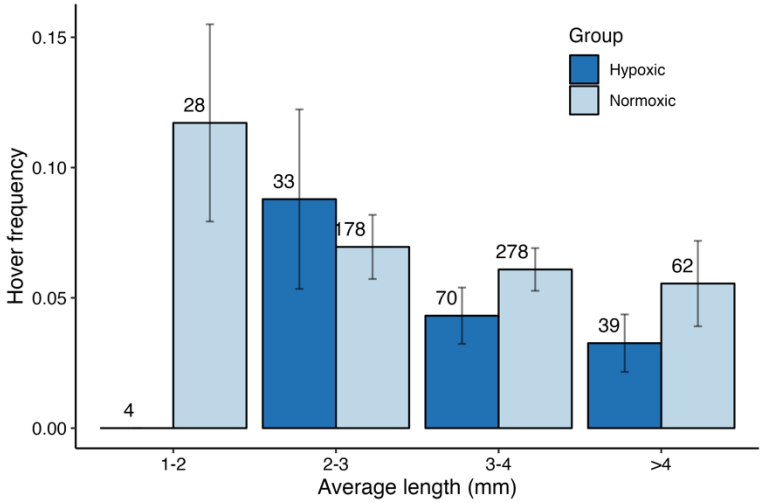

Table S9. Mean (±SE) relative amphipod abundances (amphipod per frame) between hypoxic and normoxic environments for all amphipods and amphipods 1-2, 2-3, 3-4, or >4 mm in length.

Group	Total videos	Size bin (mm)	Relative abundance
Hypoxic	80	all	0.021 ± 0.005
		1-2	0.001 ± 0.0004
		2-3	0.013 ± 0.005
		3-4	0.041 ± 0.014
		> 4	0.028 ± 0.011
Normoxic	107	all	0.062 ± 0.010
		1-2	0.006 ± 0.002
		2-3	0.062 ± 0.013
		3-4	0.137 ± 0.033
		>4	0.042 ± 0.015

Table S10. Mean (± SD) swimming speed determined by hidden Markov models for the two hidden swimming states (components 1-2) for amphipods in hypoxic and normoxic environments and for lengths of 1-2, 2-3, 3-4, or >4 mm. * Note the small sample size for amphipods 1-2 mm in length in hypoxic environments.

Group	**Size bin**	**n**	**Component 1 (mm/s)**	**Component 2 (mm/s)**
Hypoxic	all	146	15.378 ±1.1824	47.582 ± 1.0926
	1-2	4*	30.430 ±1.222	36.318 ± 1.018
	2-3	33	8.705 ±1.223	38.354 ± 1.157
	3-4	70	16.829 ±1.145	47.631 ± 1.086
	>4	39	16.615 ±1.177	51.329 ± 1.079
Normoxic	all	546	11.731 ±1.264	42.189 ± 1.116
	1-2	28	14.618 ±1.201	50.819 ± 1.065
	2-3	178	11.810 ±1.197	41.5577 ± 1.114
	3-4	278	11.764 ±1.289	42.086 ± 1.115
	>4	62	10.326 ±1.292	42.045 ± 1.1309

Multivariate analysis

Methods

Text S3. Multiple linear regressions were used to test the effects of different environmental and size metrics on average copepod cruising speed and amphipod darting speed, using the *R* package **lme4**. Speeds were log-transformed and nested models were generated using different combinations of dissolved oxygen, temperature, depth, salinity, and maximum length as continuous variables and day/night as a factor. Temperature and oxygen showed multicollinearity ($r = 0.72$), so temperature was dropped as a predictor variable. Depth and salinity showed multicollinearity ($r = 0.68$), as did salinity and oxygen ($r = 0.66$), so salinity was dropped as a predictor variable. The best models were identified using AIC values. A visual inspection of residual plots did not reveal any deviations from normality or homoscedasticity. Model predictions and confidence intervals were back transformed and plotted over raw speed data.

Results - Copepods

Text S4. Model results indicated that cruising speed increased with depth, oxygen concentration, maximum length, and oxygen*length interaction (depth: $p < 0.0001$; oxygen: $p < 0.0001$; length: $p < 0.0001$; oxygen*length: $p = 0.005$) (Fig. S10 and S11). Cruising speed increased with the concentration of dissolved oxygen, but the effect of dissolved oxygen was weaker among larger copepods. Average cruising speed also increased with depth. At 2.5 mg/L of dissolved oxygen, copepod cruising speed is predicted to be 47% faster at 100 meters than at 25 meters depth (32.5 versus 22.1 mm/s, respectively).

Figure S10. Average copepod cruising speed versus dissolved oxygen (mg/L). The trendlines (solid line) and confidence intervals (dashed lines) show predicted copepod cruising speeds for a copepod 2 mm in length and depths of 25 (blue lines), 75 (green lines) and 100 (yellow lines) meters depth from the best-fit generalized linear model.

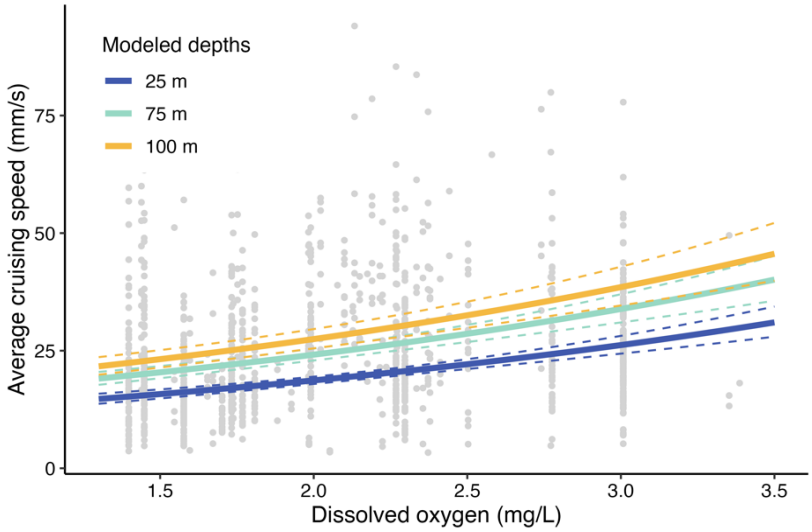

Figure S11. Average copepod cruising speed against dissolved oxygen (mg/L). The trendlines (solid line) and confidence intervals (dashed lines) show predicted cruising speeds for copepods of lengths a) 1 mm, b) 3 mm, and c) 4 mm and depths of 25 (blue lines), 75 (green lines) and 100 (yellow lines) meters from the best-fit generalized linear model.

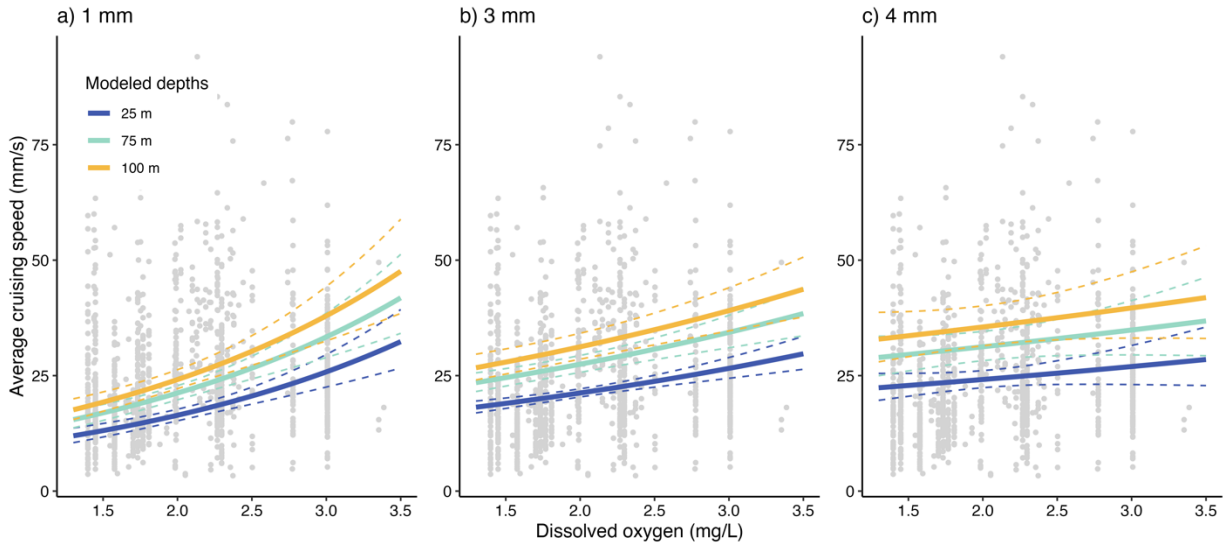

Results - Amphipods

Text S5. Amphipod darting speed significantly increased with depth and maximum observed body length. AIC values indicated that the best model included depth, length, and oxygen; however, the effect of oxygen was not significant (depth: $p = 0.019$; length: $p < 0.0001$; oxygen: $p = 0.477$) (Fig. S12 and S13). At 2.5 mg/L dissolved oxygen, amphipod darting speed was predicted to be 16% faster at 100 m than at 25 m depth (47.9 versus 41.3 mm/s, respectively).

Figure S12. Average amphipod darting speed versus dissolved oxygen (mg/L). The trendlines (solid line) and confidence intervals (dashed lines) show predicted amphipod darting speeds for an amphipod 4 mm in length and depths of 25 (blue lines), 75 (green lines) and 100 (yellow lines) meters from the best-fit generalized linear model.

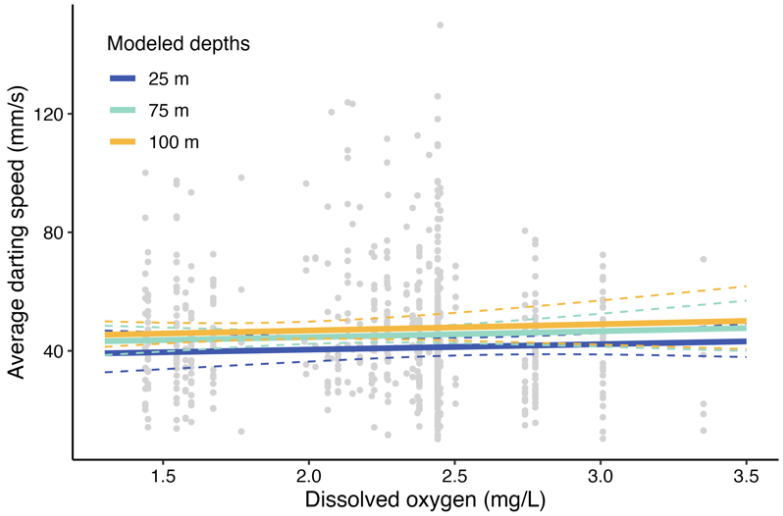

Figure S13. Average amphipod darting speed against dissolved oxygen (mg/L). The trendlines (solid line) and confidence intervals (dashed lines) show predicted amphipod darting speeds for an amphipod a) 2 mm, b) 3 mm, and c) 5 mm in length and depths of 25 (blue lines), 75 (green lines) and 100 (yellow lines) meters from the best-fit generalized linear model.

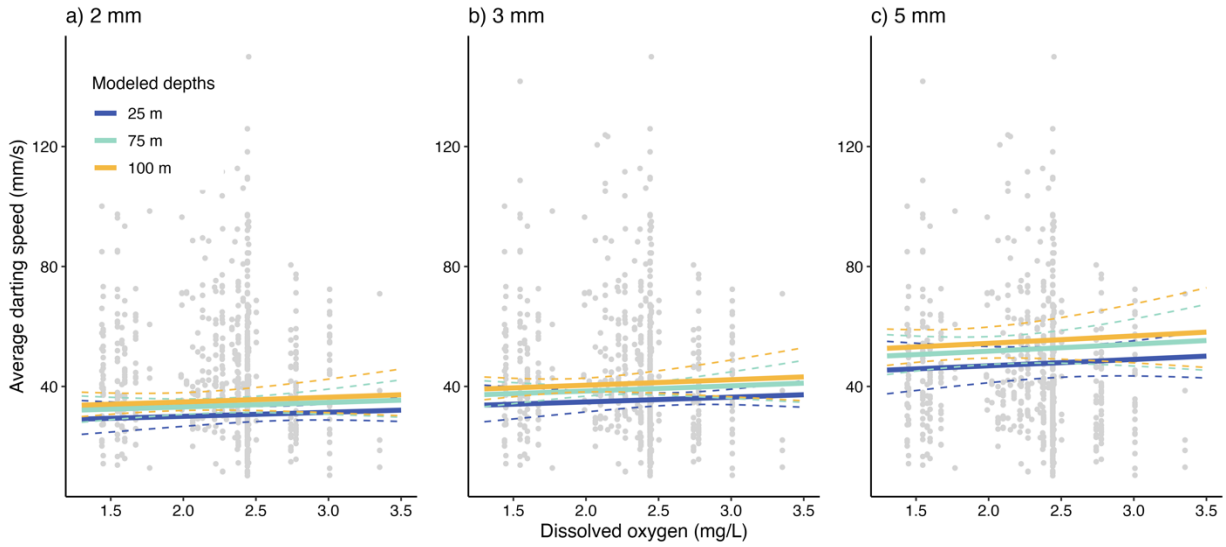

Text S6. *Discussion*

In addition to hypoxia and acidification, copepod cruising speeds also changed with depth. Statistical models predicted copepod cruising speeds to increase 47% at 100 m depth relative to 25 m depth. In Hood Canal, visibility is short: less than 1% of photosynthetically active radiation (light 400 to 700 nm) reaches 20 m and 0% reaches 50 m (NANOOS Cruise Data 2024). Lower light decreases predation pressure from visual predators, which may alter the costs and benefits of fast swimming for copepods, favoring faster speeds at depth. However, faster swimming at depth could increase their risk from nonvisual predators such as gelatinous zooplankton, which are often tolerant of hypoxia and other environmental stresses (Purcell 2012; Slater et al 2020). Our results suggest that the observed copepod responses to depth might

enhance trophic linkages with nonvisual predators in an area where visual predation is less likely. Previous studies have shown that copepods are able to modify their behaviors in the presence of predators, such as changing their diel vertical migration and vertical population distributions (Bollens and Frost 1989) or increasing their swimming speeds (Lee et al. 2005). Monitoring the presence/absence of fish predators was outside the scope of this study, but it is possible that the presence of visual predators in shallower waters may drive copepods to increase their swimming speed and seek refuge in deeper waters.

While we did not observe swimming responses to hypoxia in amphipods, we did observe changes in speed with depth. Amphipod speed increased 16% at 100 m relative to 25 m depth. Some species of pelagic hyperiid amphipods undergo diel vertical migration (Cottier et al 2006; Elder and Seibel 2014), and it is possible that changes in depth and light attenuation might drive changes in amphipod swimming behavior. Changes in amphipod speed with depth likely have impacts on trophic interactions. As with copepod behaviors, increased amphipod speed with depth may enhance trophic linkages with nonvisual predators.

Literature Cited

Bollens, S. M., and Frost, B. W. 1989. Predator-induced diel vertical migration in a planktonic copepod. Journal of Plankton Research **11**: 1047–1065. https://academic.oup.com/plankt/article-abstract/11/5/1047/1537724

Cottier, F. R., Tarling, G. A., Wold, A., and Falk-Petersen, S. 2006. Unsynchronized and synchronized vertical migration of zooplankton in a high arctic fjord. Limnology and Oceanography **51**: 2586–2599. https://doi.org/10.4319/lo.2006.51.6.2586

Elder, L. E., and Seibel, B. A. 2014. Ecophysiological implications of vertical migration into oxygen minimum zones for the hyperiid amphipod *Phronima sedentaria*. Journal of Plankton Research **37**: 897–911. https://doi.org/10.1093/plankt/fbv066

Lee, C. S., O'Bryen, P. J., and Marcus, N. H. 2005. Copepods in Aquaculture. Blackwell Pub.

NANOOS Cruise Data (2024) NVS Salish Cruises. https://nvs.nanoos.org/CruiseSalish (accessed 18 Jan 2024)

Purcell, J. E. 2012. Jellyfish and ctenophore blooms coincide with human proliferations and environmental perturbations. Annual Review of Marine Science **4**: 209–235. https://doi.org/10.1146/annurev-marine-120709-142751

Slater, W. L., Pierson, J. J., Decker, M. B., Houde, E. D., Lozano, C., and Seuberling, J. 2020. Fewer Copepods, fewer anchovies, and more jellyfish: How does hypoxia impact the Chesapeake bay zooplankton community? Diversity **12**: 1-26. https://doi.org/10.3390/d12010035

Appendix C: Chapter 3 Supplemental Materials

Methods

Table S1. Overview of sample sites within the Padilla Bay National Estuarine Research Reserve and the protocol used at specific stations to collect zooplankton samples.

Channel	Station	Latitude	Longitude	Avg Depth (m)	Protocol
Bayview	Deep	48.515986	-122.55062	19.1	Sampled during low tide (~0 ft), vertical tow
	Channel	48.496135	-122.50213	2.4	Sampled once during flooding tide and once during ebbing tide (~2.5 ft), oblique tow
	Eelgrass	48.495713	-122.50214	1.9	Sampled during high tide (~7 ft), vertical tow
Ploeg	Deep	48.557634	-122.5727	18.9	Sampled during low tide (~0 ft), vertical tow
	Channel	48.556311	-122.5309	2.0	Sampled once during flooding tide and once during ebbing tide (~2.5 ft), oblique tow
	Eelgrass	48.555819	-122.53126	1.8	Sampled during high tide (~7 ft), vertical tow

Table S2. A log of the date and time each zooplankton sample was collected in June 2023 on the two sampling transects within the Padilla Bay National Estuarine Research Reserve.

		Bayview		Ploeg	
Tidal Rep	**Date**	**Station**	**Time**	**Station**	**Time**
1	6/6/23	Flood	1658	Flood	1816
		Deep	1840	Deep	1917
		Eel	2045	Eel	1947
	6/7/23	Ebb	1212	Ebb	1103
2		Flood	1923	Flood	1754
		Deep	1613	Deep	1658
		Eel	1952	Eel	2025
	6/8/23	Ebb	1054	Ebb	1129
3		Flood	1811	Flood	1851
		Deep	1715	Deep	1645
		Eel	2044	Eel	1957
	6/9/23	Ebb	1200	Ebb	1257
4		Flood	1841	Flood	1934
		Deep	1809	Deep	1728
		Eel	2054	Eel	2016
	6/10/23	Ebb	1231	Ebb	1313
5	6/14/23	Flood	1241	Flood	1324
		Deep	1410	Deep	1350
		Eel	1552	Eel	1648
	6/15/23	Ebb	0711	Ebb	0643
6		Flood	1426	Flood	1340
		Deep	1536	Deep	1506
		Eel	1614	Eel	1659
	6/16/23	Ebb	0718	Ebb	0651
7		Flood	1423	Flood	1520
		Deep	1402	Deep	1340
		Eel	1553	Eel	1700
	6/17/23	Ebb	0814	Ebb	0750
8		Flood	1422	Flood	1506
		Deep	1604	Deep	1445
		Eel	1647	Eel	1727
	6/18/23	Ebb	0836	Ebb	0741

Figure S1. Image of the tidal heights during the 10 days of sampling conducted in June 2023, highlighting the mixed semidiurnal tide with a larger tidal cycle during the day and a much smaller tidal cycle overnight.

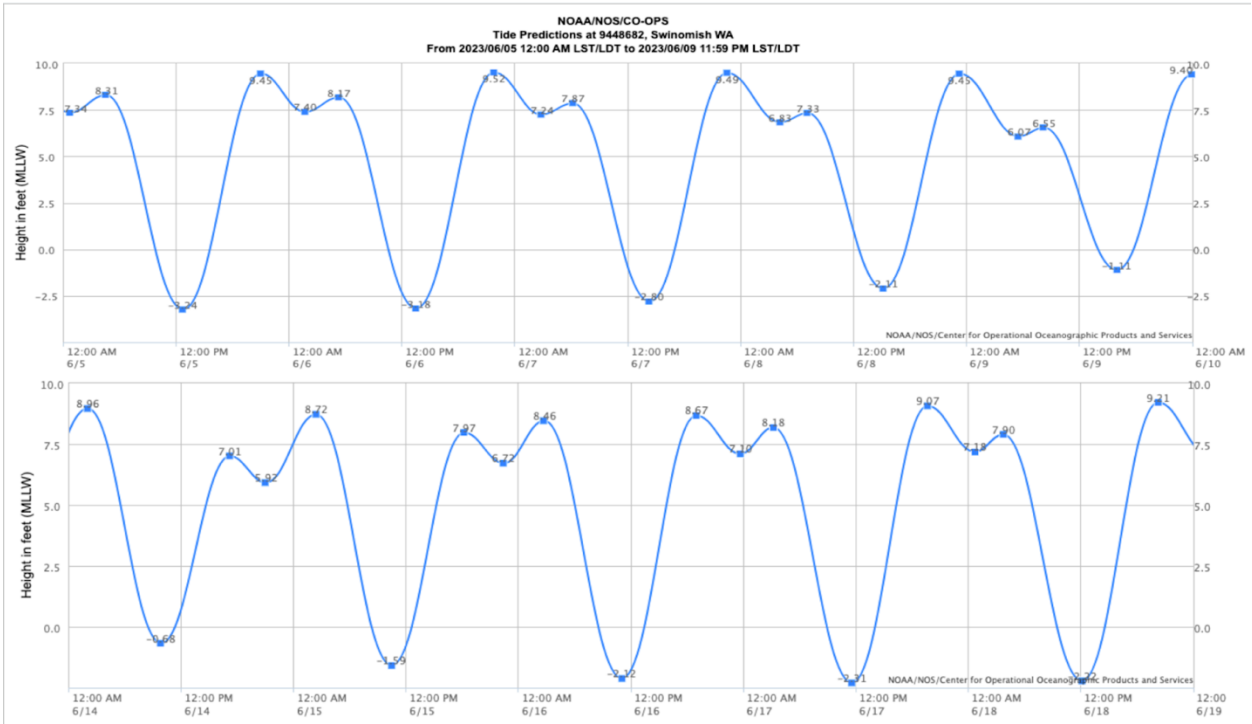

Figure S2. Copepod abundance (individuals / m^3) versus tidal replicate highlighting the consistency between replicate net tows collected back-to-back. Copepod abundance from the Bayview (green) and Ploeg (blue) channel stations during flooding (light triangles) and ebbing (dark circles) tides. Selected replicate samples are outlined in black.

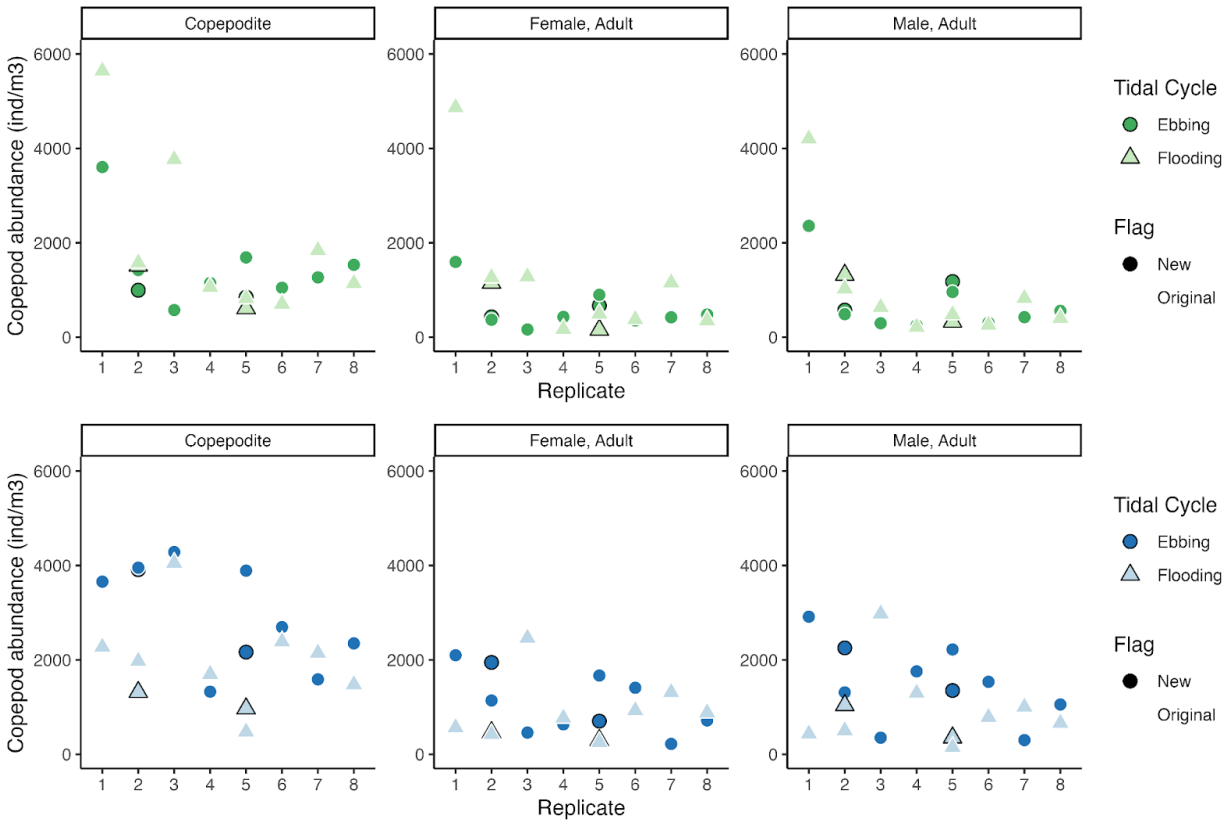

Results

Figure S3. Log-transformed mean (± SE) abundance (individuals / m^3) of copepod species/lifestage combinations recorded at the deep (D) and eelgrass (E) stations on the Bayview transect. Bars are color coded by lifestage. All copepod species are pelagic except for harpacticoids (purple).

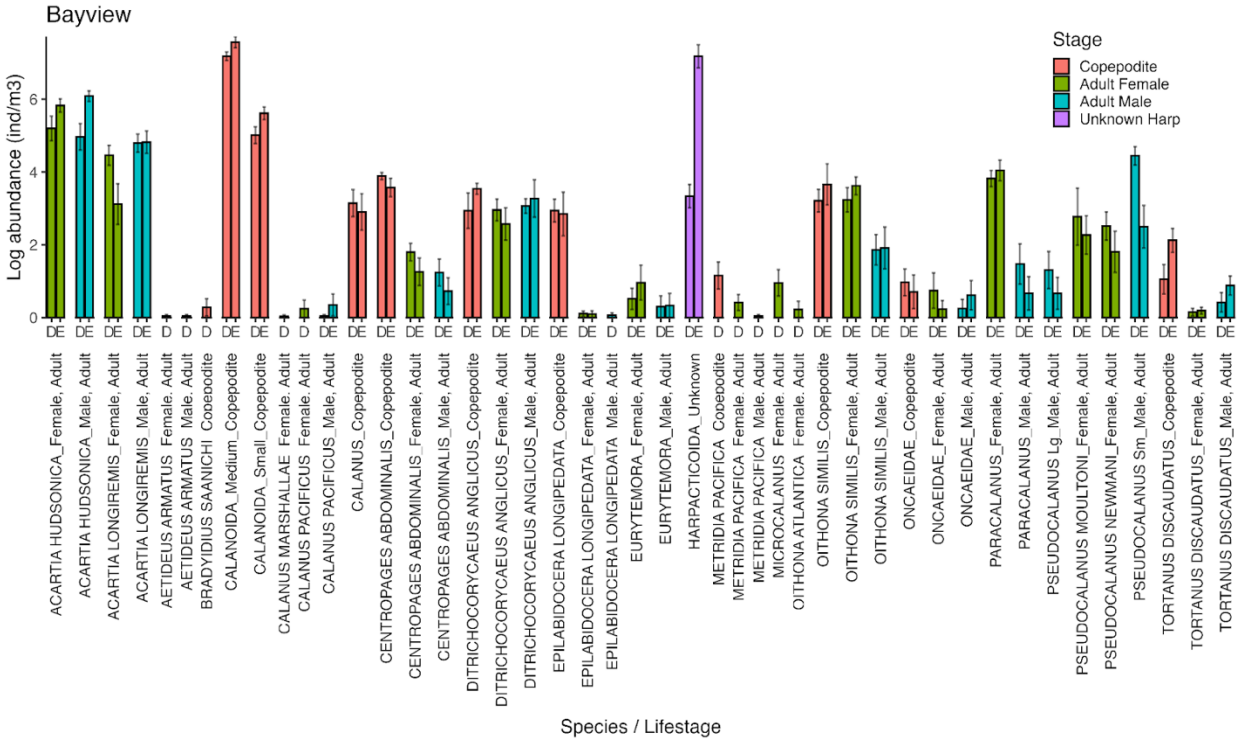

Figure S4. Log-transformed mean (± SE) abundance (individuals / m^3) of copepod species/lifestage combinations recorded at the deep (D) and eelgrass (E) stations on the Ploeg transect. Bars are color coded by life stage. All copepod species are pelagic except for harpacticoid (purple).

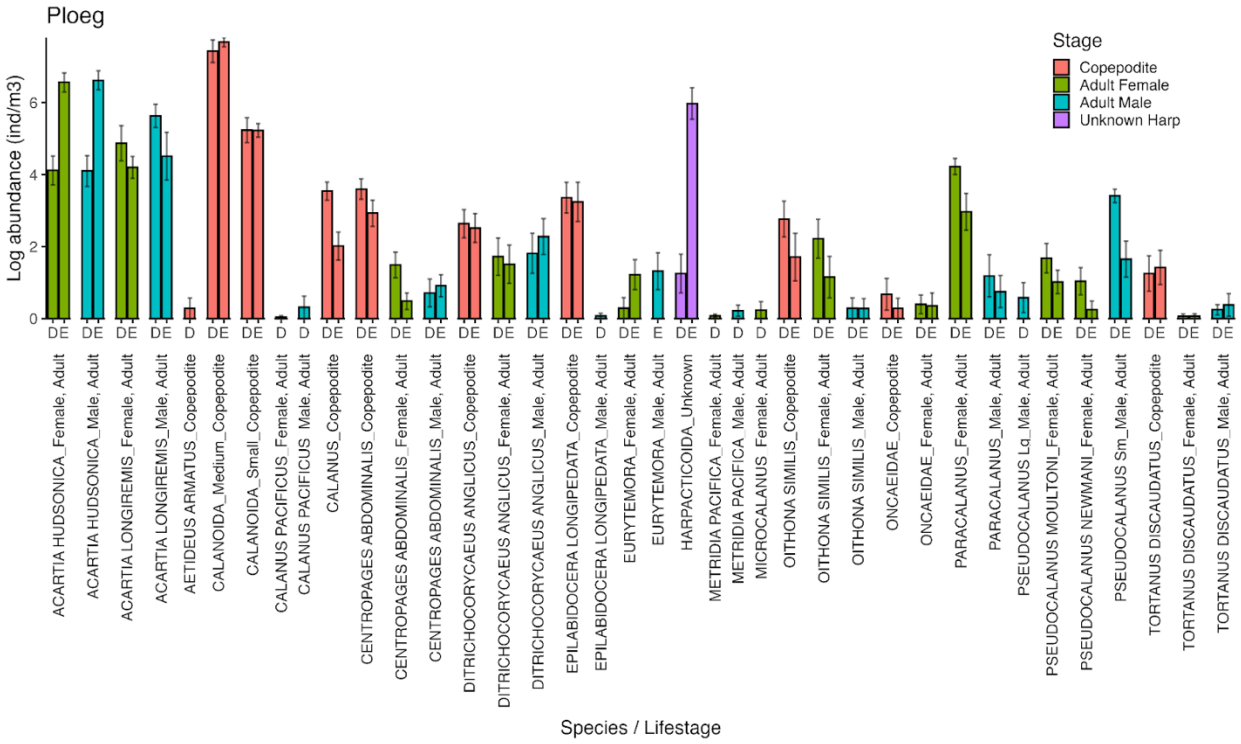

Table S3. Mean (± SE) abundance (individuals / m^3) of non-copepod species recorded at the deep and eelgrass stations on the two sampling transects. Abundances are in bold if there was a significance ($p > 0.05$) difference between deep and eelgrass abundances on that transect.

		Bayview		**Ploeg**	
Taxa	**Lifestage**	**Deep (ind / m3)**	**Eelgrass (ind / m3)**	**Deep (ind / m3)**	**Eelgrass (ind / m3)**
Amphipoda	Adult	0 ± 0	1.3 ± 1.2	0 ± 0	0 ± 0
Amphipoda	Unknown	9.2 ± 5	9.3 ± 4.2	2.5 ± 1.6	0 ± 0
Barnacles	Cyprid larva	94.8 ± 22.2	77.4 ± 15.4	55.3 ± 8.2	27.8 ± 7
Barnacles	Nauplius	2548.7 ± 317.2	2156.8 ± 312.3	**2036.2 ± 459.3**	**710.6 ± 113.3**
Bivalvia	Veliger	54.2 ± 9.2	23.7 ± 6.2	**88.1 ± 29.5**	**18.3 ± 3.3**
Caprellidae	Unknown	0 ± 0	9.3 ± 3.8	0 ± 0	1.2 ± 1.1
Chaetognatha	Unknown	**12.7 ± 5.8**	**15.1 ± 2.1**	42.4 ± 15.4	13.7 ± 3.3
Copepoda	Nauplius	105.4 ± 27.8	193 ± 40.2	398.2 ± 231.6	194.3 ± 32.4
Crabs	Megalopa	0.9 ± 0.7	0.6 ± 0.6	0 ± 0	0 ± 0
Crabs	Zoea	102.1 ± 19	176.8 ± 48.1	**34.3 ± 12.2**	**99.9 ± 21.3**
Ctenophora	Unknown	0 ± 0	0 ± 0	0.2 ± 0.2	0 ± 0
Ctenophora	Whole	2.2 ± 1.4	2.7 ± 1.6	1.4 ± 1.4	0 ± 0
Echinodermata	Larva	0.8 ± 0.8	0 ± 0	0 ± 0	0 ± 0
Echinodermata	Pluteus larva	0 ± 0	0 ± 0	5.8 ± 2.3	0.9 ± 0.9
Euphausiidae	Nauplius	28 ± 10.2	7.5 ± 3.5	25.8 ± 16.8	0 ± 0
Evadne	Unknown	99 ± 49.6	105.5 ± 49.2	**153.1 ± 74.1**	**685.1 ± 265**
Fish	Egg	1.5 ± 1.5	3.3 ± 2.2	10.6 ± 9.4	3.2 ± 2.1
Gastropoda	Adult	0 ± 0	0.1 ± 0	0 ± 0	0.2 ± 0.2
Gastropoda	Veliger	68.8 ± 7.4	77 ± 17.9	**104.9 ± 31.7**	**26.1 ± 5.3**
Obelia	Medusa	28.3 ± 8.2	33.4 ± 18.4	45.8 ± 19.6	27.7 ± 8.2
Oikopleura	Unknown	1330.3 ± 357.3	570.9 ± 111.5	**2250.8 ± 816.3**	**441.7 ± 58.6**
Oweniidae	Larva	41.5 ± 15.9	40 ± 25.2	124.6 ± 51.1	42.9 ± 20.1
Podon	Unknown	870 ± 325.2	1173.3 ± 243.7	**1593.4 ± 749.1**	**4043.8 ± 1200.6**
Polychaeta	Adult	0 ± 0	0.2 ± 0.1	0 ± 0	0 ± 0
Polychaeta	Larva	79 ± 19.1	93.2 ± 18	69.3 ± 20.8	75.8 ± 21.3
Shrimp	Zoea	32.2 ± 9.5	12.2 ± 4.5	27.6 ± 8.5	17 ± 6.6

Figure S5. Mean (±SE) total copepod abundance (individuals / m^3) across different lifestages during flooding (light colors) and ebbing (dark colors) tides from samples collected on both transects (red), Bayview (green) and Ploeg (blue). There were no significant differences between tidal phases.

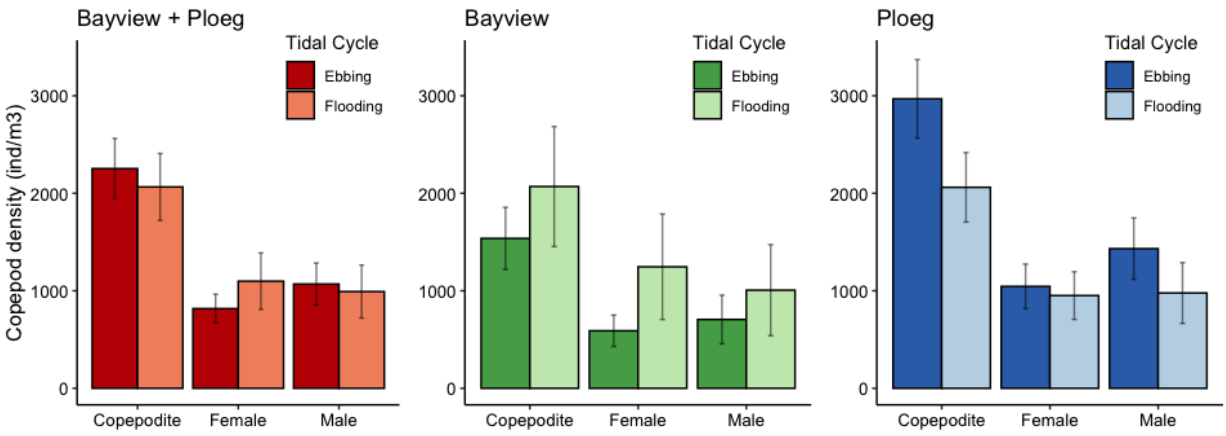

Figure S6. The relative total copepod abundance (individuals / m^3) at channel stations during ebbing and flooding tides (shown as log response ratio) on the Bayview (top panel, green) and Ploeg (bottom panel, blue) transects versus tidal replicate. Log response ratios significantly > 0 indicate that the relative abundance of copepods was higher during ebbing tides. Log response ratios significantly < 0 indicate that the relative abundance of copepods was higher during flooding tides.

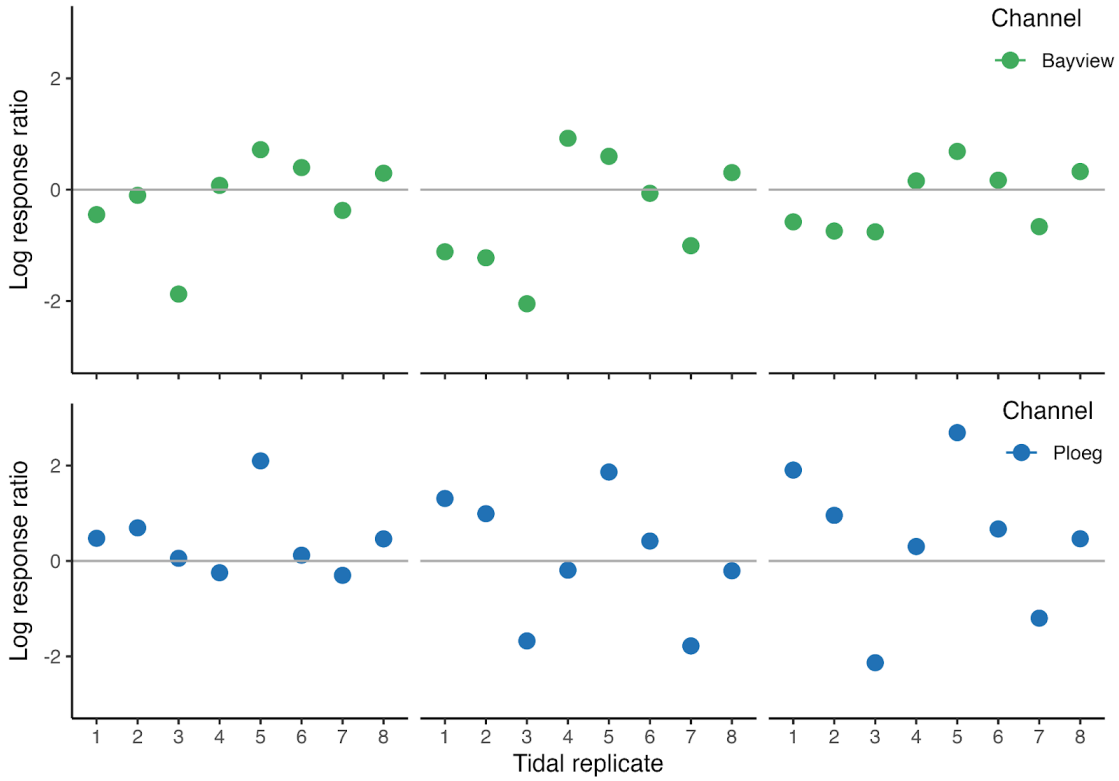

Figure S7. Mean (±SE) total copepod abundance (individuals / m^3) during flooding and ebbing tides from samples collected on the Bayview (green) and Ploeg (blue) transects. * Indicates a significant ($p < 0.05$) difference between stations.

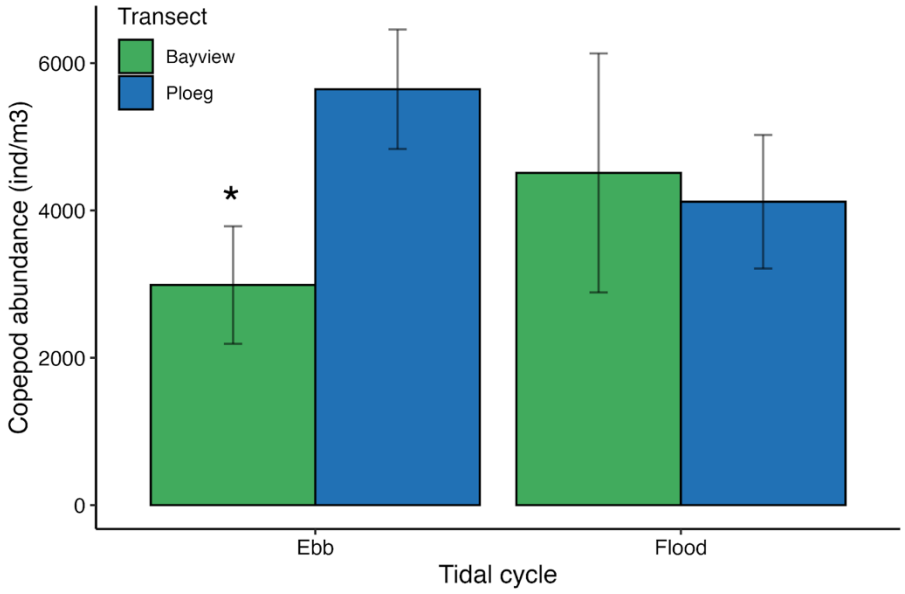

Figure S8. Variability across tidal replicates in the total abundance (individuals / m^3) of non-copepods from samples collected from Bayview (left panel, green) and Ploeg (right panel, blue) channel sites during ebbing (dark colors) and flooding (light colors) tides. There were no significant differences between flooding and ebbing tides.

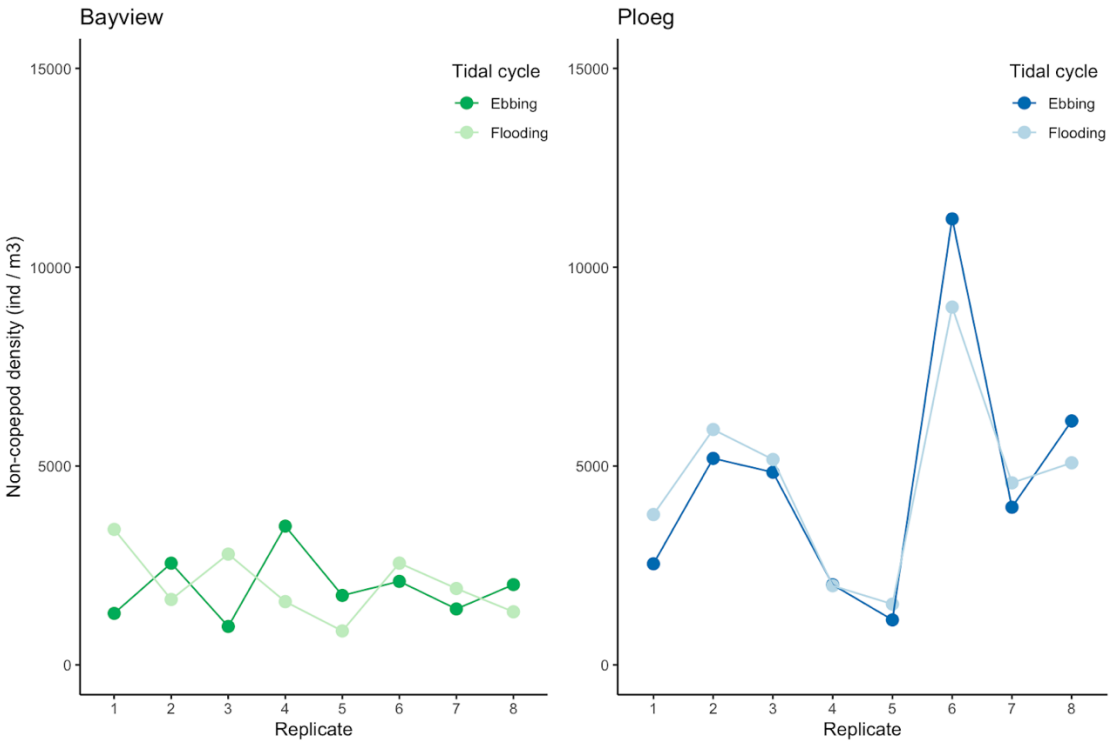

Figure S9. Nonmetric multidimensional scaling ordination of zooplankton species proportions in samples collected from the channel stations on different transects (Bayview = green, Ploeg = blue) and tidal phases (light colors = ebbing, dark colors = flooding). Zooplankton species/lifestage combinations that were significantly correlated with an NMDS axis ($p < 0.01$) are plotted. Transect ($p = 0.007$) but not tidal phase ($p = 0.483$) was significantly correlated with an NMDS axis**.**

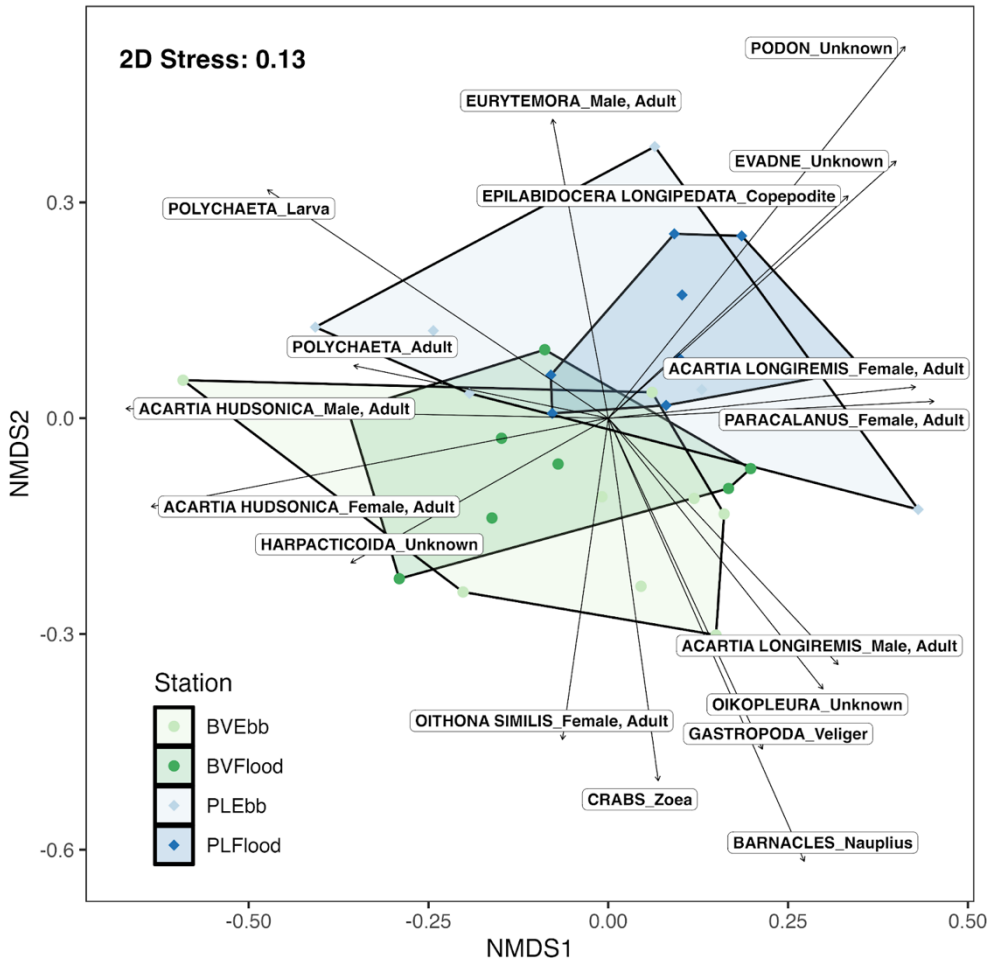

Table S4. Outputs from nonmetric multidimensional scaling ordination of zooplankton species proportions showing the relationships between ordination axes and environmental parameters at the channel stations.

Station	**Variable**	**NMDS1**	**NMDS2**	**P-value**	**R^2-value**
Channel	Temperature	-0.3515572	0.9863604	0.243	0.0945
	Salinity	-0.4928334	-0.4858765	0.574	0.0413
	Depth	0.2306645	-0.4902938	0.704	0.0253
	Wind Speed	-0.2601080	0.2069548	0.846	0.0095
	Wind Direction	-0.3235558	0.5947691	0.540	0.0395

Figure S10. Average non-copepod abundance (individuals / m^3) against turbidity (NTU). The trendlines (solid line) and confidence intervals (dashed lines) show predicted abundances on a) Bayview and b) Ploeg transects from the best-fit generalized linear model.

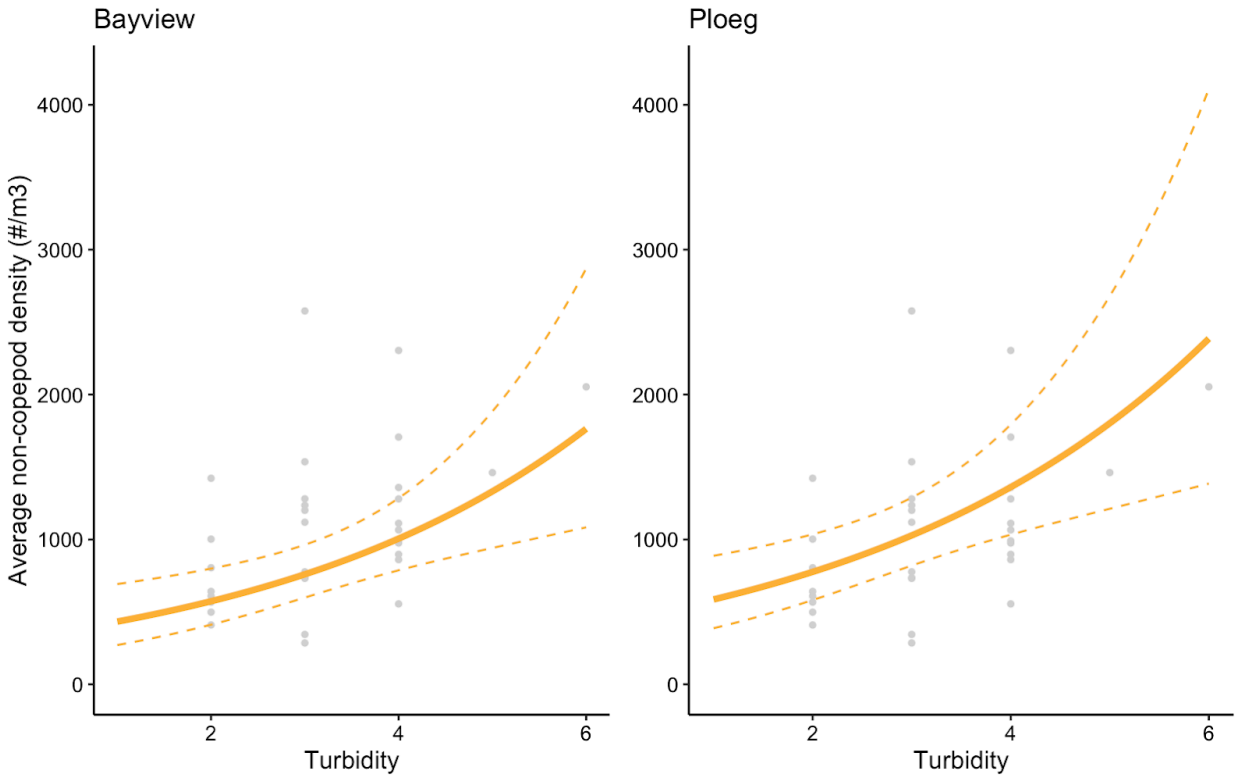

Figure S11. Log-transformed mean (± SE) abundance (individuals / m^3) of copepod species/lifestage combinations recorded at the channel station during flooding (F) and ebbing (E) tides on the Bayview transect. Bars are color coded by life stage. All copepod species are pelagic except for harpacticoid (purple).

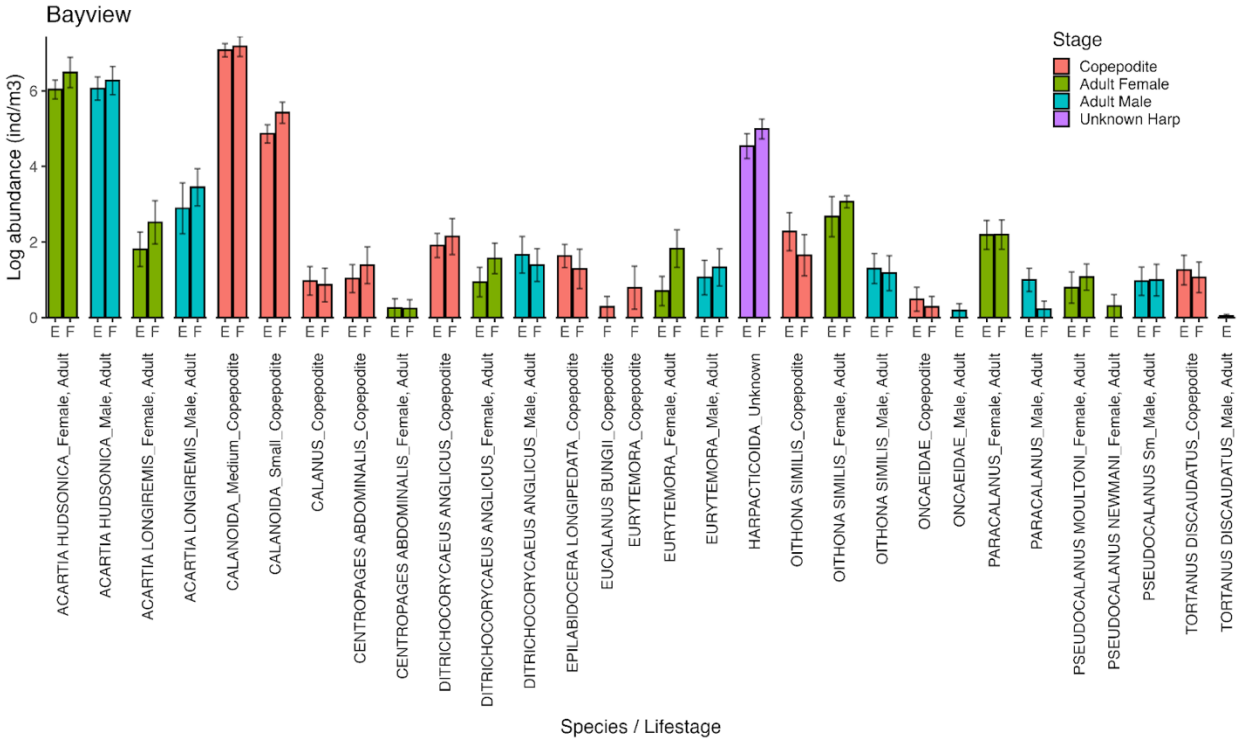

Figure S12. Log-transformed mean (± SE) abundance (individuals / m^3) of copepod species/lifestage combinations recorded at the channel station during flooding (F) and ebbing (E) tides on the Ploeg transect. Bars are color coded by life stage. All copepod species are pelagic except for harpacticoid (purple).

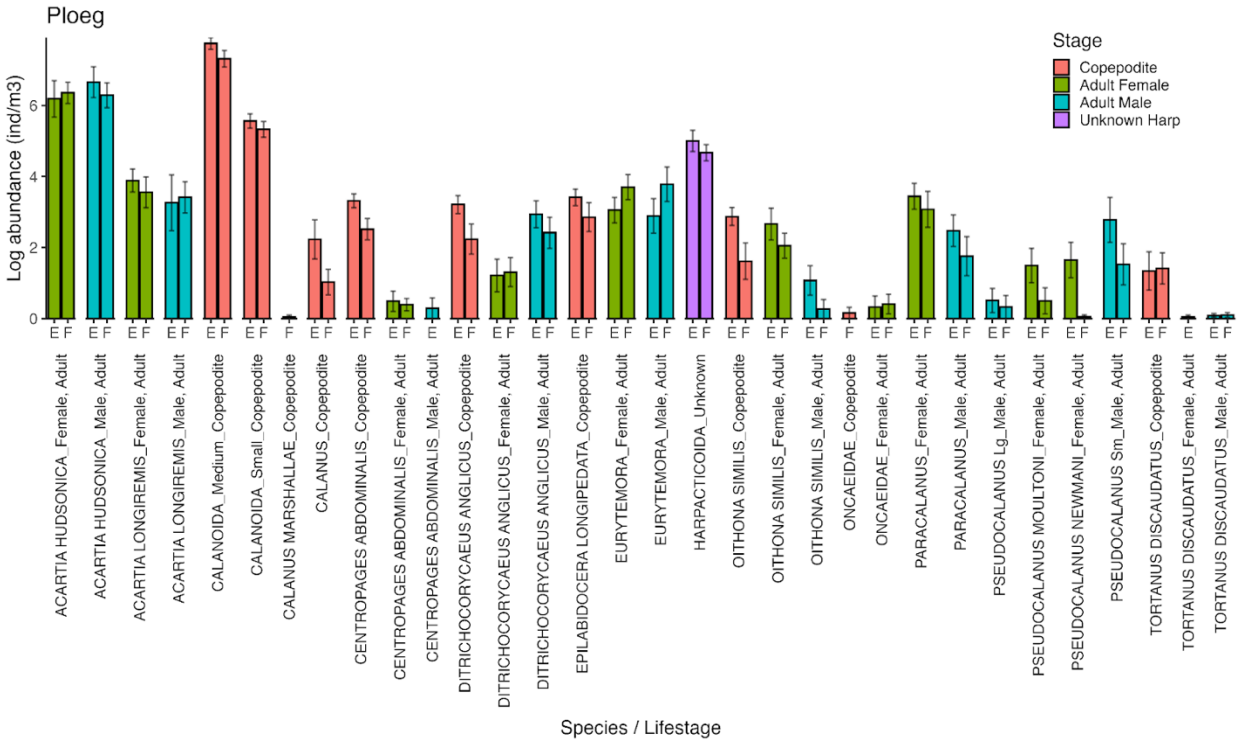

Table S5. Mean (± SE) abundance (individuals / m^3) of non-copepod species recorded at the channel stations during flooding and ebbing tides on the two sampling transects. Abundances are in bold if there was a significance ($p > 0.05$) difference between flooding and ebbing abundances within that transect.

		Bayview		**Ploeg**	
Taxa	**Life Stage**	**Flood (ind / m3)**	**Ebb (ind / m3)**	**Flood (ind / m3)**	**Ebb (ind / m3)**
Amphipoda	Unknown	0 ± 0	0.9 ± 0.6	0.5 ± 0.5	2.2 ± 1.4
Barnacles	Cyprid larva	33.9 ± 14.4	41.7 ± 16.1	84.7 ± 22.9	59.5 ± 22.7
Barnacles	Nauplius	492.2 ± 93.5	643.5 ± 191.1	382.7 ± 58.1	705.6 ± 210.1
Bivalvia	Veliger	6.7 ± 3.9	2.3 ± 1.7	25.8 ± 7.5	17.1 ± 5.3
Caprellidae	Unknown	0.9 ± 0.6	0 ± 0	0 ± 0	0 ± 0
Chaetognatha	Unknown	3.3 ± 1.5	8.2 ± 2.5	7 ± 4	5.6 ± 3.7
Copepoda	Nauplius	33.5 ± 9.8	33 ± 12.8	59.6 ± 14.1	95.4 ± 18.9
Crabs	Zoea	88.1 ± 26	184.5 ± 66.5	99 ± 34.2	103.3 ± 20.6
Cumacea	Unknown	2.5 ± 1.5	0 ± 0	0.6 ± 0.6	4.8 ± 3.6
Euphausiidae	Furcilia	0.5 ± 0.5	0 ± 0	0 ± 0	0 ± 0
Euphausiidae	Nauplius	0 ± 0	2 ± 1.3	7.4 ± 3.8	11.7 ± 5.7
Evadne	Unknown	**117.6 ± 40.9**	**49 ± 20**	354.9 ± 67.1	295.3 ± 78.9
Fish	Egg	4.1 ± 4.1	0 ± 0	5.4 ± 5.4	0 ± 0
Gastropoda	Veliger	16.6 ± 5.5	19.3 ± 7.3	24.5 ± 6.1	26.4 ± 11.6
Obelia	Medusa	8.2 ± 3.9	13.8 ± 5.9	15.5 ± 4.8	29.8 ± 15.2
Oikopleura	Unknown	167.5 ± 23.2	162.7 ± 37.2	262.1 ± 57	179.2 ± 34
Oweniidae	Larva	21.6 ± 11.9	4.4 ± 1.7	13.8 ± 4.8	1.1 ± 1.1
Podon	Unknown	749.9 ± 99.3	664.3 ± 120.3	3091.3 ± 712.5	2787.6 ± 1005
Polychaeta	Adult	0 ± 0	2 ± 2	0 ± 0	0 ± 0
Polychaeta	Larva	**252.1 ± 105.8**	**99.3 ± 57.8**	189.2 ± 90	293.1 ± 114.7
Shrimp	Zoea	11.9 ± 5.1	15.2 ± 8.9	**4.5 ± 2.4**	**11.6 ± 3.5**